The hydrodynamic stability of a ballast filled mattress in an offshore environment

Thesis

Toon Wevers

Delft University of Technology

The hydrodynamic stability of a ballast filled mattress in an offshore environment

By

Toon Wevers

Performed at

Deltares

in partial fulfilment of the requirements for the degree of

Master of Science
in Civil Engineering

at the Delft University of Technology

26th July, 2018

Student number:	4152077	
Author contact:	Toonwevers@gmail.com	
Project duration:	August 21, 2017 – June 22, 2018	
Thesis committee:	Prof. dr. ir. S.G.J. Aarninkhof	TU Delft
	Dr. ir. B. Hofland	TU Delft
	Ir. J.P. Van den Bos	TU Delft
	Ir. T.C. Raaijmakers	Deltares/TU Delft

This thesis is confidential and cannot be made public until September 1, 2021.

PREFACE

This thesis describes my graduation project to conclude my Master of Science in Hydraulic Engineering at the faculty of Civil Engineering and Geosciences of the Technical University Delft. This thesis has been accomplished in association with Deltares.

This thesis could not have been written without the help of multiple persons. First of all, I would like to thank Deltares for the opportunity to do my graduation project and their hospitality i was welcomed with. I want to thank Thijs Robijns en Pim van Steijn for sharing their knowledge. Furthermore, I want to thank all the students at Deltares I met during my thesis, and in special Thieu and Sjoerd, for the breaks, talks and occasional drinks.

would like to thank my graduation committee for their contribution to this research. First of all I would like to thank Bas Hofland. Your enthusiasm and continuous and direct supervision have helped me a lot, especially during the final stage of my thesis. Even though your enthusiasm was too much sometimes, you kept me going forward. Secondly, Tim Raaijmakers for the continuous feedback and the occasional talks about anything but my thesis during a meeting. I would also like to thank Stefan Aarninkhof and Jeroen van den Bos for being part of my graduation committee.

Last but not least, i would like to thank some people that supported me during my studies and thesis. I owe a big thanks to my parents, Toine and Ika. You have always supported me during my studies and were there when I needed it. Ellemijn, thank you for listening to me, helping me get through the last stages of my thesis and for the welcome distractions. Jochem, thank you for the time you put into reading and correcting my thesis. My old room-mates Maarten and Tomas, for cooking for me while i was writing my thesis. Lastly, Max, you know why.

Toon Wevers
Delft, July 2018

ABSTRACT

In this research the hydrodynamic stability of a ballast filled mattress under waves is investigated. There is checked if this can be applied as scour protection around a suction bucket jacket: an offshore wind turbine foundation that uses a vacuum to suck itself in position. A ballast filled mattress is a mattress made from polyester with so called *spacer threads* that take up tensile forces when the mattress is trying to deform. The combination of stiffness and combined weight make the ballast filled mattress a possible new scour protection.

Current practice for the suction bucket jacket is to pre-lay a very precise rock protection, this can negatively influence the suction process. Placing a scour protection afterwards is not possible as falling stones can damage the suction cans and anodes that prevent erosion. Furthermore, a rock protection consists of multiple layers of rock, which requires multiple vessels to bring the rock to location, and is around 1.5 to 2.0 meter high. The latter causes secondary scour that can endanger the cables running from the wind turbine. With offshore wind farms being built further offshore and to decrease the vessel movements, the ballast filled mattress can be a substitute for the traditional rock protection. The ballast filled mattress is automatically installed during installation of the suction bucket jacket after which it can be ballasted with a heavy fluid. This would reduce the amount of vessel movements. Furthermore, by keeping the mattress thin the secondary scour is significantly less, benefiting the cables.

Airgroup-Industries, a manufacturer of double walled fabrics, is looking into the possibility of bringing this ballast filled mattress onto the market, together with SPT-offshore. Within the JIP-HaSPro, coordinated by Deltares, this new innovative scour protection for the suction bucket jacket is tested on different scales for different applications and mattress characteristics. The tests were aimed at its stability and ability to follow scour. These tests are used to answer the main objective of this research: How can the hydrodynamic stability of a ballast filled mattress under waves be described?

In order to answer this question, different scale tests performed at Deltares were investigated and analysed with different methods. The failure mechanisms observed are uplift, sliding and undermining. Sliding always occurred after an uplift event and therefore uplift is seen as the main failure mechanism. The sliding mechanism was observed more often for the stiffer mattresses, but still occurred after an uplift. Undermining is scour below the ballast filled mattress, and occurs when the mattress is stable. Stable means hardly any, to no uplifts. Uplift is resisted by the weight and the bending stiffness of the mattress, undermining is stopped when the ballast filled mattress can follow changing bed topography due to undermining. The latter means that the ballast filled mattress should be flexible enough to follow the (edge) scour and stop undermining.

The tests were analysed with respect to movement or no movement to give a first indication where movement starts. This was done for different hydraulic parameters and checked which has predicting abilities. By means of an mobility analysis using uplift recognition software, more data was generated and analysed. This gave a better estimation for the beginning of motion and a conservative estimate to predict the uplift height. The parameter that was best in describing the initiation of motion and predicting the uplift is based on the Morison-equation.

The initiation of motion can be described by equation 1 for a flexible mattress.

$$\Delta d = \frac{u^2}{0.8g} \tag{1}$$

In which Δ is the relative underwater weight, d the thickness of the mattress, u the orbital velocity at the sea bed and g the gravitational acceleration. The uplift height can be estimated by using eq. 3 together with eq. 2.

$$Rul = \frac{uplift}{thickness} = 0.285\theta^2 + 1.679\theta - 1.57 \tag{2}$$

$$\theta = \frac{u^2}{\Delta g d} \tag{3}$$

Lastly a design method is given to practically apply the ballast filled mattress for irregular waves. This is done by using the Rayleigh distribution, for a given H_{m0}, T_{m02} and waterdepth, and using linear wave theory to calculate the corresponding values of θ. The design criteria are that for $H_{0.1\%}$ the relative uplift height should not exceed 1 and that the probability of exceendance of failure (relative uplift height of 3) should be below 5%. This method was tested for the German Bight and it appeared that the method can be used for a preliminary design of the ballast filled mattress. θ is based on regular waves but applied to irregular waves. The applicability is checked by applying θ_{cr} to irregular wave test performed within the JIP-HaSPro. This concluded that the design method based on $\theta_{cr} = 0.8$ gives a conservative preliminary design with respect to the initiation of motion.

A practical design criteria is given for the flexibility of the mattress that states that if the uplift height of the mattress is equal to 1 thickness, the uplift length (the length over which the mattress is lifted) should be at least 4 times the thickness of the mattress. This criteria ensures the mattress is able to follow the seabed topography due to (edge) scour.

The uplift recognition analysis showed the importance of the inertia term with respect to the behaviour of the mattress. The flexible mattress tested around a monopile the up and downstream side of the pile showed different uplift behaviour. A time domain analysis showed the importance of the under pressure from the wave fluctuations. This, together with the presence of the pile could explain the difference between the up- and downstream side for the flexible monopile mattress.
The time domain analysis also showed the uplift being dominated by inertia.

CONTENTS

List of Figures

List of Tables

List of Abbreviations

ACBM	Articulated concrete block mattress
ARC	automatic reflection compensation
BFM	Ballast filled mattress
CFD	Computational fluid dynamics
CRVs	Counter rotating vortices
EMS	Electronic current velocity meter
HSV	Horse-shoe vortex
JIP-HaSPro	Joint industry project - Handbook for Scour Protection methods
KC	Keulegan-Carpenter
LWT	Linear wave theory
SBJ	Suction bucket jacket
VIV	Vortex-Induced-Vibrations
WHM	Wave height meter

List of Symbols

u	velocity	m/s
U_m	undisturbed orbital velocity	m/s
u_w	orbital velocity	m/s
u_x	orbital velocity obtained with linear wave theory	m/s
$u_{w,max}$	maximum orbital velocity	m/s
u_{ems}	orbital velocity measured by the EMS	m/s
u_{max}	maximum orbital velocity obtained from the EMS	m/s
a	horizontal acceleration	m/s^2
a_x	horizontal acceleration according to lin. wave theory	m/s^2
a_{ems}	horizontal acceleration obtained from the EMS signal	m/s^2
a_{max}	maximum horizontal acceleration obtained from the EMS	m/s^2
T	wave period	s
T_m	mean wave period	s
T_p	peak wave period	s
T_{m02}	mean absolute wave period	s
D	pile diameter	m
F_H	horizontal force	N
F_d	drag force	N
$F_{d,up}$	uplift force due to stagnation pressure	N
$F_{i,up}$	inertia force due to pressure difference	N
F_i	horizontal inertia force	N
F_i	inertia force	N
F_T	total force	N
C_D	drag coefficient	–
C_L	lift coefficient	–
C_m	inertia coefficient	–
C_{all}	proportionality coefficient	–
ρ_w	volumetric weight of water	kg/m^3
ρ_m	volumetric weight of the material	kg/m^3
A	surface area of attack	m^2
V	volume of body	m^3
g	gravitational acceleration	m/s^2
k_a	added mass coefficient	–
Δ	relative density	–
d_s	stone diameter	m
d_{50}	median sediment diameter	m
d	mattress thickness	–
μ	dynamic viscosity	$kg/m/s$
E	Young's modulus	N/m^2

θ	mobility parameter	–
θ_i	mobility parameter for inertia	–
θ_T	full mobility parameter	–
θ_{lin}	mobility parameter according to lin. wave theory	–
$\theta_{T,lin}$	full mobility parameter according to lin. wave theory	–
θ_{ems}	mobility parameter according to EMS	–
$\theta_{T,ems}$	full mobility parameter according to EMS	–
θ_{cr}	critical stability parameter	–
$\theta_{cr,lin}$	critical stability parameters obtained with lin. wave theory	–
Θ	Shields parameter	–
Θ_{cr}	critical Shields parameter	–
λ	scale factor	–
A_x	particle excursion	m
I	moment of inertia	m^4
$\frac{\Delta p}{\Delta x}$	pressure gradient	Pa/m
w	uplift	m
κ	curvature	$1/m$
L	wave length	m
$L_{w,lin}$	wave length obtained with lin. wave theory	m
$L_{mattress}$	mattress length	m
H	wave height	m
ω	angular frequency	$1/s$
h	water depth	m
z	depth of interest	m
H_{m0}	zero order moment wave height	m
H_m	mean wave height	m
N	number of waves	–
$H_{0.1\%}$	wave height with 0.1% probability of occurrence	m

1 INTRODUCTION

There is an ongoing battle against global warming and multiple international agreements (Kyoto and Paris) have been signed to cut carbon dioxide emissions and to prevent the global temperature from rising 2°C. The results of this is that the demand for cleaner and alternative sources of energy has increased. This explains the exponential growth of wind farms being built (Ho et al., 2017). Wind is seen as a clean source of renewable energy that is freely available and has no water or air pollution.

To generate wind energy, so called wind farms are built offshore in a marine environment. There are over 3230 offshore turbines and 84 offshore wind farms currently in operation in the North Sea (EWEA, 2015). Meanwhile it is expected that the market will grow (Nghiem & Pineda, 2017). Due to the growth, the market will face new engineering challenges. More and more wind farms are planned further offshore in deeper water, see Figure 1.1. This in turn requires other foundations to coop with the increase in forces. The classical monopile, which is designed for water depths up to 30m, will lose it to space frame structures designed for deeper waters.

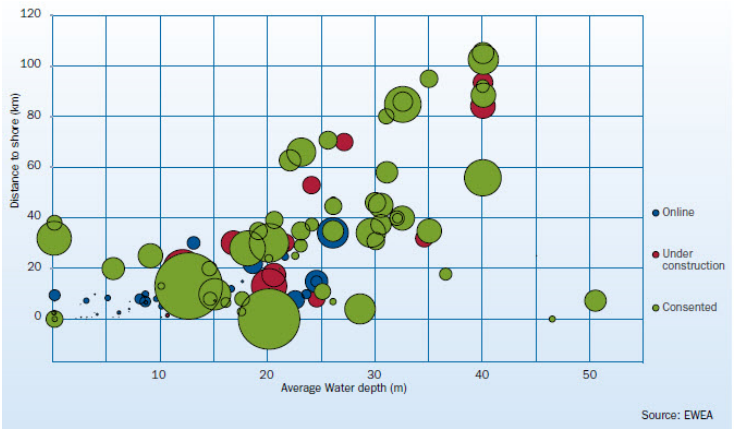

Figure 1.1: Water depth and distance to shore for offshore wind farms

1.1 BACKGROUND

For offshore structures, scour is seen as a problem for the foundation of an offshore wind turbine. For a classical monopile scour results in less bearing capacity, consequently a larger penetration depth is needed. Furthermore, a scour hole causes a drop of the natural frequency of the monopile. Due to this the natural frequency of the monopile will get closer to the frequencies of the wave loading. Lastly, a scour hole increases the lever arm of wind and wave loading which increases the bending moments in the pile. To account for all the aforementioned problems a larger diameter (or thicker wall) is needed (Zaaijer & Tempel, 2004) or a scour protection is placed around the base of the foundation to mitigate the scour around the foundation. Figure 1.2 (left figure) shows the regular lay-out of a monopile with scour protection installed offshore. For deeper waters, the loads on the substructure and foundation increase. This includes the hydrodynamic forcing and forces induced by the top structure. The material costs to strengthen the monopile will become too large and the monopile foundation and space frame structures become more economical. Space frame structures are designed for deeper waters to cope with the increasing forces, the right figure in Figure 1.2 shows the conventional jacket structure, a type of space frame structure.

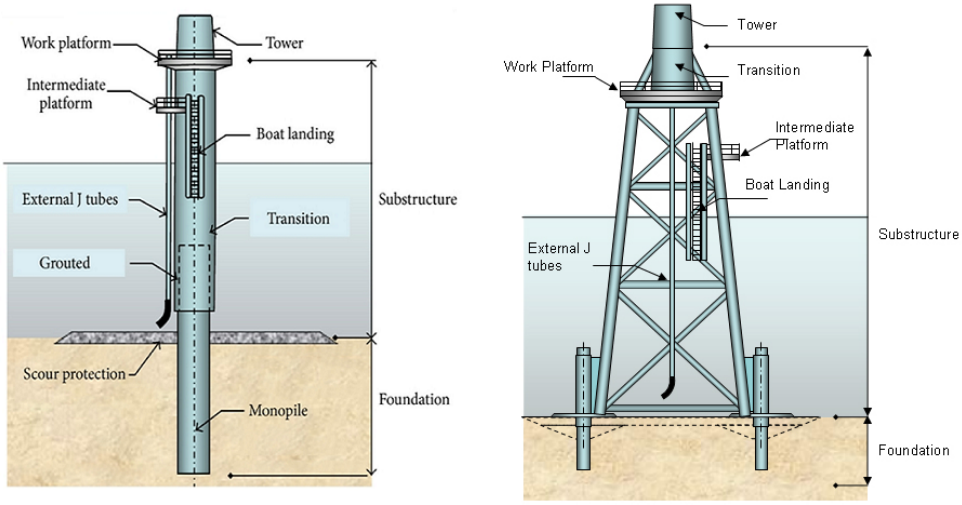

Figure 1.2: Regular lay-out monpile (L) and jacket structure (R) (Sahroni, 2015)

In general there are two ways of dealing with scour; (1) design a structure such that the scour will not be a problem. This means accounting for the extra moment and larger penetration depth needed, Or (2) protect the foundation with a scour protection to keep the scour far enough away from the foundation in order to have the stability of the foundation not endangered. In some cases (e.g. in areas with very morphodynamic seabeds) a hybrid solution is adopted, in which first (limited) scour is allowed and then a scour protection is installed inside the scour hole.

The most widely used scour protection consists of various layers of dumped rock. The various layers have the function of retaining the sediment around the base of the foundation, thus ensuring its stability. Other scour protections exist, but are not used as widely or proven to be as effective as the traditional rock protection. For the monopile foundation, the rock protection is easily installable and effective, but for the space frame structures a rock protection is more troublesome. For a space frame structure the placement of the armour layer within the structure is complicated due to the trusses between the different foundation piles. For this reason it is often chosen to design a space frame to account for the scour. But with increasing water depths, the

costs of increasing the strength of the foundation will not be profitable. Besides, large scour holes can cause free-spanning of the electricity cables, potentially resulting in failure due to Vortex-Induced-Vibrations (VIV). A specific jacked structure, the suction bucket jacket (SBJ) as shown in Figure 1.3, is a special kind of foundation. This foundation uses three suction cans to lower itself on the seabed and its stability is highly dependent on the near-surface soil around the suction cans (Zaaijer & Tempel, 2004). Traditional rock dumping is not applicable here, as falling stones can damage the suction cans, the anodes (to prevent corrosion) and the suction process itself can be negatively affected by the presence of rocks, thus an accurate protection must be placed prior to the installation of the SBJ.

Figure 1.3: Suction Bucket Jacket (Garus, 2014)

With the increasing distance to the mainland, also shown in Figure 1.1, there is a demand for solutions that are as effective as rock protections but require less work operations to be placed. I.e. a traditional rock berm requires multiple rock gradings. Each grading has to be brought to location with a vessel and placed on the seabed. With increasing distance offshore it requires these vessels to sail a greater distance, which in turn increases the costs.

1.2 Problem definition

The problem within the offshore wind industry is the lack of good scour protections for complex foundations together with the increasing distance offshore. An alternative scour protection is needed for complex foundations, especially for the suction bucket jacket. The suction bucket jacket require a new type of scour protection. One that preferably makes the installation of the suction bucket jacket easier and requires less work operations to be placed.

Within JIP-HASPRO (Joint industry project - Handbook for Scour Protection) coordinated by Deltares and supported by twenty industrial partners, new innovative scour protections are tested on different scales. Airgroup-industries, a manufacturer of double walled fabrics, is looking into the possibility of bringing a ballast filled mattress (BFM) onto the market as scour protection. This ballast filled mattress is a relatively heavy but

thin mattress, which limits edge scour and secondary scour developments. Together with SPT-offshore they are investigating a self-installable system for the suction bucket jacket, but can in theory be applied to any type of foundation. The self-installable system by SPT-offshore automatically lowers during installation of the suction bucket jacket. The ballast filled mattress is connected to the foundation and lowers at the same time. When the suction cans penetrate the soil, the support beams are lowered and the mattress will unfold. The system is comparable with opening an umbrella up-side down. After the installation of the suction bucket jacket and ballast filled mattress, the mattress can be ballasted. This system together with the mattress has the possibility to answer the demand from the market as explained above.

1.3 OBJECTIVE

This research will focus on the hydrodynamic stability of a ballast filled mattress under waves and the ballasting of the mattress. This is done by evaluating different scale tests and will lead to a preliminary design method. In order to determine the ballasting material, tests will be done with a ballasting material for the mattress. In order to set up this preliminary design method, multiple questions regarding the mattress need to be answered.
The main objective in this project is:

- *How can the hydrodynamic stability of a ballast filled mattress under waves be described?*

  To answer this objective, the following sub questions need to be answered.

  1. *What are the failure mechanisms of the ballast filled mattress?*
  2. *What are the governing hydraulic parameters influencing the stability of the ballast filled mattress under waves?*
  3. *What are the governing structural parameters influencing the stability of a ballast filled mattress under waves?*
  4. *How to ballast the mattress?*

1.4 Research approach and outline

In Figure 1.4 the approach of this research is graphically displayed and shows the steps taken in this report to get to the empirical design method. This research consists of three main components.

The first component consists of a literature study about scour, offshore foundations and forces, together with reading in on all tests performed within the JIP-HaSPro to see what and how the mattresses are tested. After this is done, filling tests are done during with respect to the filling material and filling of the mattress. This is visually shown in the left blocks of Figure 1.4.

Secondly, the video recordings from different tests are analysed. The main goal of this phase is to find the failure mechanisms, to find out the important parameters and to check what the failure mechanisms are of the ballast filled mattress. Furthermore, the tests are categorized in no movement or movement and checked against different hydraulic parameters. This analysis will also give a first estimation for the beginning of motion. The scour mitigation tests provide answers with respect to its ability to follow (edge) scour.
After the stability and video analysis, the mattresses are analysed by means of an uplift recognition software; the mobility analysis. This will also give a better understanding of the behaviour of the mattress and is compared with the earlier results found with the stability analysis and will give more information about important processes. This is shown in the middle blocks of Figure 1.4.

The third component is to combine all the results to answer the main objective of this research and to give a preliminary design method to practically apply the ballast filled mattress. Also a case study will be performed on a German Bight wind project. This research is finalized with a discussion, conclusions and recommendations, shown in the right blocks in Figure 1.4.

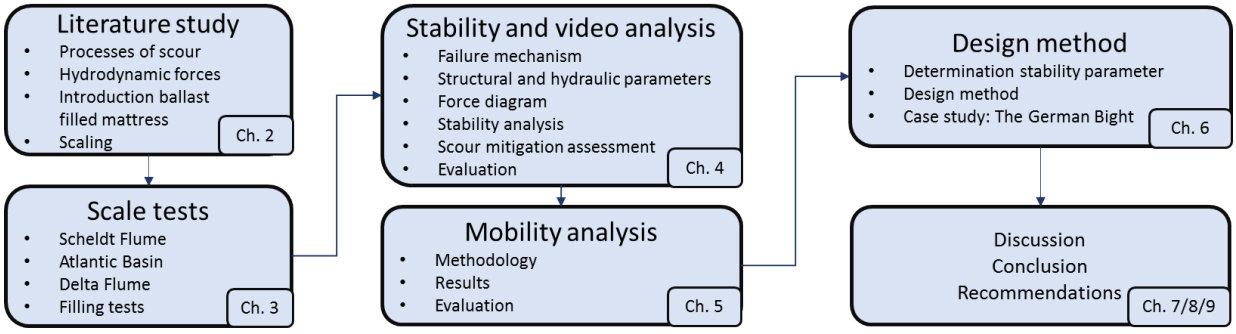

Figure 1.4: Thesis outline

2 LITERATURE REVIEW

2.1 INTRODUCTION

Structures placed in a current or waves change the flow field around the structure and cause the soil around it to erode, if erodible. Erosion is normally seen as a natural process whereas scour is the specific process where sediment around a structure is removed due to the change in flow field caused by the presence of this particular structure (Schiereck & Verhagen, 2012). Erosion only occurs when the shear stress exceeds a certain threshold that initiates the movement of particles. Shields was the first to express the removal of sediments in this way and did this for a uniform flow with no obstructions. In many cases the flow is far from uniform and this makes the shear stress a function of the flow velocity and turbulence. A structure will influence the flow pattern and induce turbulence in the wake of the structure, which enhances scour. The scour around a structure can endanger the stability and for this reason scour has been, and still is, the topic of many studies related to foundations of bridges, piers and offshore structures. The interest of these studies is on how to predict scour and how to protect against scour. For this research, only the latter is of importance.

For this research, the processes that cause scour are investigated for cables, monopiles and space frame structures. This gives insight in how scour occurs and what the governing mechanisms are. The prediction of scour and corresponding timescales are not investigated further as mentioned above. First erosion around cables is introduced after which the processes of scour around different foundation types are presented with the relevant processes per foundation. Then the phenomena edge scour and the articulated concrete block mattress (ACBM) are introduced while this resembles the ballast filled mattress. This is followed by an introduction of the ballast filled mattress (BFM) by Airgroup-Industries. Finally, different stability formulations are given and explained followed by important scaling relations and parameters.

2.2 SCOUR AROUND CABLES

Cables are crucial in the network of transporting the generated electricity towards the mainland. Cables run from each wind turbine to an offshore high voltage station, from where one cable transports the electricity towards the mainland. Besides electricity cables, other cables like telephone and internet are also present on the seabed. To protect the cables from fishing activities and anchors they are often buried within the seabed.

But due to the increase in electricity cables, more often cables need to cross one and other. This is called a *'cable crossing'*. This means that one cable must leave its buried position and cross another cable over the seabed. The unburied part of the cable will become an obstruction to the flow, as mentioned in the introduction, and this will result in scour in the vicinity of the cable.

For cables there are two processes that cause scour. The main cause for scour of cables is tunnel erosion (Leeuwenstein et al., 1985). Due to the pressure difference created by the cable, a seepage flow will start to flow beneath the cable. This pressure difference is dependent on the flow velocity, the greater the flow velocity the greater the pressure difference, thus the bigger the seepage flow and scour. For cables this mechanism is first and followed by the scour due to the shedding of vortices, called lee-wake erosion (B. Sumer & Fredsøe, 2002). When the scour hole due to the tunnel erosion has reached a certain value, this shedding of vortices will take place and will govern the scour process from that point on. The vortices that shed from the bed side of the pipe will stir up sediment from the bed and transport it downstream. Both mechanisms are shown in Figure 2.1.

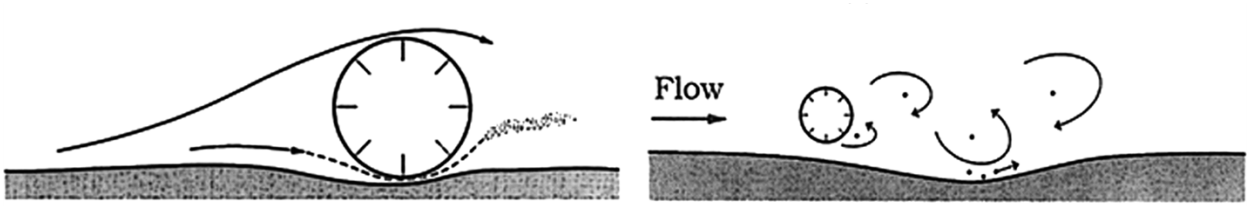

Figure 2.1: (L) Tunnel erosion (R) vortex shedding (Zanganeh et al., 2012), adjusted by author

Scour for cables is a problem in two ways, first the tunnel erosion causes a hole below the cable and this causes a freespan. A freespan is when a part of the cable is suspended in the water and part is resting on the edge of the scour hole as shown in Figure 2.2. The weight of the cable is resting on the edges and the cable must be strong enough to withstand its own weight. Secondly, a freespan can cause vortex-induced vibrations. When a vortex is shed, it causes a force on the cable alternately up and down due to the shedding. VIV can cause the cable to vibrate close to the natural frequency and reducing its lifetime due to fatigue as mentioned in Hover et al. (1997).

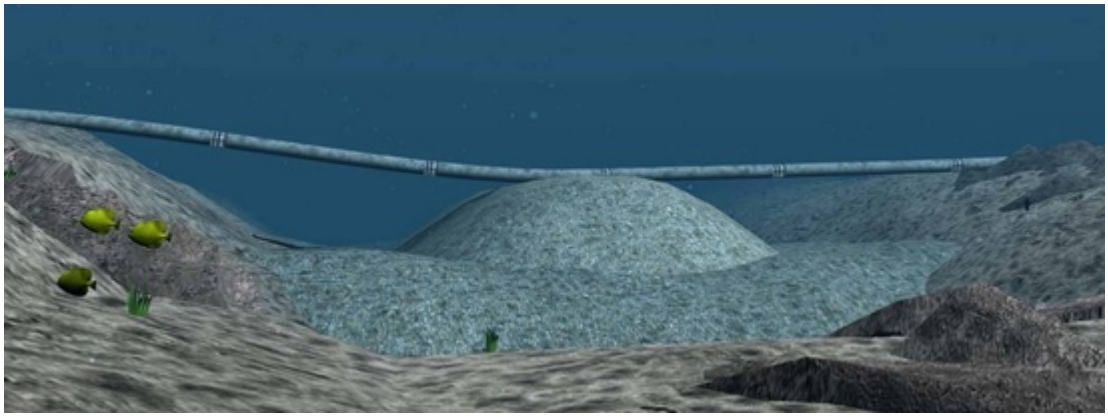

Figure 2.2: Freespanning of cables (Adhiyasa, 2015)

Freespanning and VIV also occurs at the edge of the scour protection of an offshore wind turbine where the cable enters the seabed from the scour protection. Due to edge scour, which is explained in Section 2.5, the sand around the cable is eroded and this can cause the above mentioned problems.

2.3 SCOUR AROUND A MONOPILE

Over the past decades much research has been done on scour around a monopile. This could be explained by the 66.5% of operating offshore foundations consisting of monopiles at the end of 2013 (WEU, 2013). However with increasing water depths other foundations become more competitive. Nevertheless the monopile is still widely used and developments for an extra-long monopile that can be used in water depths up to 35m are promising.

When a monopile is subjected to a current and/or waves multiple processes occur: (1) the current is pushed against the pile, (2) the current is diverted around the pile and (3) the creation of a wake area downstream of the pile. Each have their part in the scour process and are visualised in Figure 2.3. The approaching flow sets up a pressure gradient between the bed and the flow above due to velocity differences. This pressure gradient drives a flow down towards the bed along the front of the pile, with an increasing strength downwards. When this down-flow touches the bottom the boundary layer separates and forms a horse-shoe vortex (HSV) (Whitehouse, 1998), this vortex is transported downstream with the flow that is diverted around the monopile. The HSV and the accelerated flow are the main cause of erosion in front of the pile and at the transverse side of a monopile in the case of a steady current (B. M. Sumer & Fredsøe (2001) and Schiereck & Verhagen (2012)).

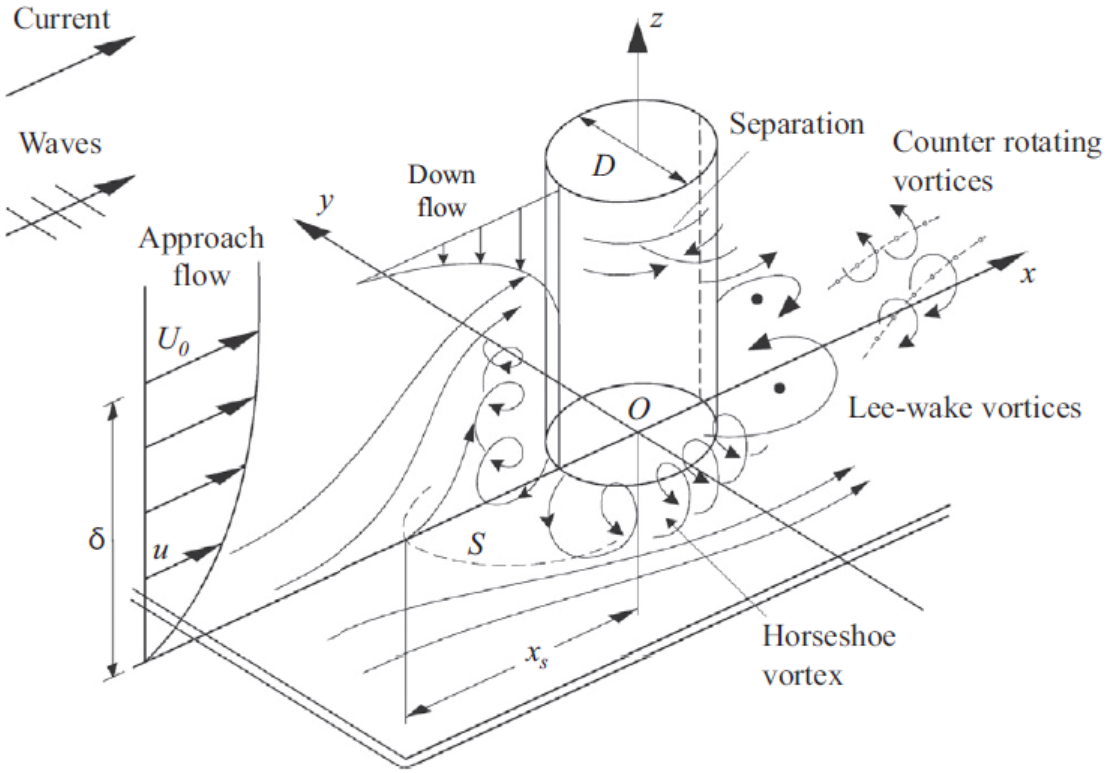

Figure 2.3: Scour processes around a monopile for current and waves combined (Baykal et al., 2017)

In the wake area, lee-wake vortices are formed. This happens because the flow cannot follow the shape of the pile and unstable shear-layers are formed between the water and the monopile. These layers roll up and the lee-wake vortices are formed (Breusers et al., 1977). Besides lee-wake vortices, counter-rotating vortices (CRVs) can occur. CRVs occur due to the HSV from upstream and the difference in lee-wake vortex shedding at the

bottom (Baykal et al., 2014). The lee-wake vortices, together with the CRVs, are responsible for the elongated scour hole downstream of the monopile. Furthermore, in the wake area a low pressure zone arises. Baykal et al. (2017) did numerical simulations that nicely show the upward directed pressures and velocity in the lee-wake area as shown in Figure 2.4. The latter study was done for waves only with a KC of 10 and 20, thus in the full vortex shedding regime according to B. Sumer & Fredsøe (2002).

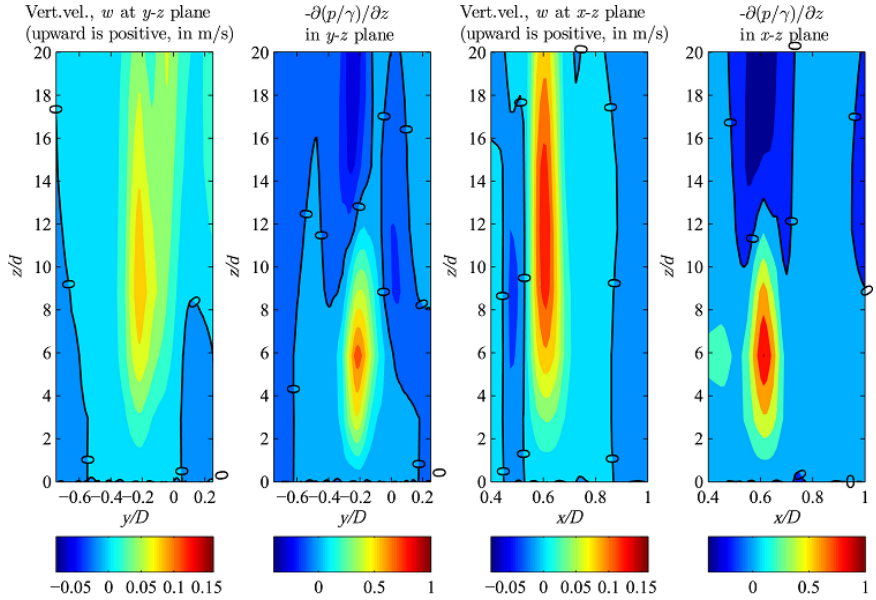

Figure 2.4: Upward directed pressure in the wake area behind a monopile for a KC of 10 to 20 (Baykal et al., 2017)

The driving force behind the formation of the HSV is a current, the shedding of the wake-vortices is governed by waves. The forming of the HSV and lee-wake vortices can be expressed in the Keulegan-Carpenter number (KC). The KC number expresses the ratio between the structural scale and the load scale, the higher the KC number the higher the load and it is defined as:

$$KC = \frac{U_m T}{D} \tag{2.1}$$

In which U_m is the undisturbed orbital velocity, T the wave period and D the pile diameter. The higher the KC number, the more the flow represents a steady current and the formation of a HSV. B. M. Sumer et al. (1992) found that for values of KC<6 the HSV is practically non-existent and also the scour is seen as insignificant. The KC number also indicated the shedding of lee-wake vortices. For KC values up to 7, the amount of vortex shedding increases. From 7 to ∞ there is full vortex shedding (B. Sumer & Fredsøe, 2002). The KC number is further explained in section 2.8

As this research focusses on the hydrodynamic stability of a ballast filled mattress under waves, the conditions during a design storm are of importance. Where the tidal current is the main cause of scour, the waves are important for the stability of the ballast filled mattress. Typical KC values of a North Sea storm are between 1 to 7 (Raaijmakers, 2014). From this it can be concluded that the HSV is practically non-existent, thus will not be a problem. A HSV could theoretically initiate uplift at the edge of a protection. For this to happen the dimension of the HSV must be in the same order as the protection. Sahin et al. (2010) and Prasad et al. (2002) found that the dimensions of the HSV are in the range of 0.2D for a rigid bed while the scour protection is in the range of 2-4D. The HSV is also responsible for scour at the perimeter of any scour protection, the consuquence of this is further explained in section 2.5.

2.4 Scour around complex foundations

Complex foundations are offshore foundations that consist of multiple foundation piles. The diameter of these piles are significantly smaller than the diameter of a single monopile. For this research only complex foundations similar to the SBJ, as introduced in Chapter 1, are investigated for reasons of practical interest. These structures are referred to as space frame structures and are shown in Figure 2.5.

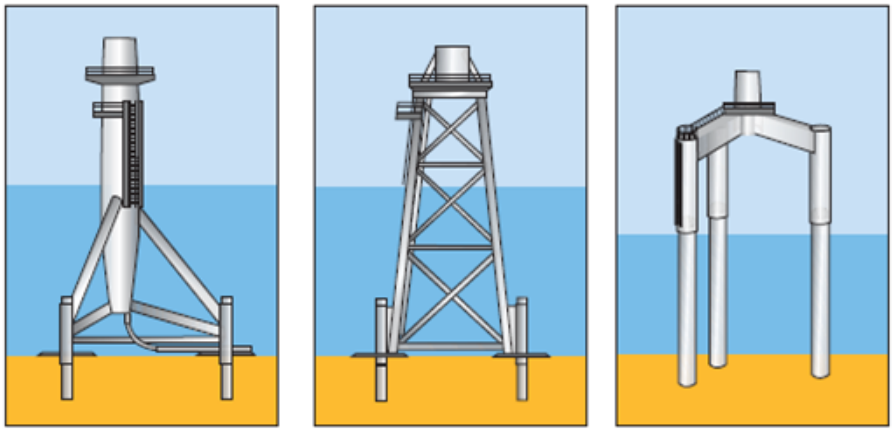

Figure 2.5: Complex foundations, from left to right: tripod, jacket and tri-pile, (Right, 2012)

Around complex foundations global scour occurs. Global scour is the scour around the entire structure where local scour is the scour around one pile (Bolle et al., 2012). Local scour has been investigated intensively as mentioned earlier by Sumer & Fredsøe, where there is a lot less known about scour around complex structures with respect to the prediction of scour. The reason is that the structures cause a more complex flow pattern and CFD is needed for the prediction of scour (Raaijmakers, 2017). Some studies have been performed for a conventional jacket and tri-pile foundations. Mostafa & Agamy (2011) studied waves against a current and found that for a tri-pile foundation the maximum scour is significantly less than for a monopile. A possible explanation according to Mostafa is that the incoming current is diverted and some of the incident current is diverted around the whole structure instead of passing through, resulting in significantly lower flow velocities within the structure. The extent of the scour hole is much larger and is attributed to the fact that the total obstruction is larger than a single pile. Chen et al. (2014) found that for the conventional jacket structure most severe scour occurred at the up-current or up-wave side. No explanation is given for this, but a possible explanation is that the downstream leg is shielded from the upstream leg. No fully developed current is directly forced on the piles. For both results the orientation with respect to the current or waves is of big importance.

A suction bucket jacket consists of a tri-pile jacket structure with a suction bucket attached to each leg. The suction buckets have a diameter ranging from 8 - 15 meters (Zaaijer, 2003). The foundation is lowered to the seabed where the bucket will suck itself into the seabed. This is done by creating a 'vacuum' within the bucket and using the weight of the water to push the foundation in place. It is impossible to completely bury the bucket within the seabed and part of it will protrude above the seabed. This has two significant consequences. As the bucket is significantly larger than legs of the jacket, it forms a protection against the HSV developed due to the legs. The protrusion of the bucket also has a negative effect. De Sonneville et al. (2010) investigated a collar type of scour protrection for monopiles. He did tests by adding a skirt at the base of the foundation, which can be seen as a bucket protruding above the seabed. This is shown in Figure 2.6. This had an adverse effect and scour was even larger than an unprotected pile. Lastly, scour is unacceptable for suction bucket jacket foundations where the suction buckets have a high reliance on the soil around (Zaaijer, 2003). In general the dimensions

of the suction bucket jacket (and other complex foundations) are smaller than a monopile, thus the processes are less pronounced as explained in section 2.3. But the complexities of the structures, i.e. the support beams between the legs, cause a different flow patterns within the foundation. In general is can be said that when a protection is stable around a monopile, it is also stable for a SBJ (Raaijmakers, 2017).

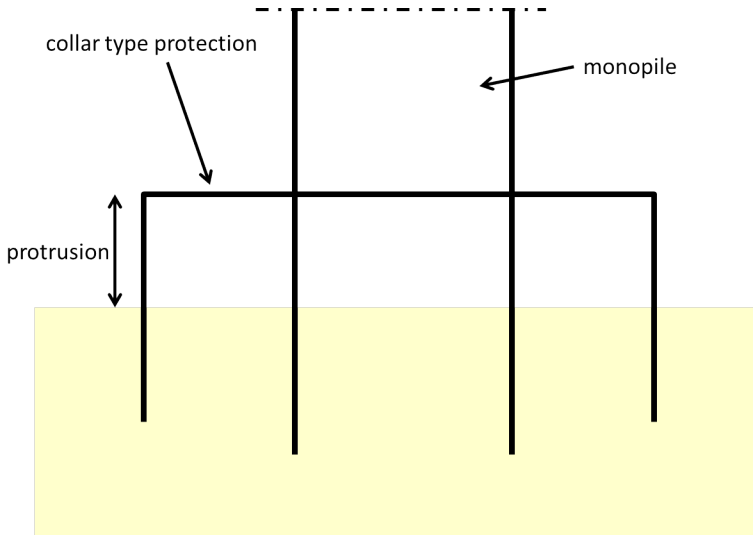

Figure 2.6: Collar type protection / Suction bucket jacket

2.5 EDGE SCOUR

A second type of scour is called *secondary scour* or *edge scour*. Edge scour is the scour initiated by a scour protection, as a scour protection will never stop scour but instead shifts it to where it will not endanger the stability of the foundation. Most processes that cause scour, as shown in Figure 2.3, are stopped with a scour protection. But a scour protection itself also causes scour at the edge of the protection, hence edge scour. Edge scour is found to be a function of the width of the berm and the diameter of the pile and the roughness of the berm (Petersen, Sumer, Bøgelund, et al. (2015) and Petersen, Sumer, Raaijmakers, & Schouten (2015)). Secondly, the height of the berm can be seen as the obstruction height to a flow to which it must adjust.

The importance of edge scour has two reasons; (1) It can cause free spanning of the cable running from the seabed onto the scour protection and in to the monopile and (2) cause instability of the scour protection. The free spanning of cables is mentioned before in section 2.2 and is not further discussed here. The instability of the scour protection can lead to failure of the protection, which in turns leads to scour that endangers the stability of the foundation. Edge scour is inevitable but can be mitigated. For a BFM is it of important that it can follow edge scour. This will stop edge scour and make the mattress more stable due to the more streamlined position. When this is not the case, sand is scoured from beneath the protection. This process is called undermining and is further explained in section 4.2.1. Secondly the mattress should be as thin as possible which reduces the scour induced by the protection. Other benefits because of a thin protection are explaned in section 2.7.

2.6 ARTICULATED CONCRETE BLOCK MATTRESS

Articulated concrete block mattresses (ACBMs) are often used as dike revetments or as bed protections for shipping channels. An ACBM consists of multiple concrete blocks tied together with a polypropylene rope. This

ensures a combined weight of all concrete blocks but keeping it flexible, see Figure 2.7. Many studies have been performed for the stability of ACBMs on a slope, where only some studies focussed on the stability of a ACBM on a river or seabed. Despite this, ACBMs are widely used as scour protection for offshore cables and structures, even though no real design guidelines exists (Godbold et al., 2014). As mentioned in the introduction of this chapter, the ACBM is similar to the BFM. Both using the total weight of the mattress and both have a certain resistance against bending/moving.

Figure 2.7: Articulated concrete block mattress (Siam Gabions, 2011)

For ACBMs the main failure mode is uplift of the edge of the mattress (Godbold et al. (2014) & Sonneville (2015)). When the hydrodynamic load becomes too large the leading edge of the mattress is lifted, allowing water to pass underneath it. Melville et al. (2006) found that the lifting of a single block would only go as far as the slack in the mattress would allow it. In other words, the adjacent blocks will stabilize the process. With an increase of the hydrodynamic load, the adjacent blocks are also lifted. This happens until a the drag force on the mattress reaches a critical value and the whole mattress is curled up and swept downstream. The process of lifting, curling and transportation downstream happens sequentially and sudden (Velzen & de Jong, 2015). Furthermore, the placements of ACBMs near structures are less stable due to the increase in hydraulic loads, i.e. turbulence (Godbold et al., 2014) which has been verified by the studies of Velzen & de Jong (2015) and Escarameia (1995).

2.7 Ballast filled mattress

2.7.1 Mattress by Airgroup-Industries

The mattress produced by Airgroup-Industries is a mattress made of polyester where the top and bottom are connected with so called 'spacer threads', see Figure 2.8. This mattress is currently used as gym tracks, tennis walls or sea rafts. For these applications the mattres is inflated with air, which requires the mattress to have a special airtight coating. The function of the spacer threads is to take up tensile forces when the mattress is trying to deform; the threads contribute to the stiffness of the mattress. The density of the spacer threads can be varied, with a maximum of about 50 000 threads/m^3 (Peters, 2017), but alterations in the pattern are possible.

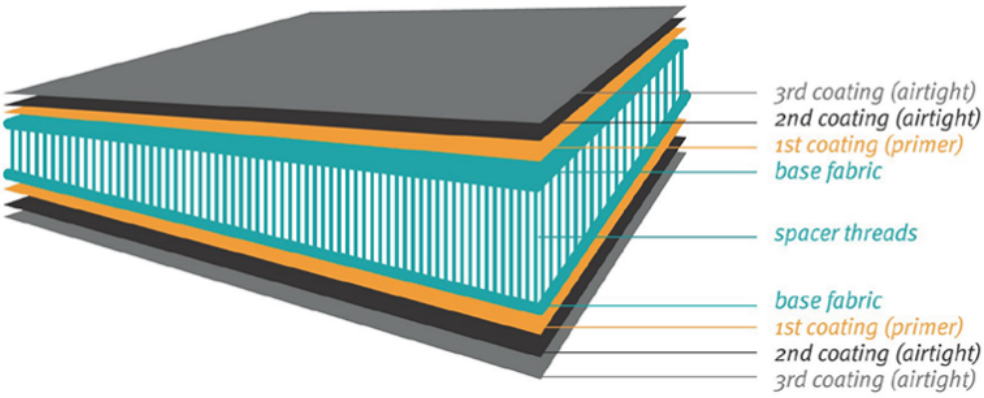

Figure 2.8: Double-wall mattress by Airgroup-Industries, source: Airgroup-industries

The stiffness of the mattress is highly dependent on the pressure in the mattress and the amount of spacer threats. When an overpressure is present in the mattress, left figure in Figure 2.9, the spacer threats are lengthened and contribute to the stiffness. An increasing pressure inside will increase the stiffness of the mattress more and more. It should be noted that this increase is two-fold. The stiffness increases due to the overpressure. Secondly, the spacer threats are lengthened further due to an increase in tensile force. This reduces their capacity to lengthen further under a tensile force. A stiff mattress is more resistant to uplift but more prone to undermining. When there is an under pressure within the mattress, right figure in Figure 2.9, the spacer threats will not experience a tensile force. When this is the case the stiffness of the mattress is determined by the filling material and the material of the mattress.

As mentioned in Chapter 1, the advantage of a ballast filled mattress is the combined weight which allows for a lower obstruction height. The thickness of the ballast filled mattress should be kept as small as possible to keep the advantages of a thin layer protection. This will results in less edge scour and secondary scour effects. Less secondary scour is in turn beneficial for the cable burial depth near the monopile. The maximum thickness that currently can be achieved by Airgroup-Industries is around $0.6m$ (Peters, 2017).

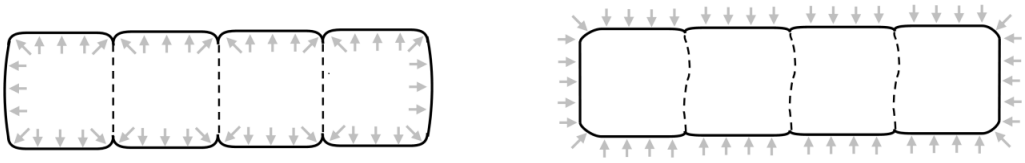

Figure 2.9: Left: mattress with overpressure, right: underpressure within the mattress

2.7.2 SELF-INSTALLABLE CONCEPT

The goal of Airgroup-industries is to compete, together with the self-installable system by SPT-offshore, with existing scour protections for offshore foundation with their ballast filled mattress. The system is designed for the SBJ but can in theory be applied to any foundation type with some changes. The self-installable system can provide a new scour protection for the SBJ that does not require a precise pre-laid rock protection and requires

less work operations to be placed. The self-installable system is shown in Figure 2.10 around a monopile.

The self-installable system is designed for the SBJ and during installation the system will automatically unfold. At a certain point the system will touch the seabed and the system will unhook. The protection will unfold automatically, analogous to opening an umbrella, and will provide protection around the suction cans. After the installation of the SBJ is the mattresses can be ballasted. The mechanism responsible for the unfolding of the protection is not further looked at in this research.

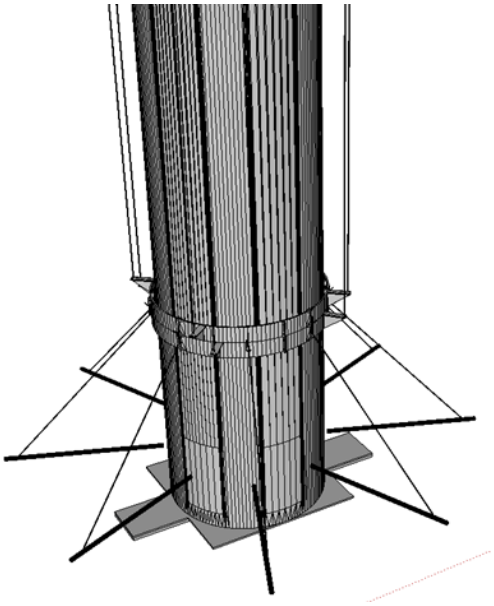

(a) Self-installable concept

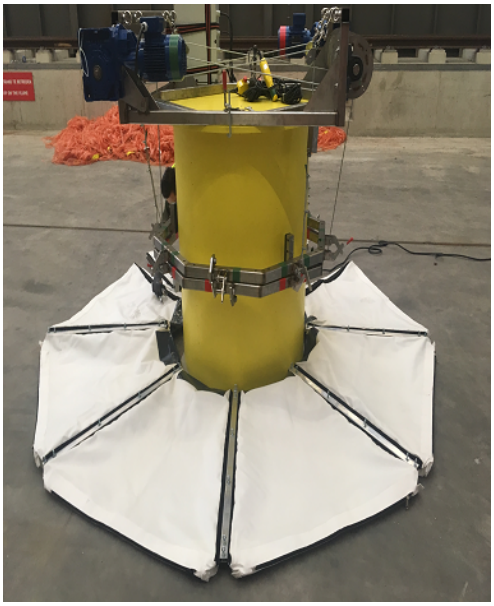

(b) Test system of the self-installable system

Figure 2.10: Self-installable concept SPT-offshore

2.7.3 BALLASTING MATERIALS

The ballasting of the mattress is crucial as mentioned section 2.7.1 . The mattress needs to be ballasted and, due to practical reasons, preferably with non-solids. A pre-ballasted mattress, with e.g. stones, will require a strong self-installable system. For this reason it is chosen to investigate on filling the mattress with a high density fluid. A fluid can be easily transported to the self-installable system and mattress by a pipeline once installed on site. However, the practical application of this is not further investigated in this research.

A high density fluid can be achieved with a drilling fluid. Drilling fluids are often referred to as water-based muds and consists of water and clay (bentonite or kaolin, the latter one is also referred to as china clay) together with other additives. The additives change the rheology of the mud such that they become, for example, more viscous. Secondly a weighting agent can be added that will increase the weight of the drilling fluid. Commonly used weighting agents are: barite and hematite. By adding the clay to the water, the clay expands and it creates a very viscous, gel like slurry that acts as a lubricant. This causes the slurry to have a higher sand carrying capacity with respect to normal water; the sand particles stay suspended within the mixture. The result of this is that higher densities can be achieved (Mastbergen, 2017). Mastbergen (2017) also did experiments at Deltares with a high-density fluid of approximately $2100 kg/m^3$ that is still pump able, Guo & Ma (2009) even formulates high-density drilling fluids up to 2.9 kg/m^3 that are still applicable as drilling fluids. Another interesting effect of drilling muds is that they are thrixorop. This means that after some time not being agitated,

the fluid becomes gel-like. The fluids becomes more stiff and viscous and will only start to flow when a certain shear stress is exceeded (Huisman, 1999). Lastly, by adding the clay a so-called *filter cake* is formed. The filter cake is formed at the wall of a drilling hole, or in this case the mattress, and prevents water from flowing out of the drilling hole/mattress (Glossary, 2017).

2.8 MOBILITY PARAMETERS

In order to set up an empirical design formula for the BFM under waves, different stability parameters are investigated. Parameters that include the forcing (drag,lift and inertia) are investigated, where the most commonly used stability parameters used (Shields) is not investigated further, where Shields focuses on stones and not bluff bodies.

2.8.1 MORISON AND MORISON-TYPE EQUATIONS

Morison estimated the forces on an object in an oscillating flow based on the velocities and accelerations. He did this by looking at the force exerted on a cylindrical pile in waves. According to Morison et al. (1950) the drag force, that is proportional to the square of the velocity, and the inertia force, proportional to the horizontal component of the acceleration, are the two components of the force. A Morison-type approach uses the same reasoning, namely the forces are approximated based on the velocities and accelerations. Instead of only an inline force; drag and inertia, a lift force is also generated by the obstruction of the object. This approach leads to the following Morison-type equations as used for the stability of subsea cables and pipelines (Godbold et al., 2014).

$$F_h = 0.5 C_d \rho_w u_w^2 A + \rho_w C_m V \frac{du}{dt} \tag{2.2}$$

$$F_L = 0.5 C_L \rho_w u^2 A^2 \tag{2.3}$$

in which:
- F_h = horizontal force
- F_L = lift force
- $C_{d/L}$ = drag/lift coefficient
- C_m = inertia coefficient
- ρ_w = volumetric weight of water
- A = surface area on which the force acts
- V = volume of the body
- u_w = orbital velocity
- $\frac{du}{dt}$ = horizontal acceleration

In order to apply the Morison-type equations, the coefficients C_d,C_w and C_L need to be known which in turn depend on the shape of the object. For specific types of structures there are several ways to determine this, e.g. subsea pipelines (Godbold et al., 2014), or the coefficients have already been determined. The latter is done for objects in a steady current. For objects placed in an oscillating flow, only research is done on the coefficients for subsea pipelines. The problem for oscillating flows is that the coefficients are not constant and change with the KC-number (Morison et al., 1950). Moreover it was also found that the lift force is highly dependent on flow history effects ,e.g. the wake formed due to the object (AS, 2010). This makes it hard to exactly predict the force with the morison-type equations.

To simply equations 2.2 and 2.3, they can be split up in two components.

1. Velocity forces: This includes the drag and lift force due to the horizontal velocity

2. Inertia force: The force due to the acceleration, which is directly linked to the pressure by Euler.

This makes it possible to combine the total force expression to:

$$F_t = 1/2 C_B \rho A u^2 + C_m \rho V \frac{du}{dt} \tag{2.4}$$

But can be further simplified to

$$F_t = \rho A u^2 + C_{all} \rho V \frac{du}{dt} \tag{2.5}$$

in which: F_t = total force
C_b = bulk coefficient for the forces due to horizontal velocity
C_{all} = proportionality coefficient between the velocity and acceleration force

Eq. 2.5 is the total force acting on an object where the response of the object is not yet incorporated in this formula. Keulegan & Carpenter (1958) found that the different coefficients depend on period parameter (also called the Keulegan-Carpenter number) and, as mentioned above, depend on the flow history around the object. For the BFM the uplift force due to the curvature can be neglected, this is only very locally and assumed to be insignificant. If a lift force is present, it is assumed this force is directly from pressure difference of the mattress and therefore assigned to the acceleration term.

2.8.2 RESISTING FORCE

There are a couple or resisting forces that try to resist the movement of any object. The first is the underwater weight of an object. The underwater weight of the stone is given in eq. 2.6.

$$W = (\rho_m - \rho_w) g V \tag{2.6}$$

in which: W = weight
ρ_m = volumetric weight object
ρ_w = volumetric weight water
g = gravitational acceleration
V = volume

Secondly the added mass. A moving object must also displace an amount of water in order to move. This is called added mass and contributes to the stability of an object. Added mass is often incorporated in the inertia term while it depends on the acceleration of the object. The resisting intertia term can be spit up in two terms according to (Dean & Dalrymple, 1991):

$$C_m = 1 + k_a \tag{2.7}$$

The k_a represent the added mass that depends on the shape of the object. Lamb (1945) showed that for an elliptical cylinder the added mass component can be described as $k_m = b/a$ (see Figure 2.11).

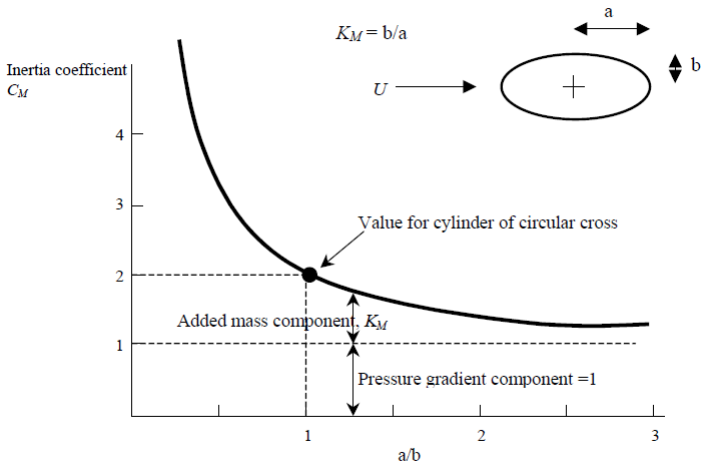

Figure 2.11: Inertia coefficient for a cylinder of ellipsoid cross section (Dean & Dalrymple, 1991)

When considering a small uplift of the BFM with the dimensions of one thickness, k_a is in the order of 1, however Figure 2.11 assumes flow around the object, which is not the case for the BFM. Lastly, Figure 2.11 assumes a streamlined object while the BFM is not. All in all it appears that C_m should be greater than unity.

2.8.3 MOBILITY PARAMETER

The Morison-type equations have a theoretical background but, as explained above, the coefficients need to be determined. The mobility paramater is a simplified form that does not show a physical background (van Gent & Wallast, 2001), but a similarity based on a balance in forces can be drawn. The drag and lift force, both proportional to u^2 in eq. 2.2 & 2.3, is seen as the forcing-parameter as shown in eq. 2.8. The mobility parameter does not take the inertia nor the coefficients in account.

$$\theta = \frac{u_{w,max}^2}{\Delta g d} \tag{2.8}$$

in which: θ = mobility parameter
$u_{w,max}$ = maximum orbital velocity
Δ = relative density
g = gravitational acceleration
d = stone diameter

θ gives the ratio between the drag/lift force and the resistance, given by the (underwater) weight of the stone. This is found by neglecting inertia and C_b and dividing eq. 2.4 by eq. 2.6.

For a ballast filled mattress, the stagnation pressure protruding below the mattress is also of importance. This is sometimes referred to as *hydraulic jacking* and is caused by a protuding object (Trojanwoski, 2006). The pressure due to the object is transferred below the object and causes a lift force. This force depends on u_w^2 and is shown further explained in Appendix A.

van Gent & Wallast (2001) compared eq. 2.8 against eq. 2.2 & 2.3 and found that the mobility parameter gives a remarkable better reult with respect to drag, however inertia was not included because of the small objects tested. The inertia force would be insignificant w.r.t. drag and lift. For the lifting failure mechanisms

the mobility parameter and morison-type equation performed the same, but due to simplicity the mobility parameter is preferred. It must be noted van Gent did his research on stone stability instead of bluff bodies.

2.8.4 SIMPLIFIED INERTIA TERM

As shown in eq. 2.2, the forcing is not only due to drag or lift ,but inertia also exerts a force. The inertia is proportional to the acceleration ($\frac{du}{dt}$) of a fluid which results in an inertia term that is out of phase with maximum drag and lift force for regular waves. The mobility parameter can be rewritten to express the inertia force as given in eq. 2.9. This is done the same way as for the mobility parameter regarding drag and lift.

$$\theta_i = \frac{a_{max}}{\Delta g} \tag{2.9}$$

in which: θ_i = mobility parameter for inertia
a_{max} = maximum acceleration
Δ = relative density
g = gravitational acceleration

How acceleration exerts a force is further explained in Appendix A.

2.8.5 COMBINATION OF DRAG AND INERTIA

For regular waves, the maximum velocity is out of phase with the maximum acceleration and vice versa. Still it is still possible that both forces occur simultaneously. To account for both forces, eq. 2.8 and 2.9 can be combined. This results in:

$$\theta_T = max(\frac{u^2 + ad}{\Delta g d}) \tag{2.10}$$

Eq. 2.10 is eq. 2.5, without the coefficient C_{all}, divided by the weight of the mattress given in eq. 2.6. Figure 2.12 shows that the occurrence of the maximum acceleration is just prior to the maxium velocity. It is assumed the maximum force occurs somewhere between the maximum acceleration and velocity.

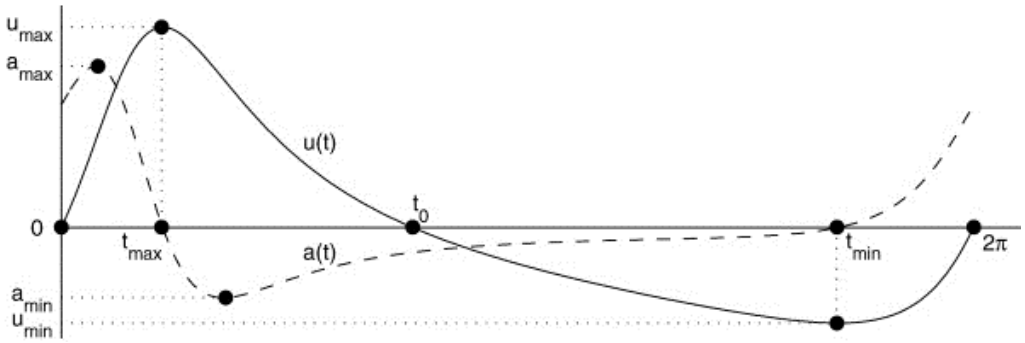

Figure 2.12: Maximum acceleration and velocity (Malarkey & Davies, 2012)

2.8.6 KEULEGAN-CARPENTER NUMBER

The Keulegan-Carpenter number has already been introduced in section 2.3 where it is used to express the formation of the lee-wake vortices. But Keulegan & Carpenter (1958) did research on forces on cylinders and plates and found that the KC number expresses the relative importance of drag over inertia. For higher KC

numbers the force that a body in waves experiences decrease. The drag will become dominant which results in a lower force.

The KC number can be found in eq. 2.1.

2.9 SCALING

To investigate offshore structures or scour protection, which typically have large dimensions and size, scale model tests are often performed. This is done by scaling the structure down to laboratory scale. To have a representative model and hydrodynamic conditions, it is required to scale the dimensions and flow parameters down in such a way that the relevant processes are the same as the prototype scale.

For hydraulic modelling non-dimensionless scaling laws give the relation between different force ratios to scale down specific processes correctly. Which scaling law to apply depends on the governing forces that need to be scaled down properly. For offshore and coastal engineering the Froude scaling law is often applied. This however has a side effect; using the Froude criterion, the Reynolds number will always be smaller in the model than for the prototype (Hughes, 1993). To keep this effect as small as possible, it must be assured that the Reynolds number is sufficiently high enough to be in the turbulent regime. For this research the Froude, Reynolds, Cauchy scaling laws and sediment mobility are important and are further explained below.

Froude scaling

The Froude number expresses the inertial force over the gravitational force. From Hughes (1993) it is found that for short wave models the Froude criterion can be used, where the fluid motions and velocity distribution is governed by inertia and gravitational effects.

$$Fr = \frac{u^2}{gL} \tag{2.11}$$

in which: Fr = Froude number
u = velocity
g = gravitational acceleration
L = characteristic length scale

The Froude criterion states that the Froude number in the prototype equals that of the model, when using full geometric scaling. From this and 2.11 it follows that length-parameters are scaled by λ and time and velocity parameters are scaled with $\lambda^{0.5}$.

Reynolds scaling

The Reynolds number expresses the inertia forces over the viscous forces. And as mentioned earlier, Froude scaling can be applied as long as the flow is sufficiently within the turbulent regime, $Re > 1 * 10^4$ (Hughes, 1993), while they cannot be satisfied simultaneously. This can be checked with eq. 2.12.

$$Re = \frac{\rho L u}{\mu} \tag{2.12}$$

in which: Re = reynolds number
ρ_w = density of water
u = velocity
μ = dynamic viscosity

Cauchy scaling

The Cauchy number is used when scaling down system that include bending stiffness and elasticity and is given by:

$$Ca = \frac{\rho u^2}{E} \tag{2.13}$$

in which: Ca = Cauchy number
ρ_w = density of water
u = velocity
E = Young's modulus

When scaling according to Froude, the E of the object or structure scales linearly with the scale factor, resulting in a to stiff scale model (Heller, 2011). For the prototype used in the scale tests, no elastic modulus is known.

2.9.1 SEDIMENT MOBILITY

When including sediment in a scale tests and focus on scour, froude scaling is not applicable anymore. Using Froude scaling, the sediment size will become to small and the sediment properties will change. E.g. particles smaller $< 62\mu m$ will behave as clay, changing the chemical properties of the sediment. Clay is cohesive and has a different erosion behaviour than sand (Hughes, 1993).

For physical model test, the smallest sediment grain diameter that can still be compacted and drained is about 110-130 µ m. The sand for prototype situations is said to have a median grain size of µm. When applying this with Froude scaling is becomes clear that this would only allow for very large scale factors ($\approx$ 1:2). In order to work with sediment mobility and smaller scale factors, the Froude-scaled hydrodynamic loading can be increased. By doing this, it is possible to achieve similar mobility in the model as field. The mobility is than expressed as relative mobility (MOB) and is defined as follows:

$$MOB = \frac{\Theta}{\Theta_c} \tag{2.14}$$

in which: MOB = relative mobility [-]
Θ = Shield parameter [-]
Θ_c = critical Shields parameter [-]

Equation 2.14 is called the mobility similarity criterion and is used to correctly scale sediment (but also rock) gradings to ensure similar mobility for physical testing and prototype scale.

3
SCALE MODEL TESTS

This chapter will present the different scale test campaigns done within the JIP-HaSPro. The different tests have been performed in the Scheldt Flume, Atlantic Basin and Delta Flume at Deltares. First the facility and the test set-up are introduced, followed by the scaling and possible scale factors. Lastly the scale model characteristics and test series are introduced. All of this is done per test campaign.

3.1 EXPERIMENTAL SET-UP SCHELDT FLUME

The first tests within the JIP-HaSPro are performed in the Eastern Scheldt Flume of Deltares. The goal of these tests is to determine the parameters that are of importance for the BFM under hydrodynamic loading around monopiles and on cables. This is done for different BFMs with different characteristics.

3.1.1 FLUME DESCRIPTION

The Eastern Scheldt flume is a 55 m long flume with a width of 1.0 m and a height of 1.2 m with glass walls. The flume is equipped with a piston-type wave generator with Active Reflection Compensation (ARC) technology. Furthermore the flume is capable of generating a current. Both fixed bed experiments and movable beds can be tested within the Eastern Scheldt Flume. Table 3.1 shows the technical specifications of the flume. For this test campaign a permeable wave spending slope is placed at the end of the flume. This will minimize the wave reflection while the current can still pass through. The slope can be adjusted manually to achieve maximum wave damping for different wave conditions.

3.1.2 GENERAL TEST SET-UP

Within this test campaign multiple innovative scour protections are tested for the JIP-HaSPro. The multiple innovative protections are tested throughout the flume simultaneously for different applications. In total three monopiles and two cable sections are placed in the flume, as shown in Figure 3.1. Pile 1 and 2 are used during the BFM tests around the monopile and cable section 2 is used for the cable protection tests. Each test section is placed 5 meters apart in order to ensure a recovered flow for the next test section. The obstruction by the monopiles should, by rule of thumb, be smaller than 1/6 of the total width of the flume according to Whitehouse (1998). This assumption was checked in the JIP-HaSPro by means of numerical modelling in OpenFOAM. The

Technical specifications Eatern Scheldt Flume		
Length	55.0	m
Width	1.0	m
Height	1.2	m
Maximum water level	1.0	m
Max. significant wave height	0.3	m
Max. regular wave height	0.4	m
Max. pumping capacity	0.6	m^3/s

Table 3.1: Technical specification Eastern Scheldt Flume

cable has a diameter of 0.03 m and is half buried in the seabed. The cable section does not cover the total width of the flume. This allows for testing different configurations at the end of the cable, see section 3.1.4. The bed of the flume is smooth compared to the sea bed. For this reason at both the monopile and cable section a roughness patch is glued to the flume bed. This represents the seabed and increases the friction between the bed and scour protection.

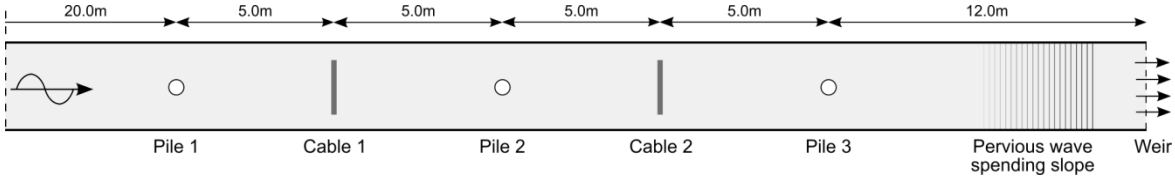

Figure 3.1: Eastern Scheldt Flume test set-up

3.1.3 MONOPILE SET-UP

To provide a continuous observation during the experiments, each section has multiple cameras. The monopile is a transparent pile with a diameter of 0.15 m. Within this pile a fisheye camera with a 360°-view is placed that records at frame rate of 8 Hz. Outside the flume a normal camera is placed that records at 5 Hz.

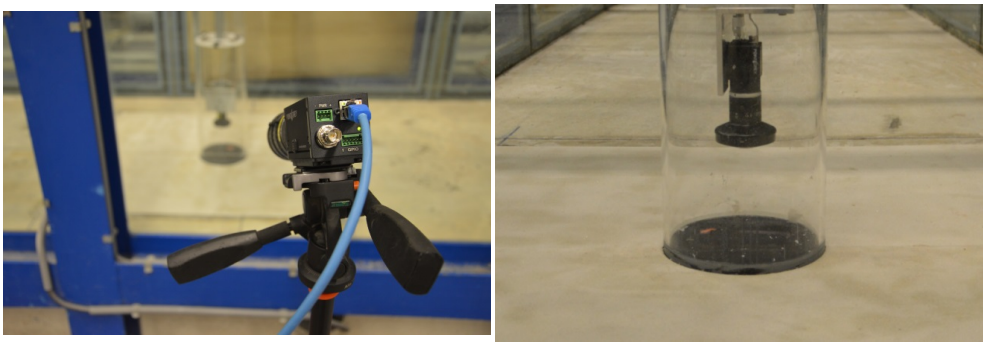

Figure 3.2: External camera (L) and internal camera (R)

The BFM is made up of two half circles that are placed around the monopile, each with a diameter of 0.15m. The two halves are not joined together. A wave height meter (WHM) and electronic current velocity meter

(EMS) are placed approximately 2.10 m in front the monopile to record the undisturbed signal, both recording at 20 Hz. During the tests three different types of flexibility of the mattresses are tested, each with two different weight/thickness ratio. The different types of mattresses are further described in chapter 3.1.5; Figure 3.3 shows the monopile test setup with a flexible mattress shown in the picture.

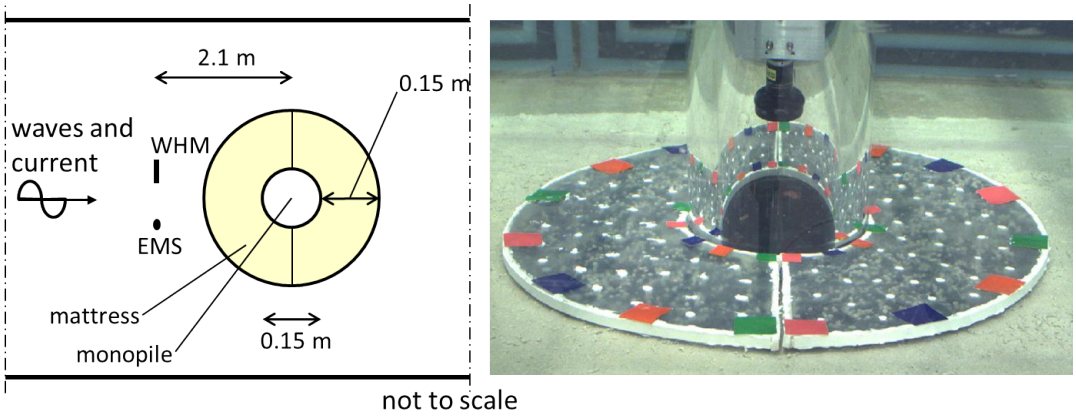

Figure 3.3: Eastern Scheldt Flume test set-up. Left figure shows a schematised top view of the monopile test set-up in the Eastern Scheldt Flume (not to scale); (right) photo of monopile set-up with a light flexible ballast filled mattress, looking perpendicular to the flow.

3.1.4 CABLE SECTION SET-UP

At the cable section only an external camera (5Hz) is placed for continuous observations. Like the monopile section, the WHM and EMS are placed approximately 2.10 m in front of the section. Only one type of mattress is tested with two different weights/thickness ratio. In total three different configurations of mattress position are tested, Figure 3.4 shows one layout. The remaining two layouts can be found in Appendix B.1.1.

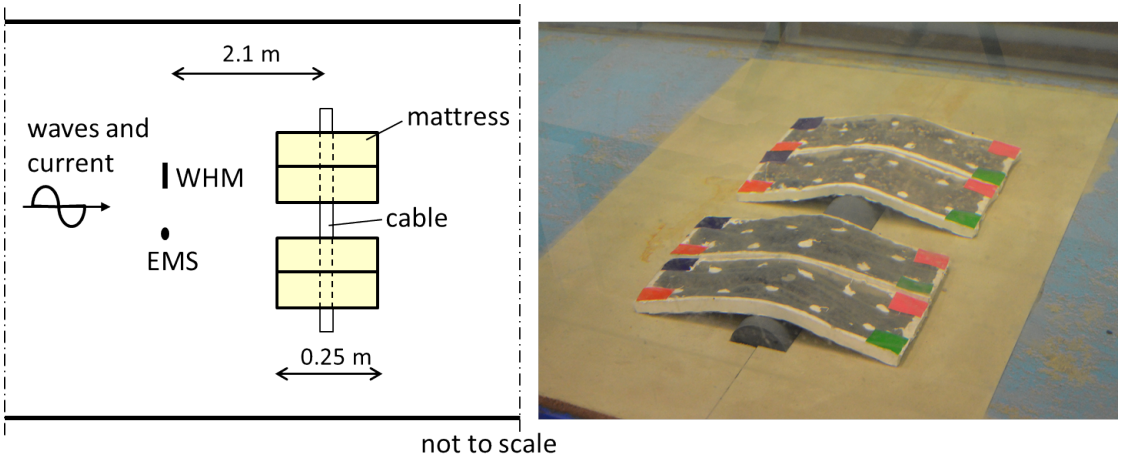

Figure 3.4: Eastern Scheldt Flume test set-up. Left figure shows a schematised top view of the cable test setup (layout one) in the Eastern Scheldt Flume (not to scale); (right) photo of cable test set-up (layout 3) with both the light and heavy flexible ballast filled mattress.

3.1.5 SCALE MODEL CHARACTERISTICS

The mattresses used during the Scheldt Flume campaign are made inhouse by Deltares. The 'frame' of the mattress is made of rubber on which sheets of another type of rubber is glued. The mattress is filled and globally spacer threads are mimicked, see the right picture in Figure 3.3.

The mattresses tested in the Scheldt Flume have different characteristics as mentioned in section 3.1.3, also they differ for the monopile and cable section. For the monopile three types of flexibility are tested and for each flexibility it has two different weight/thickness ratios. For the cable section only a flexible mattress is tested with two different weight/thickness ratios. The characteristics can be found in Table 3.2 & 3.3.

Flexibility [-]	Filling	Thickness [m]	Weight [kg]	Volume [m^3]	Δ [-]
Flexible	60% stones 40% pvc	0.0106	0.8842/0.8421	0.0014985	0.2669
Flexible	100% stones	0.0126	1.2592/1.2519	0.0017813	0.3705
Medium-flexible	60% stones 40%pvc	0.011	1.0038/0.8523	0.0007775	0.3215/ 0.27
Medium-flexible	100% stones	0.013	1.361/1.363	0.0018378	0.4135
Stiff	100% stones	0.012	1.0647/1.072	0.0016965	0.3065
Stiff	100% stones	0.014	1.4242/1.4269	0.0019792	0.3940

Table 3.2: Mattress characteristics for the monopile section, Scheldt Flume

Flexibility [-]	Filling	Thickness [m]	Weight [kg]	Volume [m^3]	Δ [-]
Flexible	60% stones 40% pvc	0.0106	0.349/0.3493	0.000265	0.6037
Flexible	100% stones	0.0126	0.4695/0.4722	0.00315	0.8253

Table 3.3: Mattress characteristics for the cable section, Scheldt Flume

The length of the cable mattresses is 0.25 m and the width is 0.10 m.

In both Tables 3.2 & 3.3 two weights are given. For the monopile the mattress consists of two halves and for the cable section two mattresses of each filling are tested. The weights are thus given for each half/mattress. The Δ is corresponding to the lightest half/mattress. From Table 3.2 and 3.3 it can be seen that Δ differs significantly between the monopile mattresses and cable mattresses. This is explained by the filling, already explained in the previous section, which is done significantly better for the cable mattresses than for the monopile mattresses.

3.1.6 SCALING

No prototype yet exists of the BFM and for this reason the mattress is not scaled down according to a scale factor but instead the hydrodynamic conditions are scaled down according to Froude scaling in such a way that they represent a wide range of typical North Sea conditions.

3.1.7 Limitiations of the Scheldt Flume

In order to minimize the scale effects the scale factor must be chosen as small as possible. Unfortunately every test has its limitations induced by the testing facility. For the Scheldt flume the limitations consist of the water depth, width and the wave generator. But as mentioned in section 3.1.2, the diameter of the monopile is limited to 1/6 of the width of the flume. This leads to a pile diameter of 0.15 m, which is the starting point of selecting hydrodynamic conditions, using Froude scaling.

3.1.8 Hydrodynamic scaling

For the Scheldt Flume campaign the monopile diameter range from 6 to 10 m is considered. This leads to a scale factor of:

$$\lambda = \frac{6-10}{0.15} = 40-65 \tag{3.1}$$

To represent offshore conditions of the North Sea, different hydrodynamic conditions are chosen that stay within the range of wave conditions and such that the Reynolds number is large enough. The range of hydraulic conditions tested during the Eastern Scheldt Flume campaign can be found in Table 3.4 below.

Hydrodynamic conditions Eastern Scheldt Flume campaign						
	D [m]	h_w [m]	H_s [m]	T_p [s]	u_w [m/s]	KC [-]
Min.	6	15	6	11	1	1
Max.	10	40	12	18	3	9

Table 3.4: Hydrodynamic conditions testing range

As mentioned earlier the purpose of the small scale tests performed in the Eastern Scheldt Flume is to explore the stability behaviour and the main failure mechanisms of the ballast filled mattress. These can serve as a first input to preparing design for BFM's that can be applied in the field. Hence, the parameters must therefore be translated back to a prototype case.

3.1.9 Scale effects and model effects

Scale effects

As mentioned in section 2.9 complete similarity between model scale and reality is not possible for a model scale factor being larger than 1, consequently scale effects are introduced. Scale effects can lead to differences in behaviour.

By applying Froude scaling, that assumes gravity as the dominant force, the other forces like viscosity, elasticity, surface tension etc. are scaled incorrectly (Hughes, 1993) and initiate scale effects. However, the scale effects due to this are negligible for waves but for the flexibility of the mattress are not.

The material of which the models is made can be smoother or less smooth than that of the prototype. This will under- or overestimate the shear force on the mattress. But the influence of the shear force is assumed to be small compared to the uplift force, it will not have a large influence on the outcome of the test but should be kept in mind while analyzing.

Model effects

Instead of hydrodynamic scale effects, the use of a model or the test layout also initiates unforeseen effects. By applying multiple test sections within the flume, interference from an earlier test section is possible in the next section. Secondly, the mattress is made up of two halves which are not joined together. The loose connection at the transverse side of the pile can influence the stability. This can be the case when multiple tests are performed one after another. A slight movement can cause the mattress to move and a front of the mattress is exposed. The hydraulic loads at the transverse side increase due to the acceleration and with less combined weight this could lead to an earlier failure of the mattress.

The different configurations tested at the cable section do not cover the whole cable. As shown in Figure 3.4, there are big gaps between the mattresses. Furthermore the wave can easily travel below the BFM due to the open sides. This can increase the stability of the mattresses while the pressure differences can be smaller.

Doing tests with waves in a wave flume will give rise to a return current. The continuity equation requires a zero net transport otherwise the water would pile up against the end of the wave flume. In order to balance the mass due to the wave, a return current is initiated. This return current effects the velocity measurement by the EMS (Bosboom & Stive, 2011). Furthermore, as metioned in section 3.1.2 artificial roughness is applied at the test sections. The bottom friction might be different than in a real life situation.

The spacer threads inside the BFM are mimicked by applying a connection between the top and bottom rubber sheets. This can be seen in the picture of Figure 3.3 and 3.4. The applied connection is different than that of the prototype shown in Figure 2.8. The spacer threads are mimicked with rubber and is more elastic than a polyester thread on prototype scale. For this scale it is unknown how these relate. Lastly, the filling of the mattresses has only been done partly and the ballast material is able to move freely throughout the mattress, which may not be representative for the prototype case, depending on which type of filling material or fluid is chosen. Figure 3.5 shows the degree of filling of the mattress, in this case the light flexible monopile mattress.

Figure 3.5: Photo showing the partly filled flexible ballast filled mattress

3.1.10 Test Series

Within the test series multiple hydrodynamic conditions are tested, see Table 3.4, but as mentioned in chapter 1.3, this research focuses on the stability of the BFM under waves. For this reason Table 3.5 shows the range of tested conditions for waves imposed by the wave board. For the full test series, see Appendix B.

Mattress	Water depth [m]	waves	wave height [m]	Wave period [s]	No. of test
Flexible, monopile	0.45 - 0.75	regular	0.1 - 0.35	1.1 - 2.6	31
Medium-flexible, monopile	0.45 - 0.75	regular	0.1 - 0.35	1.6 - 2.9	63
Stiff, monopile	0.45 - 0.75	regular	0.2 - 0.35	2.0 - 3.2	24
Flexible, cable	0.45 - 0.75	regular	0.15 - 0.35	1.6 - 2.9	76

Table 3.5: Range of hydrodynamic conditions per mattress

For each test a different range was tested and the amount of tests differ. Due to weight difference of the medium-flexible mattress (60% rock, 40% pvc) as seen in Table 3.2, 23 tests that included this mattress provide 23 extra data points due to this difference.

3.2 Experimental set-up Atlantic Basin

The second test series within the JIP-Haspro is performed in the Atlantic Basin at Deltares. The aim of these tests is to look at the ability of the protection to mitigate scour and their performance with respect on following edge scour.

3.2.1 Flume description

The Atlantic Basin is a 75 m long, 8.7 m wide and 1.3 m high basin. The basin is equipped with a cradle type wave generator, consisting of 20 individually controlled wave paddles. Each paddle is equipped with ARC to damp out reflected wave energy. The basin is also capable of generating a current in both directions to simulate the tide. Furthermore, the Atlantic Basin consists of a mobile bed section which allows for testing morphological and scour related cases. Table 3.6 show the technical specifications of the Atlantic Basin.

Technical specifications Eatern Scheldt Flume		
Length	75.0	m
Height	1.3	m
Maximum water level	1.0	m
Max. significant wave height	0.25	m
Max. regular wave height	0.45	m
Max. pumping capacity	3.0	m^3/s

Table 3.6: Technical specifications Atlantic Basin

3.2.2 General test set-up

During the Atlantic Basin campaign two cases for the BFM are tested ; around a monopile and for the SBJ. No cable protection is tested in the Atlantic Basin for the BFM. First the general test set-up of the Atlantic Basin is explained after which the specific cases are presented.

Both tests are placed on a test section that is shown in Figure 3.6 that consists of a mobile bed ($D_{50} = 170\mu m$). This figure also shows the general layout of the Atlantic Basin.

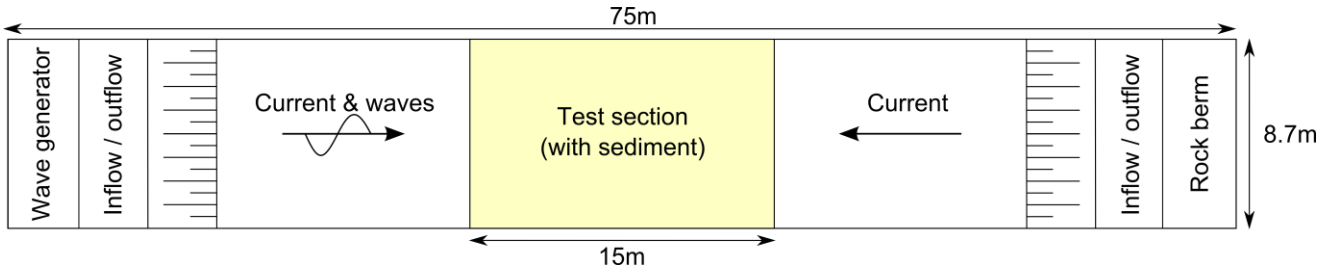

Figure 3.6: General layout Atlantic Basin

3.2.3 MONOPILE TEST SET-UP

During the monopile test-series, four monopiles are placed adjacent to each other which allows for testing multiple scour protections. To prevent any disturbance from the adjacent piles, the maximum pile diameter is chosen to be 200 mm, for a specific type of scour protection the pile diameter is chosen as 300 mm. The test test set-up of the monopile test series is shown in Figure 3.7.

Similarly to the Scheldt Flume campaign the monopile is transparent and equipped with a 360°-view camera. An underwater camera is placed downstream of the piles to provide a continuous observation, both camera system are previously explained in section 3.1.3. The WHM and EMS are placed 3.0 m in front of the test section and in between the piles a GRSM (WHM and EMS in one) or WHM is placed. Furthermore behind the test set-up a WHM is placed.

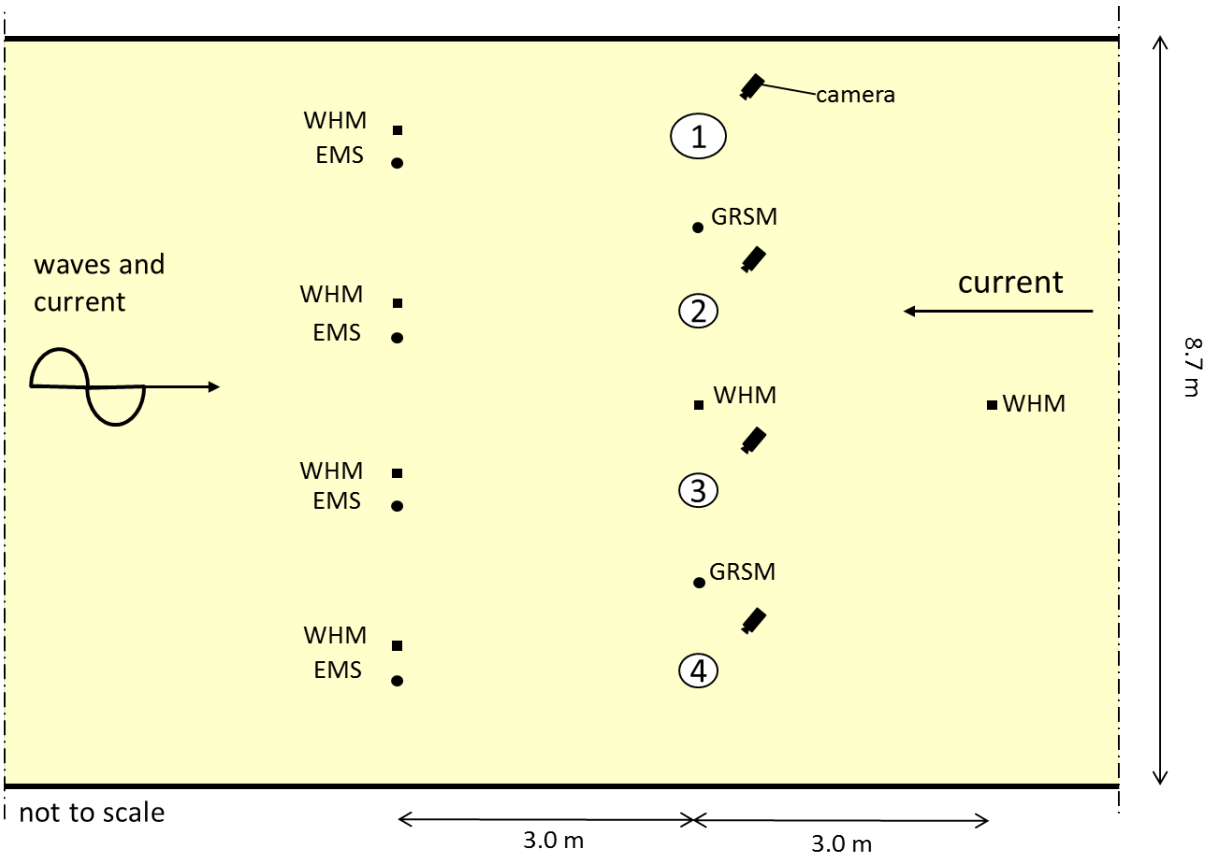

Figure 3.7: Test set-up for the monopiles zoomed in on the test section in the Atlantic Basin

The BFM is placed around pile 4 and is similar to the mattresses used in the Scheldt Flume. However, one continuous mattress is used instead of two halves, see Figure 3.8. The white dots on the mattress are to resemble the spacer threads, as explained in section 3.1.9.

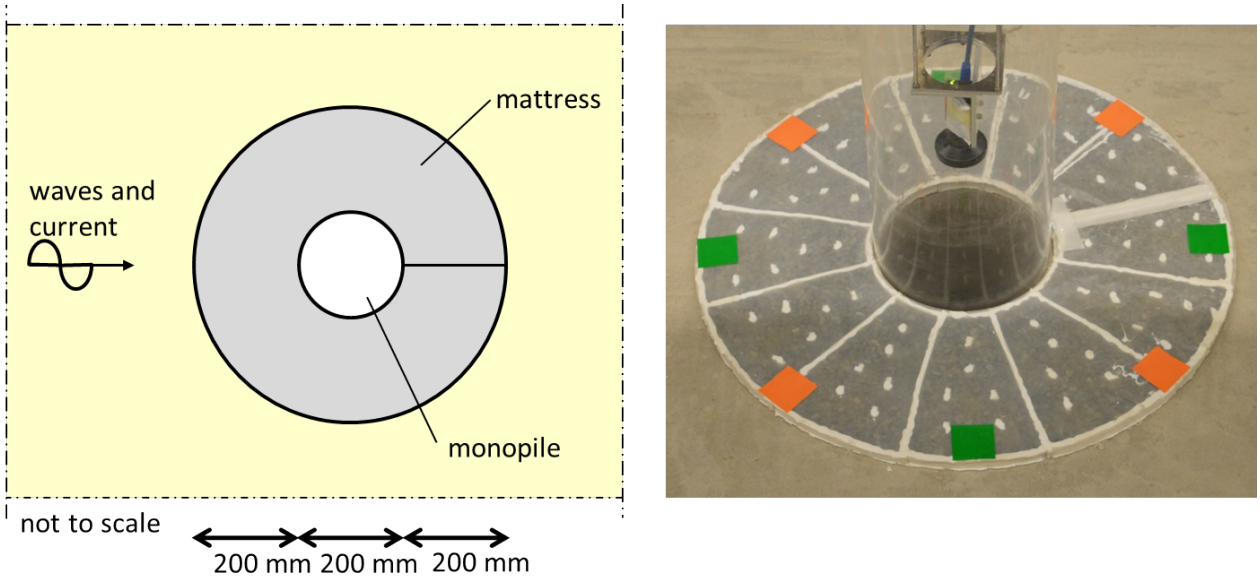

Figure 3.8: Atlantic Basin monopile test set-up. Left figure shows a schematised top view of the monopile test set-up in the Atlantic Basin (not to scale); (right) photo of monopile set-up with a ballast filled mattress.

3.2.4 SUCTION BUCKET JACKET TEST SET-UP

An additional scope was done for SBJs. Two SBJs are placed 2.1 m from the wall and in between a cable section is placed. The aim of the test is the same as for the monopile tests. The buckets have a diameter of 300 mm and are again transparent with a 360°-view camera. On both sides of the SBJ an underwater camera is placed that records at 5 Hz. For the general layout see Figure 3.9. The WHM and EMS are again placed 3.0 m in front of the SBJ and one WHM is placed 3.0 m behind the SBJ. Furthermore, above the cable section a WHM and EMS is placed, both recording at 20 Hz.

During this test series two different mattresses are tested around the SBJ: the flexible and medium-flexible mattress. The mattresses have a radial extent of of 225 mm. See Figure 3.10 for the layout of the SBJ.

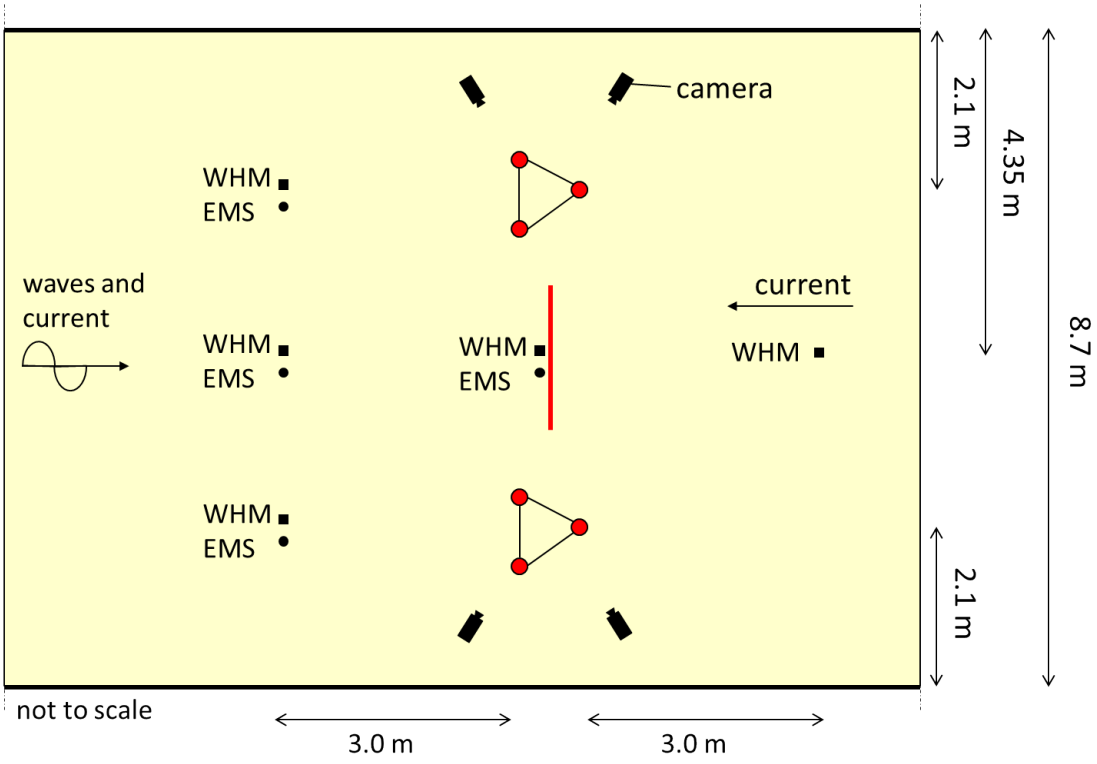

Figure 3.9: Test set-up for the SBJ zoomed in on the test section in the Atlantic Basin

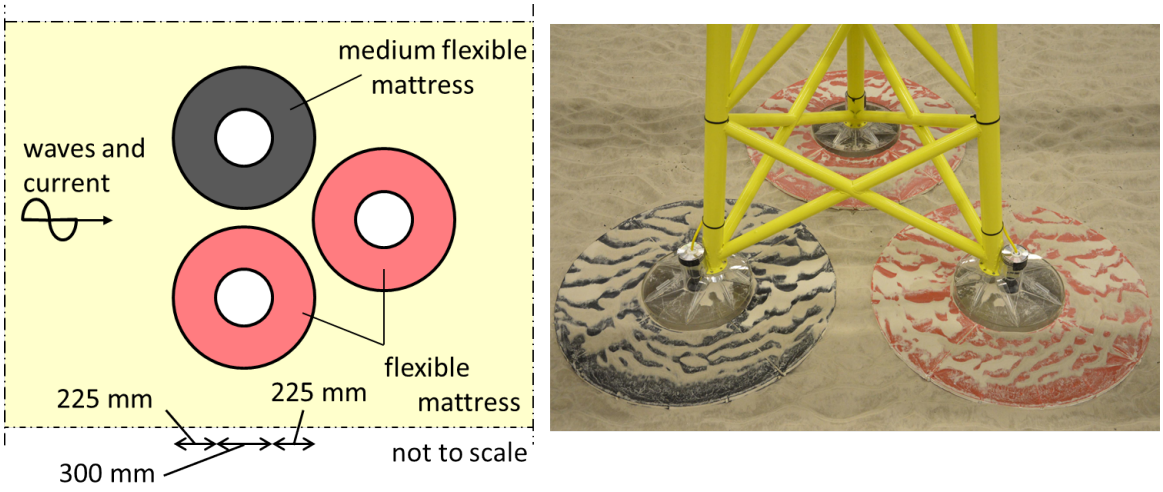

Figure 3.10: Atlantic Basin SBJ test set-up. Left figure shows a schematised top view of the SBJ test set-up in the Atlantic Basin (not to scale); (right) photo of SBJ set-up with a two types of ballast filled mattress. The black mattress is the medium-flexible mattress, red the flexible ballast filled mattress.

3.2.5 SCALE MODEL CHARACTERISTICS

The focus of the Atlantic Basin test was scour mitigation and edge scour following abilities and not on the stability of the mattresses. Therefore, mattress weights were selected that were expected to be hydraulically stable. Indeed, no movement or failure was observed during the test series. For this reason the tests performed in the Atlantic Basin have not been used in the stability analysis.

As mentioned in section 3.2 the diameter of the monopile test differed from the suction bucket, as a result the weight of the different mattresses also differed. For the SBJ, the weight difference was little. The flexible mattress weighing 7.56kg and the medium-flexible weighing 7.60kg.

3.2.6 SCALING

3.2.7 HYDRODYNAMIC SCALING

The focus of the Atlantic Basin test campaign is on scour, therefore the processes of scour must be represented correctly. For this reason, the full hydrodynamic conditions as explained in section 3.1.8 are not achieved. The scale of the Atlantic Basin test is approximately 25-40.

3.2.8 SCALE AND MODEL EFFECTS

Scale effects

The scale effects discussed in section 3.1.9 with respect to the mattress are also relevant for the Atlantic Basin, because a similar mattress is used. In contrast to the Scheldt Flume, the sediment availability in the Atlantic Basin gives rise to scale effects.

Due to the the incorrect scaling of sediment some phenomena are not represented correctly. An example is the formation of small ripples due to wave action on the seabed. This does not represent a correctly scaled morphological feature but is in fact a scale effect. The ripples are assumed not to have an effect on the stability of the protection. But can influence the scour around the protection.

Model effects

The cameras for the monopile series are placed downstream of the monopile. In tidal conditions however the flow is directed from both the upstream and downstream side. When the flow is directed from downstream, which is the case for the ebb-tide, the cameras disturb the flow. However, the cameras are placed at some distance behind the pile and not on the same line, limiting the effects of this disturbance.

Similarly to the Scheldt Flume, the filling of the mattresses tested in the Atlantic Basin is only done partly, but significantly better than for the mattresses of the Scheldt Flume. The degree of filling if important for the stiffness. For a prototype case it is considered to fill the mattress with particles and water; the water might drain out at some point, as long as the weight of the remaining particles is still sufficient, the mattress will be stable. But for a first filling of the mattress the degree of filling is assumed to be such that it has a certain stiffness. Where the Atlantic basin focus lies on scour mitigation and the ability to follow scour, this could influence the ability of the mattress to follow the scour; the mattress could be too flexible due to an incomplete filling. However, is could be that this incomplete filling relates to the goal of the prototype.

3.2.9 TEST SERIES

Contrary to the Scheldt Flume tests, the Atlantic Basin tests series consisted of a sequence of increasing hydrodynamic conditions to simulate different North Sea storms. Only for the monopile, one series of regular

waves was tested. The test series of the Atlantic basin tests for the monopile and SBJ can be found in Appendix B.2.1.

3.3 Experimental set-up Delta Flume

The last test series within the JIP-Haspro is done in the Delta Flume at Deltares. The objective of the Delta Flume test series is to verify the results obtained from the Scheldt Flume and Atlantic Basin test. For the latter two the test series were performed at a small scale and are prone to scale effects as explained in section 3.1.6 and 3.2.6. The Delta Flume tests will give the opportunity to test at a large scale, eliminating the scale effects.

Due to geometrical and technical constrictions of the Delta Flume, wave-only tests are performed and the tests are again aimed at the stability under waves.

3.3.1 Flume description

The Delta Flume is a 300 m long, 5.0 m wide and 9.5 m deep wave flume that makes it the largest wave flume in the world to date. At the beginning of the flume there is a 10 m high piston-type wave board that is driven by 4 pistons and equipped with ARC. At the end of the flume there is a fixed rubble mound structure for wave damping. But for this test campaign only 200m of the flume is used and a concrete slope is placed at the end. The full technical specifications of the Delta Flume can be found in Table 3.7.

Technical specifications Delta Flume		
Length	300	m
Width	5.0	m
Height	9.5	m
Max. significant wave height	2.2	m
Max. regular wave height	3.3	m

Table 3.7: Technical specifications Delta Flume

3.3.2 Test set-up

In the Delta Flume the BFM is tested around a monopile and as a cable protection. This is done simultaneously throughout the flume. The general lay-out of the Delta Flume test is shown in Figure 3.11.

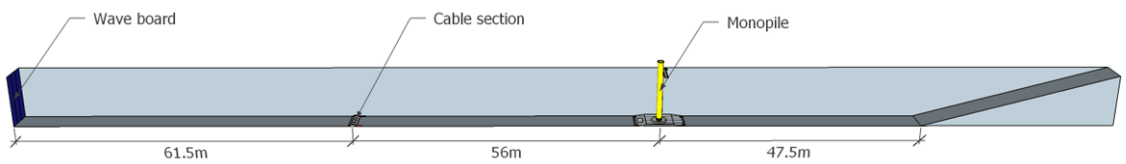

Figure 3.11: General layout Delta Flume

3.3.3 MONOPILE TEST SET-UP

The monopile used in the Delta Flume has a diameter of 1.02 m and is placed on an elevated section of 25 m^2 with a height of 0.3 m above the flume bottom. The elevation is placed at a distance of 127.5 m from the wave board. The diameter makes the monopile bigger than 1/6 of the flume width as previously mentioned in section 3.1.2. This has been verified by an OpenFOAM model and showed that this did not lead to a significant influence of the wall. Around the monopile a sand bed is placed that extends 1.02 m from the pile. The purpose of the sand pit is to check the protections with their mitigation ability against winnowing. Note that these tests are therefore carried out in a clear water regime (instead of a live bed regime), which results in a conservative setup for testing winnowing.

Throughout the Delta Flume WHMs are fixed to the flume wall. On the elevated section 2 EMSs are fixed to record the orbital velocities, all recording at 20 Hz. Four underwater cameras are placed around the monopile to provide a continuous observation. Lastly, the monopile is equipped with transparent windows at the bottom for an internal camera to provide continuous observation throughout the tests. The frame rate of the cameras can be adjusted to have a higher frame rate during the tests when higher waves are incoming. Figure 3.12 shows the lay-out.

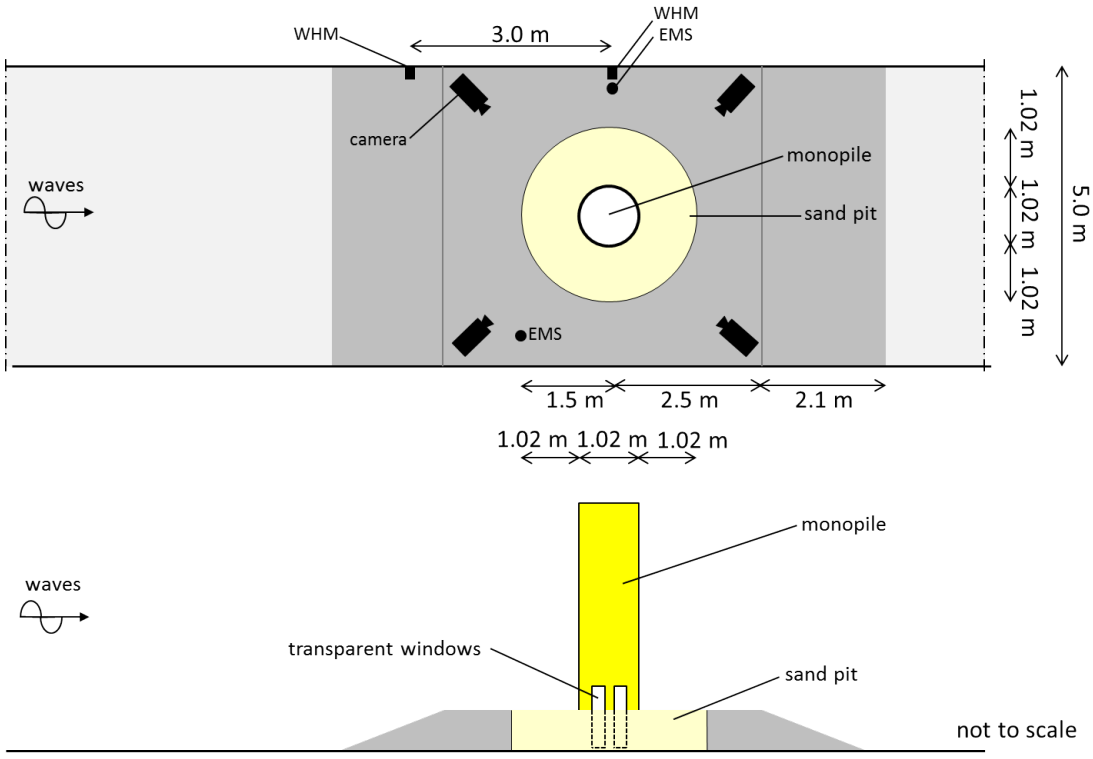

Figure 3.12: Delta Flume monopile test set-up. Top figure showing a schematised top view of the Delta Flume monopile test set-up. Bottom figure showing a schematised side view of the Delta Flume monopile test set-up

The BFMs that are tested in the Delta Flume are different than the BFM tested in the Scheldt Flume and Atlantic Basin. The BFMs used are made by Airgroup-Industries and made from the same material as the gym tracks explained in section 2.7, thus with the real spacer threads and an air-tight coating. During the Delta Flume tests two test configurations are tested. The first test series consists of 8 separate parts placed around the monopile which is shown in the left photograph in Figure 3.13. The second configuration is done with the same mattresses

but with a connection between the mattresses using aluminium bars as shown in the right photograph in Figure 3.13 . The latter is done to test the importance of the combined weight and to represent a BFM-system that is self-installable. In order to prevent winnowing from occurring the sand bed around is modified to prevent winnowing as much as possible, because this is not the aim of the BFM tests. This was achieved by placing a small scour protection at the interface of the monopile. This scour protection against winnowing did not interfere with the mattress.

Figure 3.13: Left figure showing loose BFMs around the monopile, right showing the connected BFMs around the monopile

3.3.4 CABLE SECTION TEST LAY-OUT

The cable section is placed 61.5 m from the wave board and 4 BFMs are placed over a cable with a diameter of 50 mm. The BFMs used at the test section are the same shape as the mattresses around the monopile, but slightly smaller. A WHM is present just downstream of the cable and underneath an EMS is placed. Another EMS is placed at the same position but on the opposite wall. Furthermore, there is a fixed WHM 11.0 meter in front of the cable section with again two EMSs, one directly beneath the WHM and the other on the opposite side of the wall, see Figure 3.14.

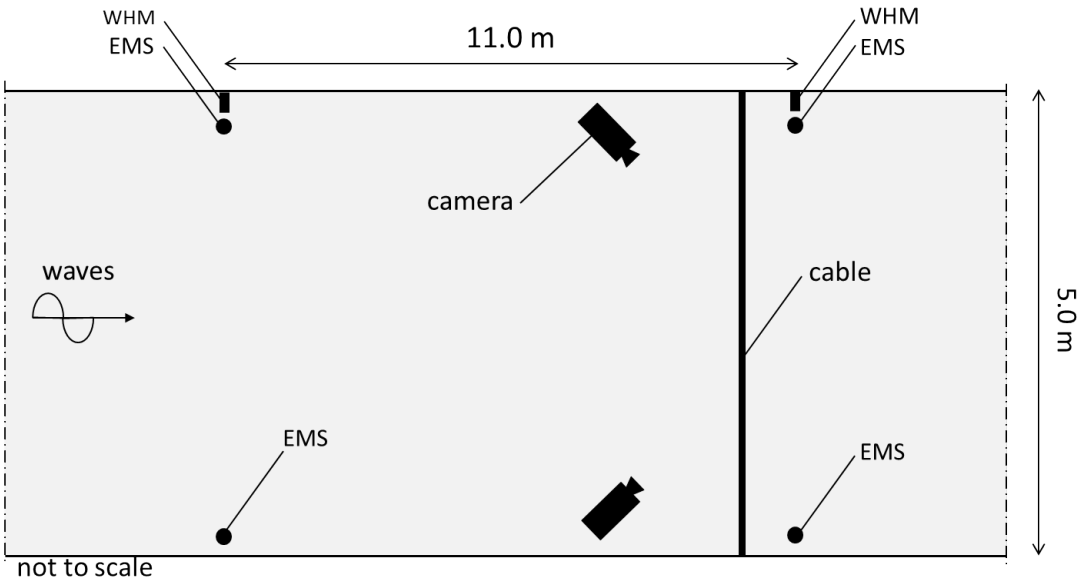

Figure 3.14: Schematised top view of the Delta Flume cable test set-up (not to scale)

The BFMs used at the cable section are filled with the same material as the BFMs around the monopile, this is further explained in section 3.3.5. During the test series, 2 different orientations are tested, as shown in Figure 3.15. Below the cable section a sheet of geotextile is fixed to the flume bottom to obtain a more realistic friction between the mattress and the bottom of the flume. The geotextile will increase the roughness of the bed, as the flume bottom is very smooth. Lastly, two different weights are tested for the cable section; this is also shown in the figure below and indicated with the different colours.

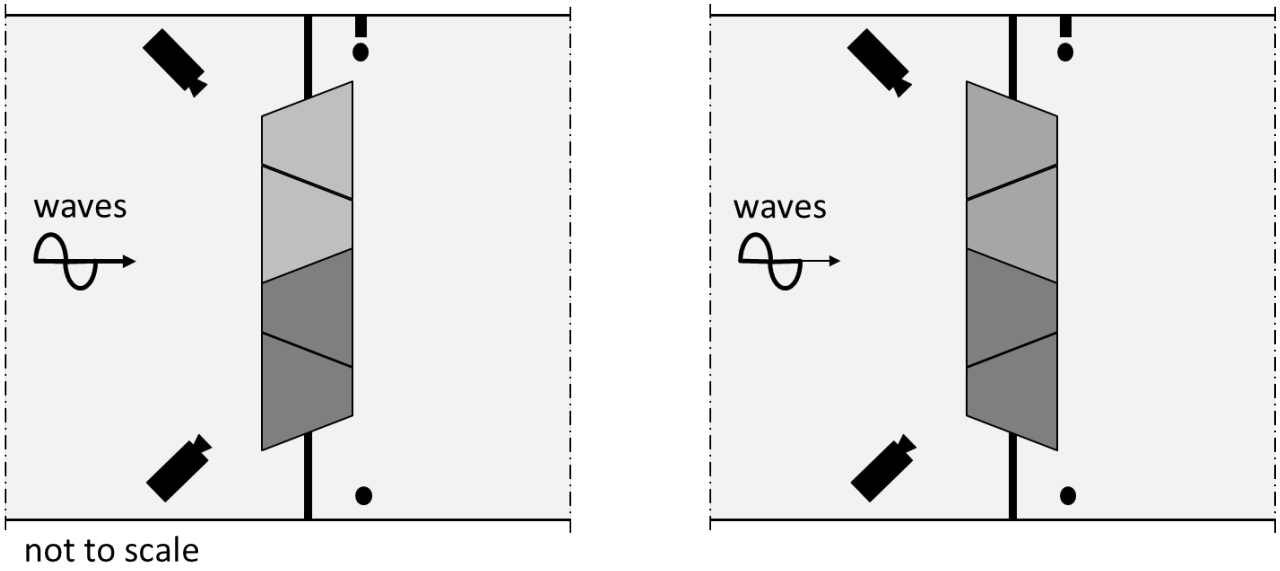

Figure 3.15: Zoomed in schematised top view of the Delta Flume cable test section. The light coloured mattresses indicating the heavy cable mattress, the dark coloured mattresses indicating the light cable mattresses.

3.3.5 SCALE MODEL CHARACTERISTICS

The mattresses used in the Delta Flume are made of the same material as the prototype mattress will be, thus as shown in Figure 2.8, only the spacer thread configuration is different. The spacer threads are bundled in groups with a distance of 0.14 m in both directions as shown in Figure 3.16. Figure 3.17 show the dimensions of the tested mattresses for the monopile and cable, the height of both mattresses is approximately 0.12 m. All dimensions shown below should be interpreted with care. The exact dimensions are hard to measure due to the shape and the sagging of the mattress.

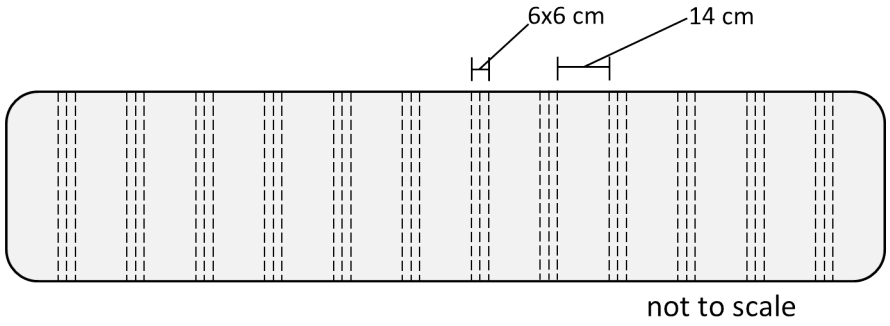

Figure 3.16: Delta Flume spacer thread configuration

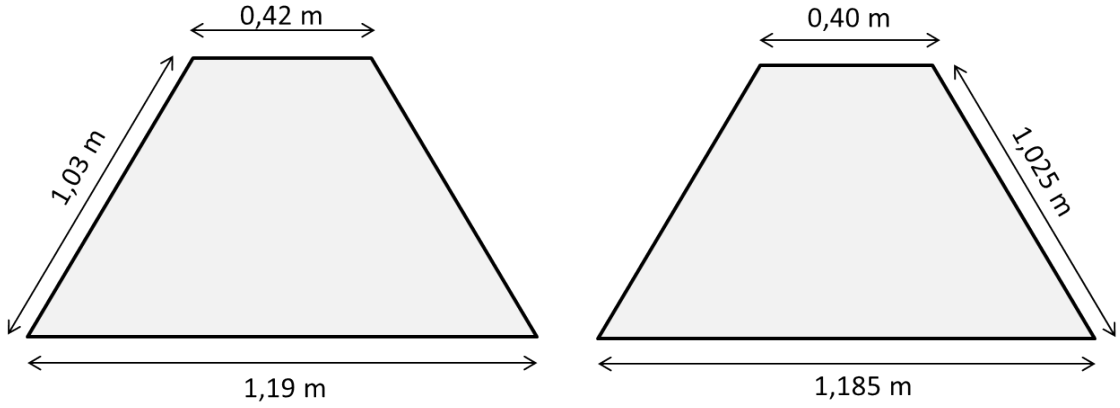

Figure 3.17: Dimension of the Delta Flume mattresses, (L) monopile mattress (R) cable mattress

The mattress is ballasted with 2-5 mm rock together with rubber granulate. The rubber is used as filling material where the amount of rock put in the mattress is not enough to fill the whole mattress. The other reason is to obtain the right weight of the mattress. And also to be able to compare when using ballast fluids, which are typically lighter. The density of the rock that was used is $\approx 2600\ kg/m^3$ and the rubber had a density of $\approx 1.02\ kg/m^3$. The characteristics of the models can be found in Table 3.8.

Test section	Weight [kg]	Submerged weight [kg]	Volume $[m^3$	Δ [-]
Monopile	91.98-92.16	39 (+/- 0.5)	0.094	0.4159
Cable	88.43	33 (+/- 0.5)	0.090	0.3834
Cable	80.81 & 81.41	26 (+/- 0.5)	0.090	0.2884

Table 3.8: Delta Flume mattress characteristics

3.3.6 SCALING

Scaling is again done similarly to the Scheldt Flume; for the BFM there is no specific scale and the required weight is estimated with help of the previous test on gabions. The hydrodynamics are again scaled with Froude scaling.

Hydrodynamic scaling

The scale factor of the Delta Flume can be found by applying eq. 3.1 but with the diameter of the monopile used in the Delta Flume.

$$\lambda = \frac{6.0}{1.02} = 5.88 \tag{3.2}$$

Scale effects

Scale effects in the Delta Flume are assumed to be eliminated due to the large scale size at which is tested.

Model effecs

The cameras and EMSs placed near a test section can change the flow. The EMS is small and the effects are minor, the cameras are placed close to the wall so their influence is insignificant. The effect of testing in a confined wave flume is already explained in section 3.1.9.

The filled mattress consist of many pores that must be filled with water in order to get rid of the air, especially underwater. Due to the airtight coating and only one escape possibility for the air, it is possible that air remains present within the mattress during the tests. Even with all the effort that is put in to remove this air. Lastly, in contrast to the Scheldt Flume and Atlantic Basin tests, the filling ratio of the mattresses for the Delta Flume is higher then the filling ratio of the Scheldt Flume and Atlantic Basin.

3.3.7 TEST SERIES

Only irregular waves are being tested in the Delta Flume, the test series can be found in Table 3.9 and 3.10. One test series, e.g. F02, consisted of multiple wave files with an imposed H_{m0}. The small difference in H_{m0} and T_p for the cable and monopile is due to the fact that the wave analysis is performed on a WHM near a test section. The full test series can be found in Appendix B.3.1.

Test Series	h_w[m]	H_{m0} [m]	T_p [s]
F02	5.11	0.68 - 1.57	3.68 - 6.21
F03	5.11	1.01 - 1.63	4.55 - 6.08

Table 3.9: Delta Flume test series for the monopile

Test Series	h_w [m]	H_{m0} [m]	T_p [s]
F02	5.11	0.68 - 1.53	3.58 - 5.72
F03	5.11	1.01 - 1.62	4.55 - 5.73

Table 3.10: Delta Flume test series for the cable

3.4 FILLING TEST

Beside all hydraulic scale tests, the scaled prototype mattress (similar to the Delta Flume mattresses) has also been tested for a ballasting material. The aim of these tests was to check if it is possible to fill the mattresses with a drilling fluid and if the material will be distributed evenly. Two different type of mattresses are tested: one square mattress and one mattress shaped similar as the prototype, given in Figure 3.13.

3.4.1 FILLING MATERIAL

The filling fluid used is a mixture of water, bentonite and sand. By adding the bentonite to the water, it will get more carrying capacity for ballast sediment resulting in less settling of sand. This has already been explained in Chapter 2. In Table 3.11 the composition of the filling fluid is given.

Material	Density			Material	Amount	
Bentonite	2600	kg/m^3	Amount of betonite	Water	320	L
Water	1000	kg/m^3	90 g/L	Bentonite	28.8	kg
Sand	2650	kg/m^3		Sand	310	kg

Table 3.11: Filling fluid characteristics

Measuring the density of this mixture resulted in $1440 kg/m^3$.

The left photo in Figure 3.18 shows the test setup. The capacity of the pump was set to approximately 2 m^3/s. Both tests showed no difficulties in pumping the mixture into the mattress. The increase in stiffness due to the overpressure is clearly noticeable and the spacer thread pattern, as presented in Figure 3.16 is shown nicely, see the right photo in Figure 3.18. The mattresses have also been weighed after filling and it was found that the theoretical weight only differed slightly from the measured weight. From this it can be concluded that the mixture keeps its consistency after being pumped.

Figure 3.18: Left photo showing the set up of the filling tests. Right photo shows the square mattress filled with the fluid.

4

STABILITY AND VIDEO ANALYSES

4.1 INTRODUCTION

The goal of this research is to describe the hydrodynamic stability of the ballast filled mattress under waves. To do this, a first analysis is performed with respect to the initiation of motion. In this chapter only the tests performed in the Scheldt Flume and Atlantic Basin are discussed. First a general analysis of the mattresses is given with respect to its failure mechanisms that are obtained from analysing the different video recordings made of the different tests. Next, a stability analysis is performed with respect to initiation of motion. Further a qualitative analysis is done for the Atlantic Basin scour mitigation tests.

4.2 FAILURE MECHANISMS AND CHARACTERISTIC PARAMETERS

4.2.1 FAILURE MECHANISMS

From the different scale tests the failure mechanism of the BFM is observed. This is done by analysing the video recordings of the tests. It was expected that the failure mechanisms of the BFM are similar to those of the ACBM, which is verified by the recordings. The different failure mechanisms are shown in Figure 4.1.

The follow can be said about the failure mechanisms:

1. Uplift Uplift of the (edge) of the mattress is considered the main failure mechanism. Uplift has three possible forcing mechanisms.

1. Drag force: The flow velocity exerts a force on the protruding mattress. This force is balanced with the resistance against sliding and the gravitational force. A small uplift will result in an increased area of attack and a moment around the turning point of the mattress which enhances uplift. An increase in uplift will result in a larger area of attack, increasing the drag force again. This is explained further in section 4.2.3.

2. Stagnation pressure: The flow pushing against the protruding mattress give rise to a stagnation pressure. A very small gap between the bed and mattress will result in the

stagnation pressure to transfer below the mattress and cause an uplift force, trying to lift the mattress.

3. Wave induced pressure: Waves travelling over the mattress give rise to pressure differences. The pressure difference is proportional to the acceleration of a fluid according to Euler. This pressure difference is either over the length of the mattress or over the distance between top and bottom. The pressure difference over the length of the mattress is resisted by its resistance against sliding but is assumed to be small due to the $L_w >> L_{mattress}$. The pressure difference over the thickness of the mattresses is due to the hydrostatic pressure below the mattress and wave-induced pressure fluctuations above the mattress. This pressure difference causes an upward force. This is further explained in Appendix A.

Uplift at the edge of the mattress will expose the seabed below to the flow. This can result in significant undermining of the mattress. This is not considered a problem if the mattress is flexible enough to follow this scour at the edge and the uplifts are limited so the mattress is not washed away.

2. Undermining Undermining is the scour beneath the protection; the scour protection remains stable under the hydrodynamic conditions. Undermining is due to edge scour as mentioned in section 2.5. When the mattress is not able to follow edge scour development, the mattress will be slowly undermined. This leads to lowering of the mattress and the possibility of scour reaching up to the foundation. A flexible mattress will be able to follow edge scour and provide protection against further scour (thus undermining) as it will '*hang*' on the slope (Schiereck & Verhagen, 2012). The stiffer the mattress, the harder it becomes to follow this scour and undermining will be significant.

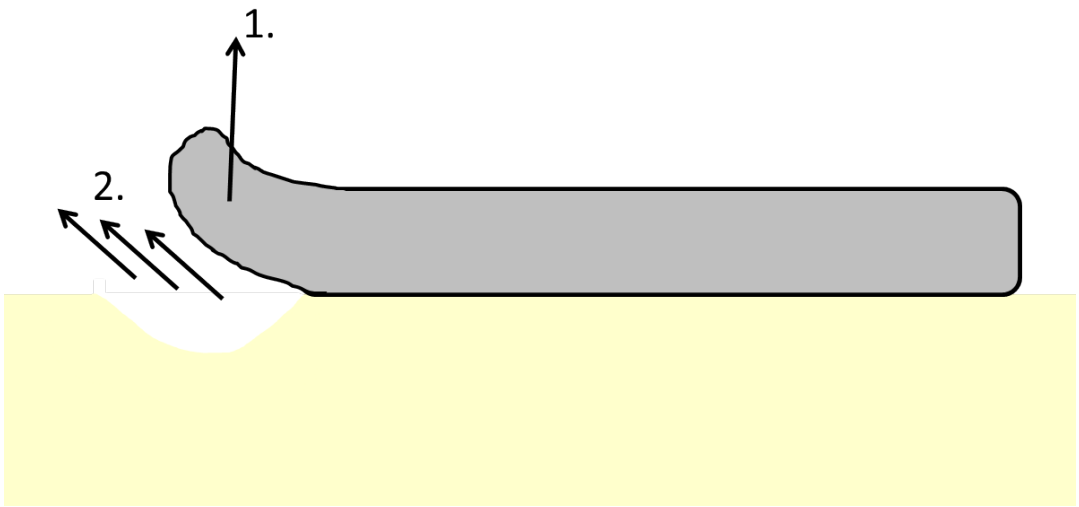

Figure 4.1: Ballast filled mattress failure mechanisms

Winnowing is the washing out of sediments from between the mattress and foundation pile and is also seen as a failure mechanism. Winnowing happens when there is a gap between the mattress and monopile and can lead to significant scour hole development near the pile. For this research winnowing is not taken into account. This

is because winnowing is not attributed to the stability of the mattress but to the placement/installation of the mattress.

As mentioned in section 2.6 sliding is also considered as failure mechanism. Sliding is the last phase of the sequence of uplift that leads to failure. If the uplift is sufficient and (depending on the stiffness) the contact area is reduced sufficiently, then the resisting friction force becomes smaller than the destabilizing force. Depending on the stiffness, this happens very fast. For the medium-flexible and stiff mattress, the uplifts were significantly less than those of the flexible mattress. The medium-flexible and stiff mattress have significantly smaller uplifts with respect to the flexible mattress and the mattress moves as a whole. Sometimes the whole mattress is lifted but it does not yet slide away. This has two possible reasons: (1) the monopile blocks the movement downstream or (2) the wave has not lifted the mattress sufficiently enough to be carried up- or downstream by the wave trough.

To conclude, the failure mechanism of the ballast filled mattress is defined as follows: A ballast filled mattress has failed when the seabed below the mattress is exposed which in time leads to ongoing undermining of the mattress.

This failure mechanism assumes the mattress to be stable. For the mattress to be stable it is preferred that is has no systematic significant uplifts.

4.2.2 CHARACTERISTIC PARAMETERS

Since the model tests are mainly aimed at finding the parameters of importance for the stability, with the failure mechanisms known the mattress can be systematized with the parameters based on the failure mechanisms and video recordings.

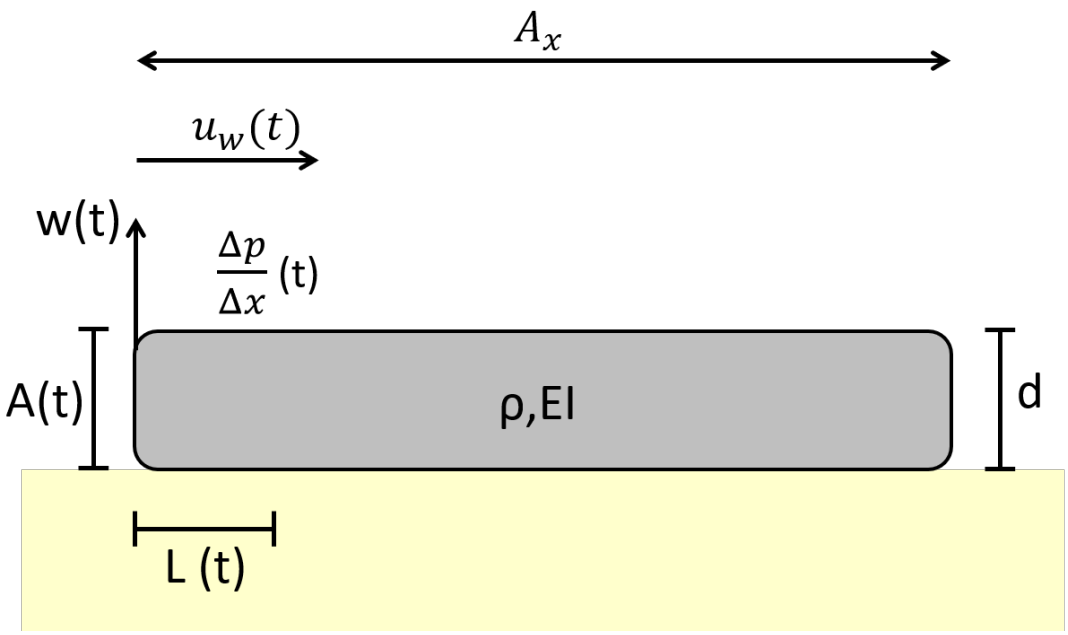

Figure 4.2: Characteristic parameters of the ballast filled mattress

in which: L = uplift length of the ballast filled mattress
d = thickness of the mattress
ρ_m = density of the mattress
EI = bending stiffness of the mattress
u_w = orbital velocity
A = area of attack
Δp = pressure gradient
A_x = particle excursion
w = uplift of the ballast filled mattress

Many parameters depend on time. For the orbital velocity and pressure gradient, this is due to the wave passing over. The uplift length and area of attack also change in time with increasing uplifts.

4.2.3 MOMENTUM BALANCE

This section will show the force mechanisms assumed to be responsible for the start of motion. Figure 4.3 shows the force balance for a simplified 2D case of the BFM. Lifting of the edge will occur when the lift (due to a pressure difference or *hydraulic jack*), drag and inertia forces are bigger than the resisting force and is expressed by the momentum balance around point A in Figure 4.3. The moment around point A is defined as given in eq. 4.1. For this momentum balance the added mass term is neglected.

$$F_d L_d + F_{d,up} L_l + F_i L_d + F_{i,up} L_l = F_w L_w + EI\kappa \tag{4.1}$$

The drag force (F_d) is due to the orbital velocities and the obstruction of the flow by the ballast filled mattress. This also causes a stagnation pressure that is transferred below the mattress and acts like a hydraulic jack and causes a lift force ($F_{d,up}$). The other lift force, $F_{i,up}$ is assumed to be due to the pressure difference over the over the thickness of the mattress due to the wave. Finally the inertia force (F_i) in line with the flow also causes a force. The lift force due to accelerating flow is neglected in eq. 4.1, this force is assumed to be very local and small. The bending stiffness of the mattress (EI) gives an additional resistance against uplift. An increase in uplift, will result in an increase in drag (bigger area of attack), as given in eq. 2.2. On the other hand, an increase in uplift will also result in more mobilization of mass ($L_{eff,up}$ increases). The resistance due to the bending stiffness depends on κ and depends on the uplift behaviour of the mattress; it depends on where the turning point of the mattress is. The increase of drag together with the increase in mobilized mass will be discussed later and is not yet of importance as the focus is on the initiation of motion.

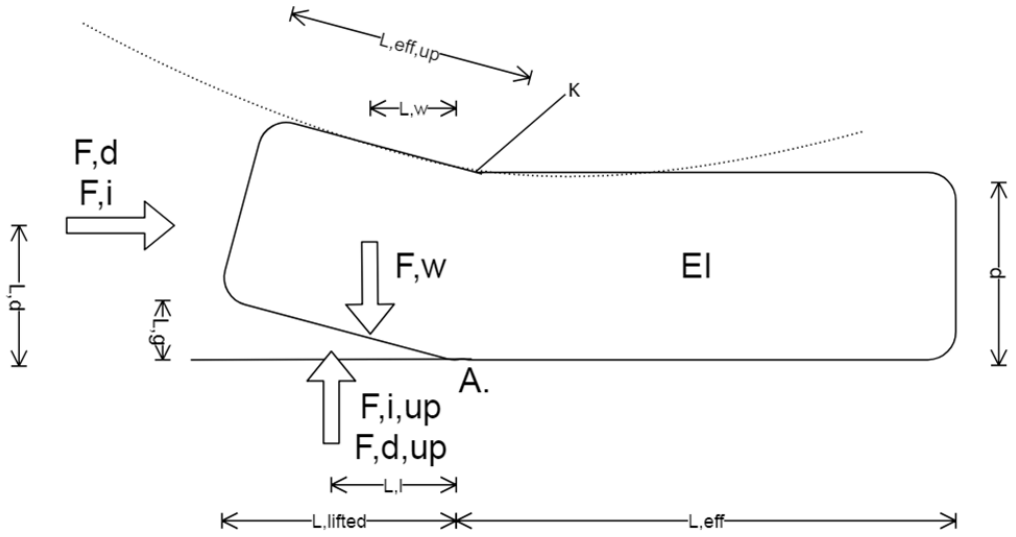

Figure 4.3: Simplified force balance

If for eq. 4.1 a block with $L_{eff,up}$ = d is assumed to determine the initiation of motion and $0 < L_g << d$, the equation can be rewritten as follows:

$$(F_d + F_{d,up})\frac{1}{2}d + (F_i + F_{i,up})\frac{1}{2}d = F_w\frac{1}{2}d + EI\kappa \tag{4.2}$$

Which results in:

$$(0.5\rho_w C_d u_w^2 d + 0.5\rho_w u_w^2 d)\frac{1}{2}d + (\rho_w C_m a d^2 + \rho_w C_m a d^2)\frac{1}{2}d = \rho_m g d^2\frac{1}{2}d + EI\kappa \tag{4.3}$$

Neglecting $EI\kappa$, the coefficients and assuming the inertia force due to the horizontal pressure difference is small ($L_w >> L_{mattress}$) will lead to the simplified Morison-equation:

$$\theta = \frac{u_w^2 + ad}{\Delta g d} \tag{4.4}$$

in this equation u_w^2 thus contains both contributions due to drag and stagnation pressure. The lift occurs due to the under pressure due to the wave fluctuations over the mattress.

It must be noted that this analysis does not include the difference in time of occurrence.

4.3 Stability analysis

A stability analysis is performed with the data from the Scheldt Flume with respect to the initiation of motion. With the obtained values an analysis is made for the different stability parameters presented in section 2.8. The data that is used and the methodology is explained below.

4.3.1 Methodology

The stability analysis is performed on the video recordings made off the Scheldt Flume tests and is done to check the mattresses for movement or not. The tests are categorized as (1) no movement or (2) movement. The

movement category covers the entire range from initiation of motion up to failure. The initiation of motion starts at any slight movement of the edge of the mattress. This threshold is chosen due to the fact that it is hard to differentiate between uplifts and just small movements of the edge of the mattress with just one camera angle.

From the WHM the mean wave height and mean wave period are obtained by a zero-down crossing analysis, this is explained in Appendix C.1. These values are subsequently used in linear wave theory, given in eq. 4.5 and 4.6, to determine the characteristic values.

$$L = \frac{gT^2}{2\pi} tanh(\frac{2\pi d}{L}) \tag{4.5}$$

$$u_x = \frac{\omega H}{2} \frac{cosh(k(h+z))}{sinh(kh)} sin(\omega t) \tag{4.6}$$

The categorization is plotted against the different stability parameters by using the data obtained from the data analysis and linear wave theory. The tests used are found in Table 4.1.

Facility	Structure	Flexiblity	Wave type	H/h [-]	H/L [-]	No. of tests
Scheldt Flume	monopile	flexible	regular	0.16 - 0.55	0.04 - 0.07	31
	monopile	med-flex	regular	0.25 - 0.56	0.04 - 0.08	63
	monopile	stiff	regular	0.35 - 0.53	0.03 -0.06	24
Scheldt Flume	cable	flexible	regular	0.26 - 0.61	0.04 - 0.06	28

Table 4.1: Range of hydraulic parameters used in the stability analysis (wave parameters determined with linear wave theory)

4.3.2 VISUAL OBSERVATIONS

From the video analysis, several important observations were made, of which some have a direct influence on the stability of the mattress.

1. For the flexible and medium-flexible mattress, the connection between bed and mattress worsened during the test series. Parts of the mattress permanently lost connection with the flume bed leaving gaps below the mattress in the course of the test series. This gap is of influence of the stability on the mattress explained in the section 4.2.3. Furthermore, the uplifted part has an increased area of attack for the drag force. Appendix C.3 show the gaps for the flexible and medium flexible mattresses.

2. In contrast to the flexible and medium-flexible mattress, the stiff mattress seems to have a better connection with the flume. However, all three mattresses will have an opening where the pressure can go beneath the mattress. The distance from the gap to where the mattress touches the bottom again, is of importance. This distance could not be observed during the tests. This distance determines up to which point the pressure can go beneath the mattress and the influence on the stability is therefore unknown.

3. The material within the mattress was able to move freely throughout the mattress. This means that when a mattress is lifted, stones may roll or slide away from the edge. Leaving the edge of the mattress unballasted, resulting in an earlier observation of movement. This phenomena has been verified by separate uplift tests performed at Deltares given in Appendix C.5.

4. As explained in Chapter 3, there is a weight difference between the two halves of the medium-flexible mattress around the monopile while their position was varying. During the test series this difference in

weight was not known and hence the position of the two mattresses was not reported. This influences the stability (difference in Δ of approximately 0.05 as found in Table 3.2). As it is unknown during the test which is which, if one mattress failed earlier than the other it is assumed to be the light one.

5. Sometimes the mattress has already been slightly moved out of position during a previous test, this can in turn increase the stability (a new favourable position) or decrease the stability.

6. During some tests, little air pockets were present in the flexible monopile mattress. The air pockets were small and these tesst have been analysed as regular tests, where there was no sign of the little air pockets influencing the stability of the mattress. For the medium-flexible and stiff monopile mattress it was unknown if airpockets were present. The top layer of these two mattress types was not transparent, which made it impossible to check the potential presence of air pockets. It is therefore assumed that the potential effect of the presence of air pockets is negligible.

4.3.3 STABILITY PARAMETER

Monopile analysis

The stability analysis done is by applying eq. 4.7 as shown below. This first assessment only takes the drag and lift due to stagnation pressure in account. Figure 4.4 shows the boxplot for the three mattresses. The red line in Figure 4.4 indicates the median. The location of the median says something about the skewness of the data. The more distance between the median and the edge of the box, the more spread the data is. But the distance still contains 25% of all data. The total data within the box is 50%, the minimum and maximum (excluding outliers) are represented by the whiskers. Lastly, the boxplots must be interpreted with care as the data sets are small.

$$\theta_{lin} = \frac{u_x^2}{\Delta g d} \tag{4.7}$$

In eq. 4.7 u_x is the orbital velocity at the bottom of the flume is calculated with eq. 4.6. The initiation of movement can be taken as the lowest value of the boxplot, assuming this is the point where the mattress started moving. The lowest point is now seen as a stability number, the value of $\theta_{cr,lin}$ at which the mattress starts to move. When looking at this initiation of motion, a trend is observed that with increasing stiffness there is a shift in stability. Figure 4.4 only shows the boxplots with respect to movement, the full plot can be found in Appendix C.2. Table 4.2 shows the amount of test and failures per mattress.

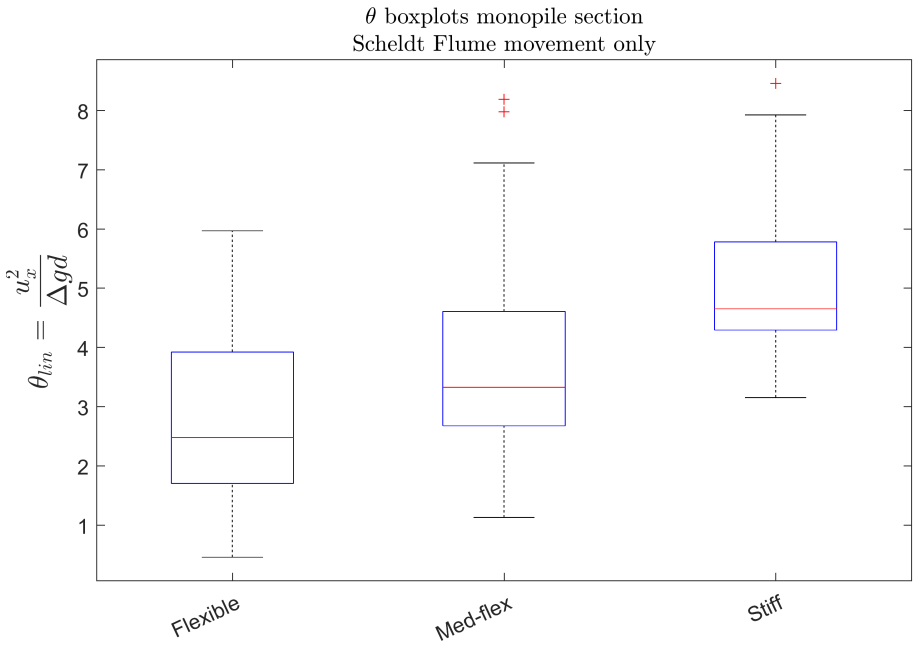

Figure 4.4: θ_{lin} boxplots monopile section, Scheldt Flume monopile tests

	No. of tests	No. observed motions
Flexible	31	30
Medium-flexible	63	63
Stiff	24	18

Table 4.2: Number of tests vs number of motions, monopile section

The data shows only failures for the medium-flexible mattress and only one success for the flexible mattress. The initiation of movement of both could therefore have an even lower value.

Cable analysis

Eq. 4.7 is also used for the cable analysis. Figure 4.5 shows the results of the analysis. Layout 1 & 2 have a significantly higher stability than the layout 3. The configuration of layout 1 & 2 are likely to affect the stability due to open sides of the layouts. The main failure mechanism of these mattresses is sliding. The stability of layout 3 is a little higher than the flexible mattress of the monopile tests and showed uplift behaviour. This can be explained by the fact that the hydrodynamic conditions at which the cable tests start is significantly higher than the for the flexible mattress at the monopile, as shown in Table 4.1.

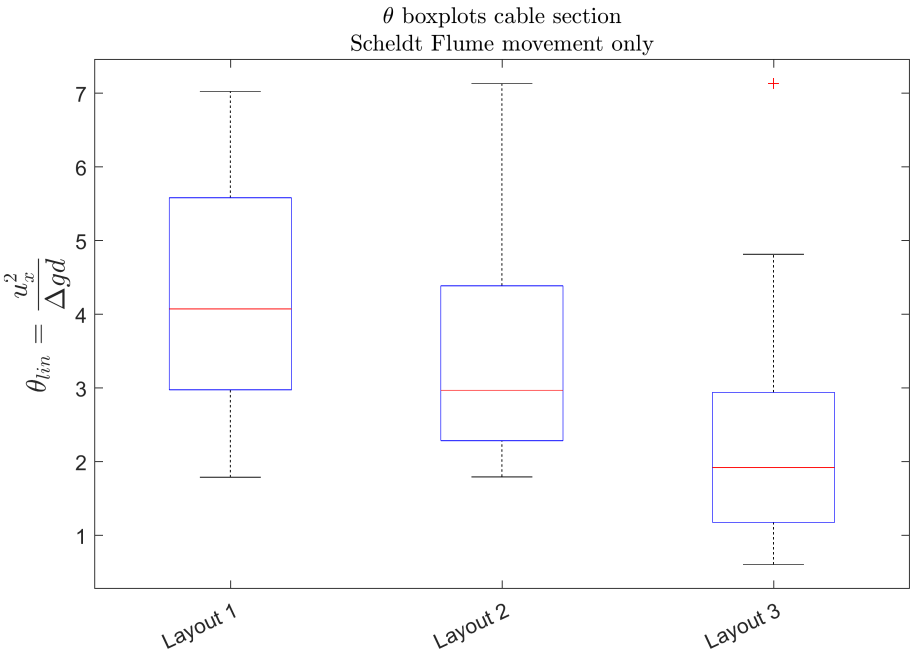

Figure 4.5: θ_{lin} boxplots cable section, Scheldt Flume cable tests

	No. of tests	No. of observed motions
Layout 1	48	8
Layout 2	56	14
Layout 3	28	28

Table 4.3: Number of tests vs number of motions, cable section

4.3.4 FULL STABILITY PARAMETER

A third analysis is performed by looking at the full stability parameter, given in eq. 4.8. By adding the force due to inertia, including the coefficient, the influence of inertia on the stability can be checked.

$$\theta_{T,lin} = \frac{u_x^2 + C_{all} a_x d}{\Delta g d} \tag{4.8}$$

The acceleration is also calculated according to linear wave theory, see eq. 4.9 below.

$$a_x = \frac{\omega^2 H}{2} \frac{cosh(k(h+z))}{sinh(hd)} \tag{4.9}$$

Figure 4.6 shows eq. 4.8 for multiple values of C_{all}. No clear effect of inertia is observed. This is explained by linear wave theory, which does not take in account the skewness of the waves as found by the EMS signal. For the flexible and medium-flexible mattress no conclusions can be drawn due to the lack of data. It is assumed that the coefficient includes the difference in time at which the velocity and acceleration occur, as explained in Chapter 2. Appendix C.4 explains the full stability parameter in full detail.

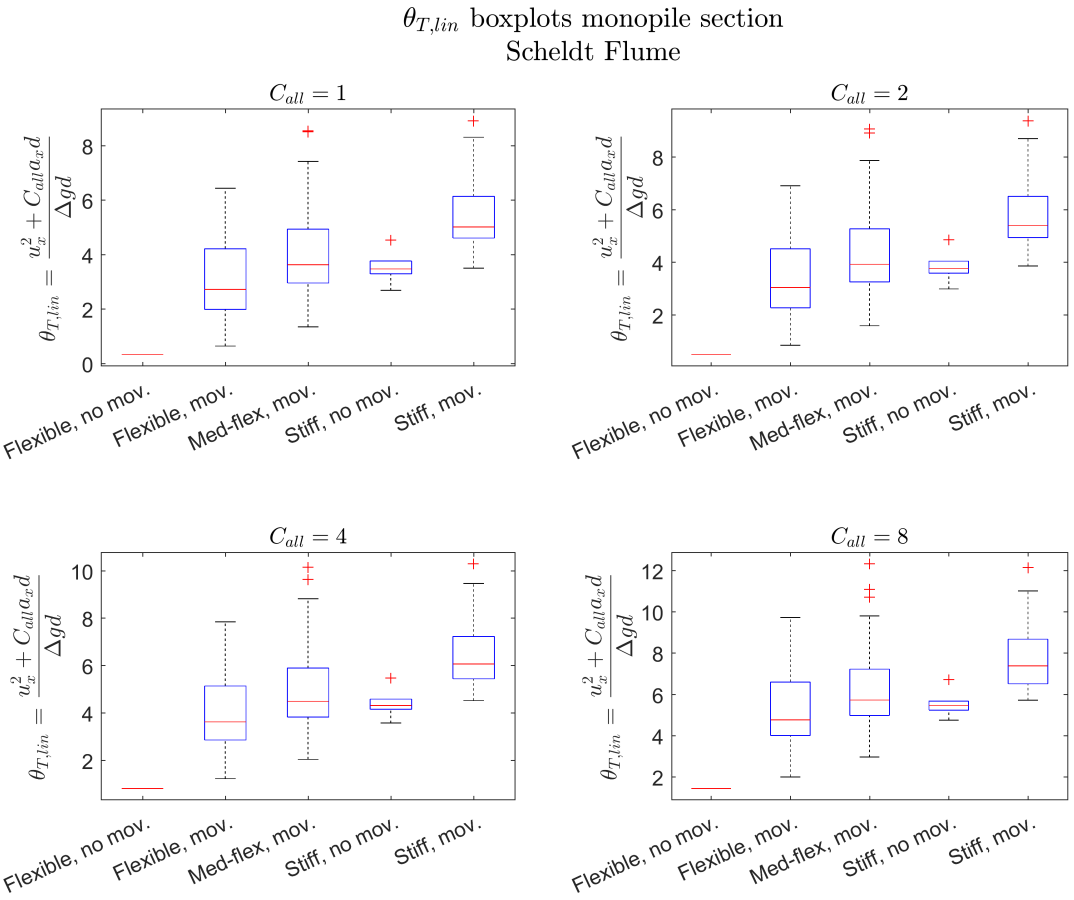

Figure 4.6: $\theta_{T,lin}$ boxplots monopile section, Scheldt Flume

4.4 Other analyses

This section will present different findings with respect to the analysed video recordings made from the Scheldt Flume and Atlantic Basin, and present the findings with respect to stiffness measurements done for the mattresses.

4.4.1 Video analyses

Scheldt Flume

As is shown in the stability analysis the failure mechanism of the mattress is highly influenced by the stiffness of the mattress. The flexibility of the mattress determines the amount of uplift and distance over which uplift happens. The difference in stability with respect to stiffness has already been presented in the previous section.

For the flexible mattress the uplifts were clearly noticeable and significant. The sliding failure mechanism did not occur that often, but when this happened it initiated most of the times at the transverse side of the pile where the two mattresses would touch. The part of the mattress at the transverse side would start to lift up and eventually move the whole mattress. At the transverse side of the pile the flow velocities are higher due to the

presence of the monopile, resulting in a significantly higher drag force when the mattress was protruding a little. Depending on the chosen installation method, the mattress can be made out of 1 piece or more individual mattresses. If the protection is made out of two or more mattresses it can fail due to this mechanism if the individual mattresses are not connected. For this remaining of this research it is assumed that the prototype mattress consists of 8 individual mattress which are connected and this mechanism does not occur. Figure 4.7 shows the side uplift for the flexible mattress.

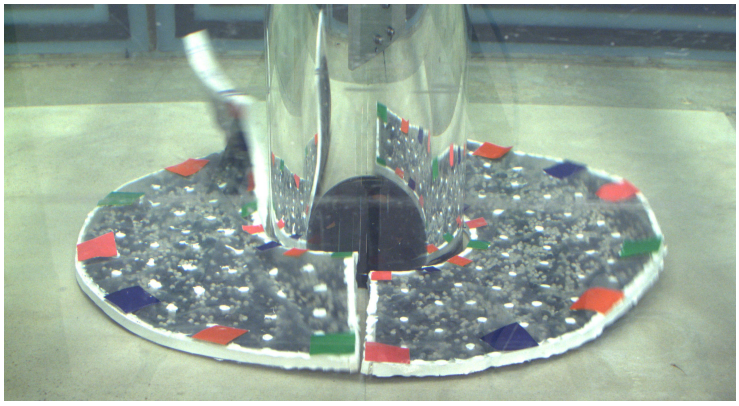

Figure 4.7: Photo showing the failure at the transverse side of the mattress

The uplifts of the medium-flexible experienced fewer uplift compared to the flexible mattress and when an uplift happened, the whole mattresses seemed to move/lift. This is in contrast to what was found during stiffness measurements taken of all mattresses. The stiffness measurements showed similar deformations to the flexible mattress (dry and underwater tests) but under wave loading the whole mattress seemed to lift. A possible explanation for this is the time scale of the force, but this has not been further looked into. The stiffness measurements are further explained in Appendix C.5.

For the stiff mattress the uplifts are even lower and the mattress was lifted as a whole. Due to this the sliding mechanism was dominant for the stiff mattress and happened after small uplifts. The lifting of the whole mattress resulted in the loss of connection with the flume bed, decreasing its resistance against sliding and being transported up- or downstream with the orbital motion.

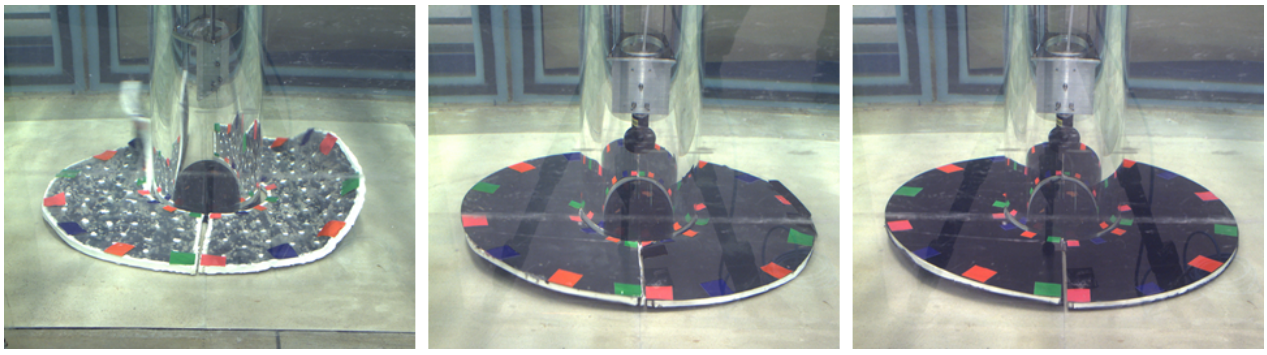

Figure 4.8: From left to right: flexible, medium-flexible and stiff mattress

Figure 4.8 illustrates a potential factor that explains the difference in stability between the mattresses with

different flexibility. For the medium-flexible and stiff monopile mattress the whole mattress seems to move, resulting in a significant amount of water that must be displayed in comparison to the flexible monopile mattress. This added mass will increase the stability as explained in Chapter 2.

Scour mitigation tests Atlantic Basin

From the Atlantic Basin scour mitigation tests stereo photos have been taken to determine the mattresses ability to mitigate scour. Figure 4.9 shows the stereo photos taken after the full test series, found in Appendix B.2.1, and are taken after the removal of the ballast filled mattress. For the SBJ only test series T02 is analysed with respect to scour mitigation.

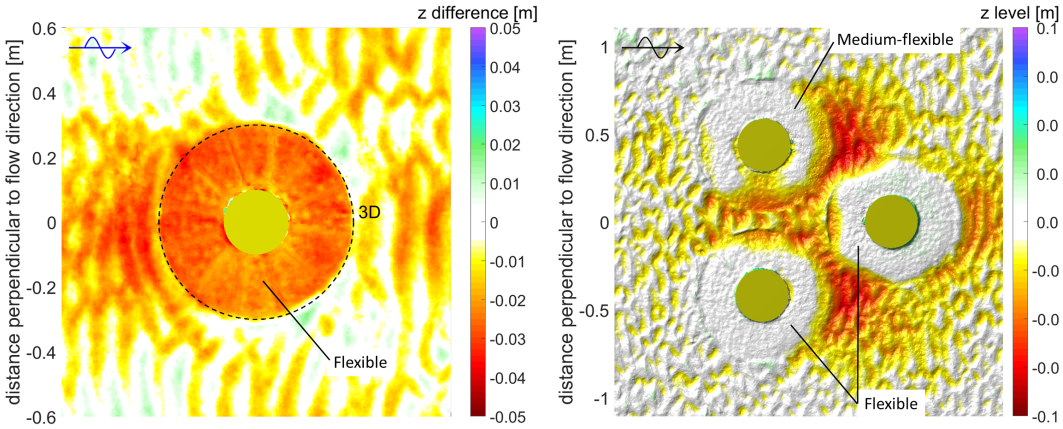

Figure 4.9: Bathymetry plots obtained by stereo-photography from the Atlantic Basin scour mitigation tests. (left) the bathymetry plot for the monopile tests, (right) bathymetry plot for the SBJ tests.

The bathymetry of the monopile shows two distinct features; winnowing and undermining. Close to the pile, on the upstream side a small scour hole due to winnowing is formed. This scour hole is very local and did not lead to significant scour at the pile interface. The amount of winnowing is limited due to a tight connection between the pile and mattress.

Besides winnowing, the left figure shows a systematic lowering of the bed level beneath the BFM of approximately 1.0 cm. This lowering was not visible during the video recordings and is not explained by winnowing or edge scour. If winnowing is the case, significant amounts of sand had to be seen leaving at the pile interface, which has not been observed. If edge scour would be the cause, the scour should be significantly lower at the edge of the protection. The reason for the systematic lowering of the mattress is unknown.

The right figure shows the stereo photography taken from the Atlantic Basin tests. The difference is clearly visible. The flow pattern due to the complex structure increases the scour at the downstream side and in between the structure. The scour downstream is significant but it also shows the most downstream mattress following the scour and reducing the scour beneath the mattress. The difference between the flexible and medium-flexible mattress is also clearly shown with respect to following (edge) scour. The undermining of the medium-flexible mattress is significant and reaches up to the suction bucket. For the flexible mattress the undermining comes to a halt because the mattress is able to follow the scour hole. By comparing scour beneath the flexible mattress of the monopile with the SBJ, it is clear that the systematic lowering of the flexible mattress is not due to the hydrodynamic loadings.

4.5 EVALUATION

In this chapter the different failure mechanisms regarding the ballast filled Mattress are given and obtained from the video recordings made from the Scheldt Flume test. The uplift mechanisms of importance are; uplift and undermining.

Sliding and winnowing of the mattress are also considered a failure mechanism. Sliding is successive to uplift and it is sufficient to incorporate this in the uplift mechanism, on the condition that the weight of the mattress is sufficiently to keep the mattress in place on the bed. Winnowing is attributed to the installation of the mattress and not linked to the mattress itself.

From the same video recordings and stability analyses the important structural and hydraulic parameters are obtained. These are given in Figure 4.2. Initiation of motion starts when a critical force is exceeded. It is assumed that this happens around a certain point and uplift starts, this is given in Figure 4.3. Once movement is started, the surface area on which drag acts increases and on the resisting side the amount of mobilised weight. This is further discussed in the next chapter.

With the stability analysis an attempt has been made to determine at which $\theta_{cr,lin}$ movement starts. The determination of movement has been done by categorizing one test in movement or no movement. The determination of movement is done by simply looking at the mattresses and this introduces many errors and uncertainties, this is reflected in the amount of movements founds per type of mattress.
For the cable mattresses, only the flat cable mattress (layout 3) is further analysed. This is done to compare with the monopile mattress and to check the influence of the pile. The other layouts (layout 1 and 2) are not representative for a cable protection and thus for not further analysed.
Furthermore the full stability parameter was used to determine the initiation of motion. This did not increase the fit, for the flexible and medium-flexible mattress there was not enough data to conclude the effect of inertia.
From the stability analysis a first critical value can be obtained and it can be concluded that the higher the bending stiffness the higher the stability, which is given in Table 4.4.

	$\theta_{cr,lin}$
Flexible, monopile	0.45
Medium-flexible, monopile	1.13
Stiff, monopile	3.16
Flexible, flat cable mattress	0.60

Table 4.4: Critical θ for initiation of motion obtained from the stability analysis and linear wave theory, Scheldt Flume tests

The values given in Table 4.4 are obtained from Figure 4.4 by taking the lowest value per mattress. These values should be interpreted with care, especially for the medium-flexible mattress where all tests have been categorized as movement. The initiation of motion can be even lower.

A final analysis with respect to the behaviour of the mattresses provided information regarding the uplift mechanism of the different mattresses. From the videos it can be seen that the medium-flexible and stiff mattress lift up as a whole. For the medium-flexible mattress this is in contrast to what has been found by stiffness measurements. Furthermore it can be concluded that the medium-stiff mattress and the stiff mattress are to stiff to follow scour and significant undermining occurs. For this reason the stiff mattress is not further analysed in the following chapter but the medium-flexible monopile mattress is still further analysed. The flexible mattress is able to follow scour.

5 MOBILITY ANALYSIS

5.1 INTRODUCTION

In this chapter the mattresses are analysed with uplift recognition software to determine the amount of uplift. The software gives information about all uplift events, together with an analysis script it provides the information about the corresponding waves. This provides a more detailed and accurate analysis than the analysis in the previous chapter. The amount of data is subsequently plotted against the mobility and full mobility parameter as explained in Chapter 4. A quantitative mobility analysis, found in Appendix D, showed that both parameters have potential for predicting the amount of uplift for the ballast filled mattress. This analysis is only performed on the flexible mattress for the monopile and cable. Table 5.1 shows the results obtained in Chapter 4 and the mobility analysis.

	Flexible, monopile	Flexible, flat mattress cable	Medium-flexible, monopile	Analysis	Method
θ_{cr}	0.45	0.6	1.13	Stability	LWT
θ_{cr}	0.53	0.69	-	Mobility	LWT
θ_{cr}	0.8	0.48	-	Mobility	EMS

Table 5.1: Found θ_{cr} per analyses. Method determines how θ_{cr} is obtained: LWT = linear wave theory and EMS = measured values

First, the methodology of the mobility analysis is given and shortly explained how the uplift recognition software determines the uplift. Second there is explained how the data is processed. The results with respect to this analysis are given in section 5.3 and section 5.5 gives the evaluation on the analysis. The stiff mattress is not analysed with the uplift recognition software as the main failure mechanism for the stiff mattress is sliding.

5.2 METHODOLOGY

During the construction of the models used during the Scheldt Flume tests, coloured squares were fixed on top of the BFMs as shown in Figure 3.3 and 3.4. These coloured squares are used by the uplift recognition software

to determine the uplift.

The uplift recognition software uses HSV-colour ranges to detect colours. For monopile and cable tests, the HSV-range is tuned to detect the desired coloured square. For the uplift recognition only two colours are analysed; red for the upstream mattress and green for the downstream mattress. The square of interest is the most upstream or downstream square.

The software analyses each frame individually for the upstream and downstream side of the pile. The software draws polygons on each square with the colour that is analysed and temporarily saves these polygons. Subsequently this is done for the next frame and the polygons of the consecutive frames are compared. When a movement with a minimum of ten pixels is detected, the software assigns it to movement and the movement found is saved as well. Once all frames are analysed, the software saves a file that includes all the coordinates of the polygons for the specific colour, the center coordinates of the polygon and when a movement is detected, the detected movement.

This output file is subsequently used in the uplift analysis script. The saved polygons are filtered with respect to the right coordinates, this assures the right polygons are used for the uplift determination. The filtered polygons are subsequently plotted and the figure is saved for reference. Figure 5.1 shows the polygons for one test and also the motion made by the mattress in time.

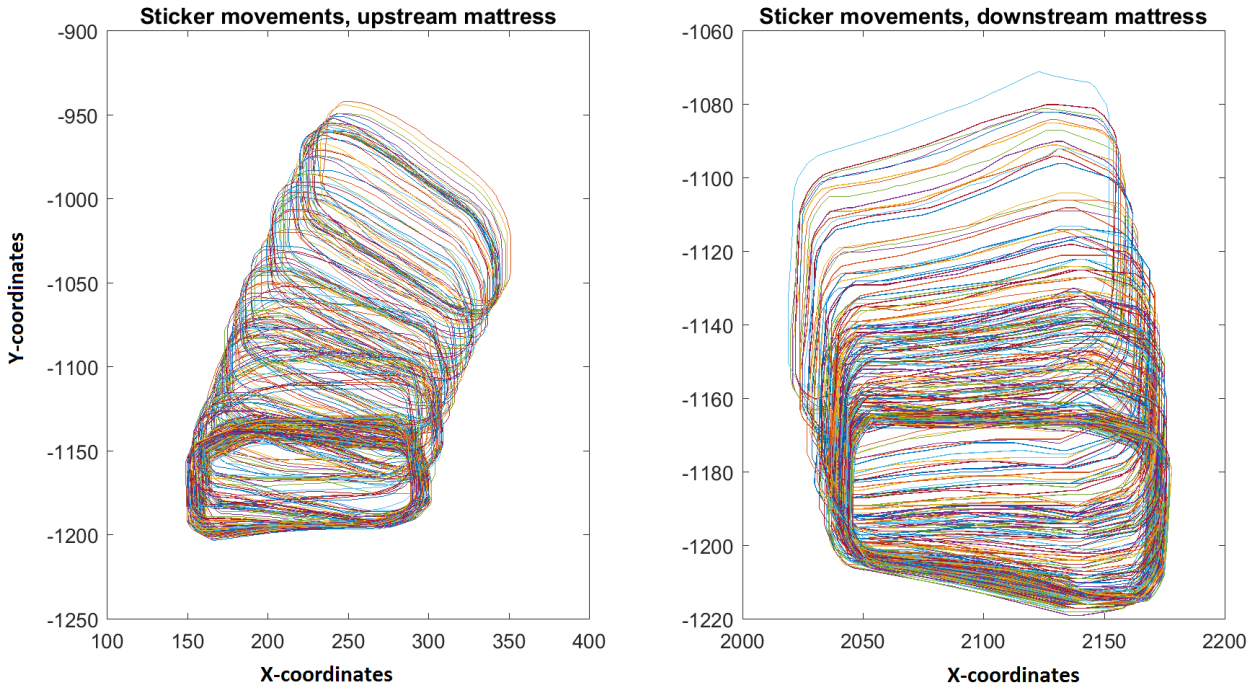

Figure 5.1: All filtered polygons for one test

From the remaining polygons only the top layer of the coloured square is used for the uplift analysis. From this remaining part of the coloured square, the maximum uplift is determined. Different tests have been analysed with respect to the maximum,95% and 90% uplift as well, but no significant difference was found comparing them with the maximum uplift.

The resulting uplift is given in pixels. To translate the pixels to centimetres, the dimensions of the coloured square are used for the conversion, the dimensions are 3x3 centimetres. As the uplift happens in the plane of the length of the square, it is assumed that the pixels ratio is the same in the vertical. By measuring the length of the coloured squares in pixels, the amount of pixels in the vertical can be converted to centimetres. By assuming the angle under which the camera stand is small, this is a reasonable assumption. This is further clarified in Figure 5.2.

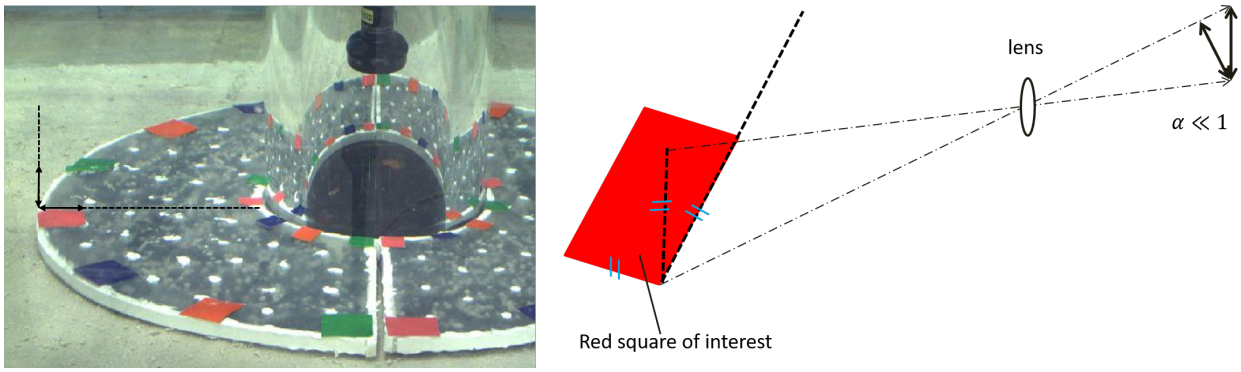

Figure 5.2: Pixel to centimeter conversion

The software analyses the frames taken by the camera that has an frequency of 5 Hz, meaning that for an uplift event, every 0.2 seconds a data point is obtained. To get a continuous uplift motion, which is assumed to have a sin-like function, all points are interpolated using a spline function as this gave the best fit. Consequently all peaks are saved with its corresponding time of occurrence. Only the maximum uplift events are used for this analysis.

Furthermore, for the corresponding test the EMS and WHM data are analysed and all zero-down crossings of the water level elevation, velocity and acceleration with each corresponding time period and time of occurrence are saved. With the dispersion relation from linear wave theory an estimate can be made about the time difference between the wave passing the EMS and the mattress. This estimate is used to assign the right wave to the right uplift event.

5.3 Results

To process all data obtained from the mobility analysis an instantaneous approach is used. This is done by only looking at movements of the mattress. This is done because the goal of this research is to come up with a empirical design method to predict the stability of the BFM. Therefore the critical value at which the movement starts is of interest and the behaviour in time of the mattress. It is important to consider that, when using the instantaneous approach, the maximum forces due to velocity and acceleration never occur at the same time, and both change in time. The time of occurrence between the two is of great importance for a correct representation of the force. As mentioned in the introduction, the simplified Morison-equation is used, followed by the full simplified Morison-equation given in eq. 5.1 and 5.2 respectively. This simplified form does not take in account the changing area of attack for drag or the increasing weight due to an increase in uplift. It is assumed this is implicitly incorporated in the data.

$$\theta_{ems} = \frac{u_{ems}^2}{\Delta g d} \tag{5.1}$$

$$\theta_{T,ems} = \frac{u_{ems}^2 + C_{all} a_{ems} d}{\Delta g d} \tag{5.2}$$

For the analysis that uses eq. 5.1 the assumption is made that the maximum velocity occurs at the time of maximum uplift, which does not necessarily have to be the case. With increasing uplift, the surface area on which the drag exerts a force increases, increasing the force due to drag. On the other hand, with an increase in uplift the amount of mobilised mass also increases. The ratio between these two mechanisms is unknown. The reliability of this assumption will be discussed later on.

For the plots in the coming section the relative uplift (Rul) is used to express the amount of uplift. The relative uplift is defined as:

$$Rul = \frac{uplift \quad [cm]}{thickness \quad mattress \quad [cm]} \tag{5.3}$$

5.3.1 FLAT CABLE VELOCITY ANALYSIS

Figure 5.3 shows the relative uplift against eq. 5.1. The highest uplifts are found at the downstream side of the mattress which cannot be explained from the data. In general the plot shows significant scatter and there is no observable trend in the data. Two possible explanations are given by the fact that the velocity and acceleration signal is deviating significantly from the regular waves. For short waves ($T < 2s$) the signal shows trough velocities higher than the crest velocities where the acceleration is approximately the same. For medium-long waves ($T < 2.6s$) the crest velocities are significantly larger than the trough velocities, but the upstream directed acceleration is larger.

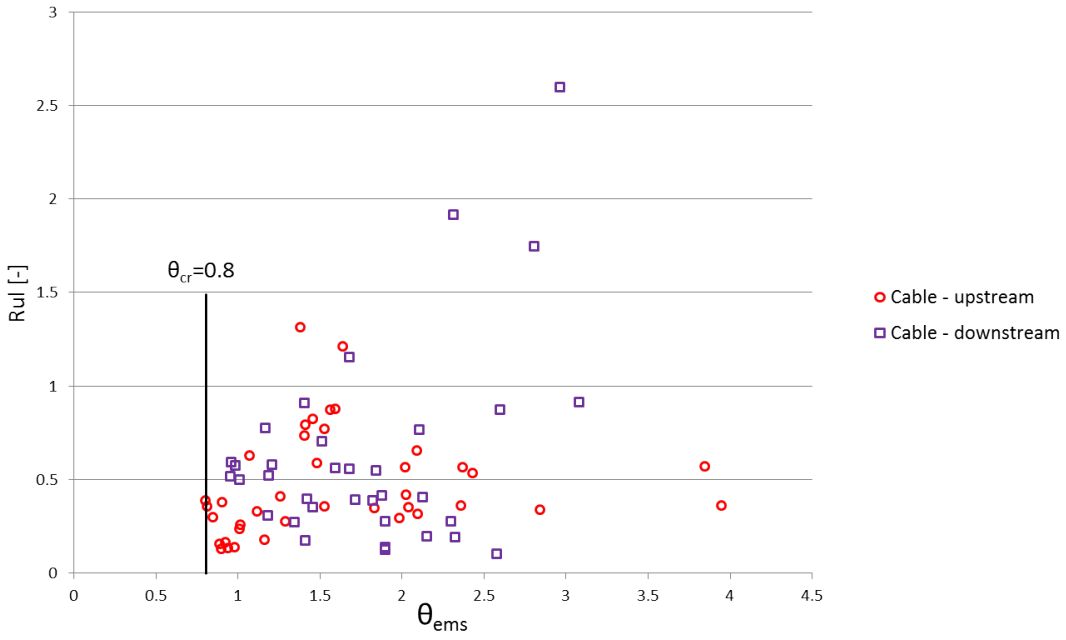

Figure 5.3: Relative uplift against θ_{ems} for the cable mattresses, Scheldt Flume

By comparing the time of occurrence of the uplift with the time of the maximum velocity, which has been translated to the mattress with the dispersion relation according to linear wave theory, an estimate is found

to what point in the wave motion the uplift happens. By analysing this difference it is not always found that the time of uplift correspond to the time of maximum velocity but in fact happens prior to the maximum velocity. As a result the acceleration term is of influence to the stability of the mattress.

5.3.2 FLAT CABLE FULL MOBILITY ANALYSIS

As explained in the previous section, the uplift happens in the upward (or downward) wave motion and not specifically at the maximum velocity. By estimating at which percentage, of the corresponding up or down crossing, the uplift happens an estimate can be made for the velocity and acceleration at the time of uplift. This is done by taking the maximum velocity and acceleration obtained from the EMS and using these values as maximum for the sine function. Assuming the velocity and acceleration follow a sine function, the corresponding velocity and acceleration can be calculated with eq. 5.4 and 5.5 respectively.

$$u = sin(\pi up_{\%})u_{max} \tag{5.4}$$

$$a = sin(0.5\pi - up_{\%}\pi)a_{max} \tag{5.5}$$

$Up_{\%}$ is the percentage that expresses at which time the uplift occurs from the crossing to the maximum velocity. Subsequently using eq. 5.2 and plotting this against the relative uplift (Figure 5.4) shows little difference with respect to Figure 5.3. The value of θ_{cr} however, is shifted to the left.

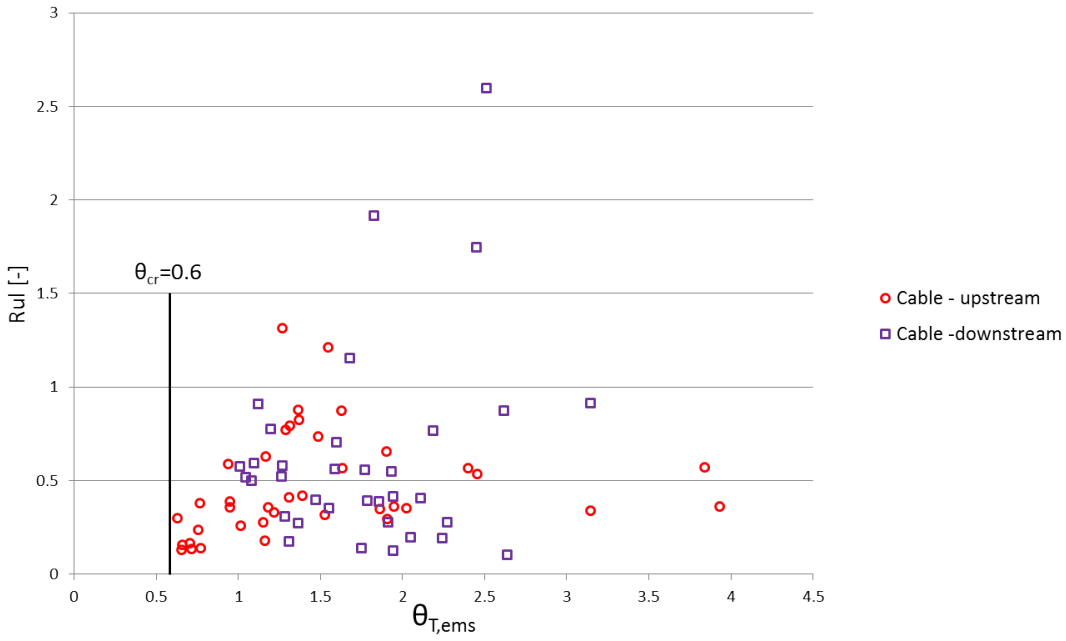

Figure 5.4: Relative uplift against $\theta_{T,ems}$ with $C_{all} = 4$ for the cable mattresses , Scheldt Flume

5.3.3 MONOPILE VELOCITY ANALYSIS

Figure 5.5 shows the relative uplift against eq. 5.1 for the flexible and medium-flexible mattresses from the Scheldt Flume tests. The flexible mattress shows a significant difference with respect to the upstream and downstream side. The downstream side shows significant lower uplifts for the same mobility number. The

medium-flexible mattress show significant lower uplifts and significantly higher mobility values. The difference between the upstream side and downstream side is less significant. The difference in uplifts is explained by the difference in failure mechanism, when the medium-mattress is sufficiently lifted it slides away as explained in Chapter 4.

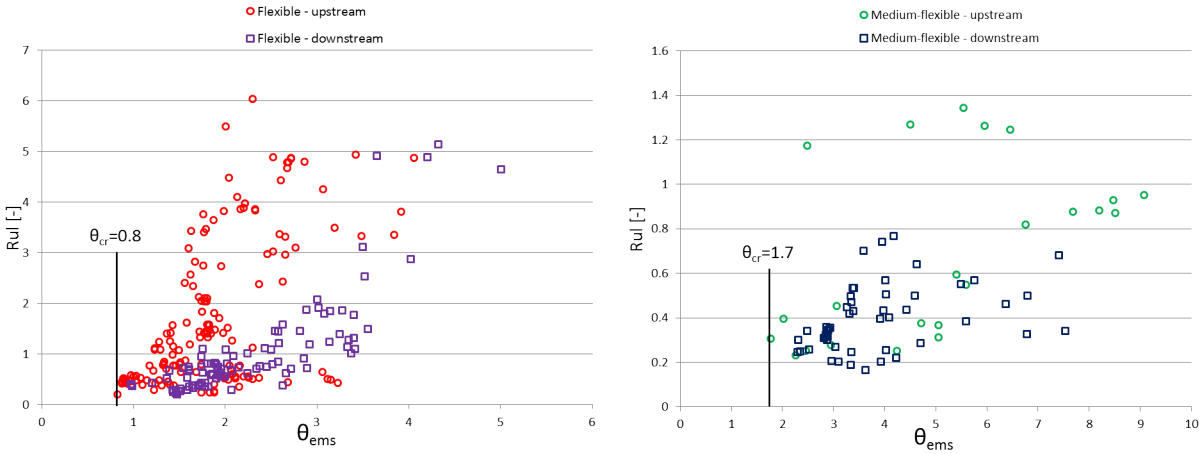

Figure 5.5: Relative uplift against θ_{ems} for the flexible (left figure) and medium-flexible mattress (right figure) for all regular wave Scheldt Flume tests

5.3.4 MONOPILE FULL MOBILITY ANALYSIS

Similar to the cable, the time of the uplift is compared to the upward (or downward) motion of the wave and the same estimation of the corresponding velocity and acceleration is performed. Figure 5.6 and 5.7 show the results.

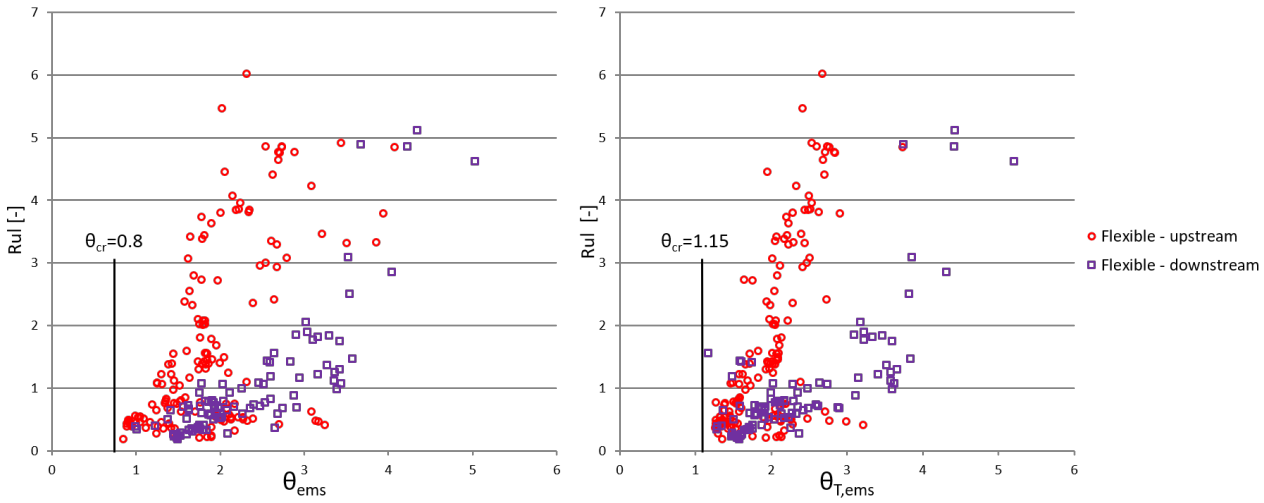

Figure 5.6: Relative uplift against θ_{ems} on the left and relative uplift against $\theta_{T,ems}$ with $C_{all} = 4$ on the right for the flexible Scheldt Flume mattress

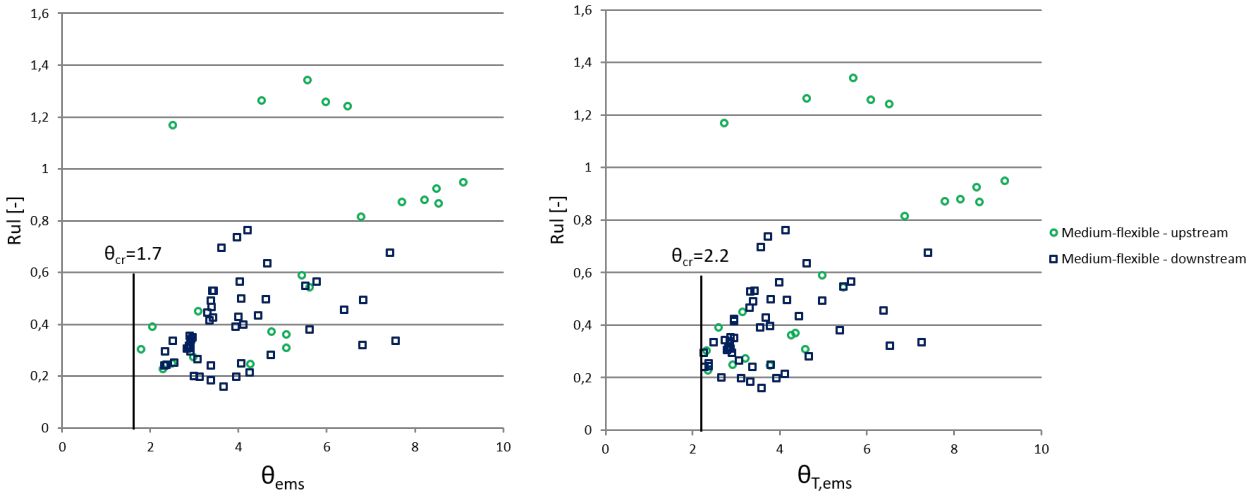

Figure 5.7: Relative uplift against θ_{ems} on the left and relative uplift against $\theta_{T,ems}$ with $C_{all} = 4$ on the right for the medium-flexible Scheldt Flume mattress

For the flexible mattress the difference is significant for the upstream side. The scatter becomes less and a clear trend is observable. The downstream scatter does not differ much. A possible explanation for this is given in the following sections.

The medium-flexible mattress shows very little difference when including the force due to inertia, just like the cable mattress. For the medium-flexible mattress θ_{cr} also shifts to the right.

The right figure of Figure 5.6 and 5.7 have been compared with the values obtained by translating the EMS signal to the edge of the upstream and downstream mattress. It was found that both methods agree well and the method described as explained in section 5.3.2 is reasonable. The comparison can be found in Appendix E.1. For both plots a coefficient of $C_{all} = 4$ is used. This value has been determine by fitting a line and looking at the correlation coefficient, R^2.

5.4 TIME DOMAIN ANALYSIS

The results from the uplift recognition software are also used in a time domain analysis. This is done by translating the velocity and acceleration to the edge of the mattress and plotting this together with the uplift in time, the forces (drag, inertia and weight) and the corresponding moments. During the force calculations the increased area of attack for the drag force is taken in account, so is the increasing weight due to the increased uplifted part. The turning point for the mattress is assumed to be at three times the uplift height. Eq. 5.6 is used to calculate the resulting moment.

$$M_{res} = F_d * arm_d + C_{all} * F_a * arm_a - F_w * arm_w \tag{5.6}$$

Figure 5.8,5.9, 5.10 and 5.11 show some results from this analysis. Figure 5.8 and 5.9 show a mattress with a large uplift. Figure 5.10 and 5.11 show a small uplift. For the momentum calculation $C_{all} = 4$ is used as obtained from the fit in the previous section, the coefficient for F_d and F_w is taken as unity. The characteristics of these test are found in Table 5.2.

Test	H_m [m]	T_m [s]	$L_{w,lin}$ [m]	h [m]
RWO_ 1cs_ 01	0.20	1.6	3.28	0.6
RWO_ 1ds_ 01	0.23	1.8	3.85	0.6
RWO_ 1bl_ 01	0.16	2	4.36	0.6
RWO_ 1bs_ 01	0.14	1.4	2.72	0.6

Table 5.2: Wave characteristics of the tests shown in Figures 5.8, 5.9, 5.10 and 5.11.

All figures below are obtained from an upstream flexible monopile mattress and show that movement starts around the maximum negative velocity, corresponding to minimum of the wave trough. The pressure difference between hydrostatic pressure and the wave trough is sufficient to lift the mattress. For Figure 5.8 and 5.9 the hydrodynamics are relative high and the uplift continues after intertia has reached it maximum. It is assumed that the drag force is big enough, due to the increased area of attack, to increase the uplift motion some more. For Figure 5.10 and 5.11 the movement starts at the same moment. But the hydrodynamics are lower in these tests and the orbital velocity is not strong enough to lift the mattress further. When analysing the moment at the maximum uplift, it can be seen that for Figure 5.8 and 5.9 this is ≈ 0 which is expected. For Figure 5.10 the resulting moment shows some strange behaviour, where Figure 5.11 shows movement starts while the moment is negative.

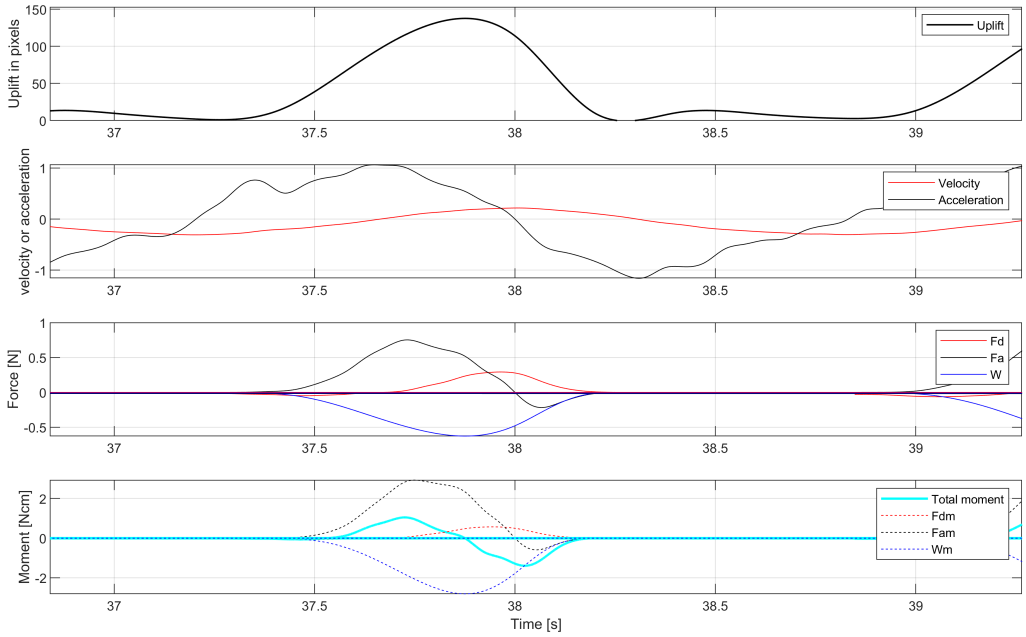

Figure 5.8: Time domain plot zoomed in on one uplift motion of test RWO_ 1cs_ 01

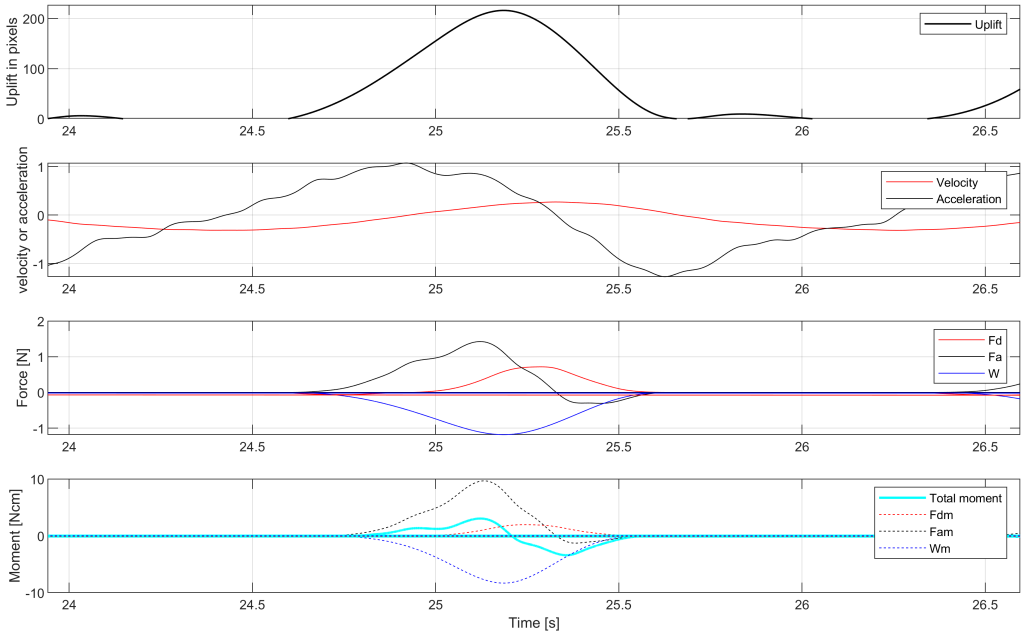

Figure 5.9: Time domain plot zoomed in on one uplift motion of test RWO_ 1ds_01

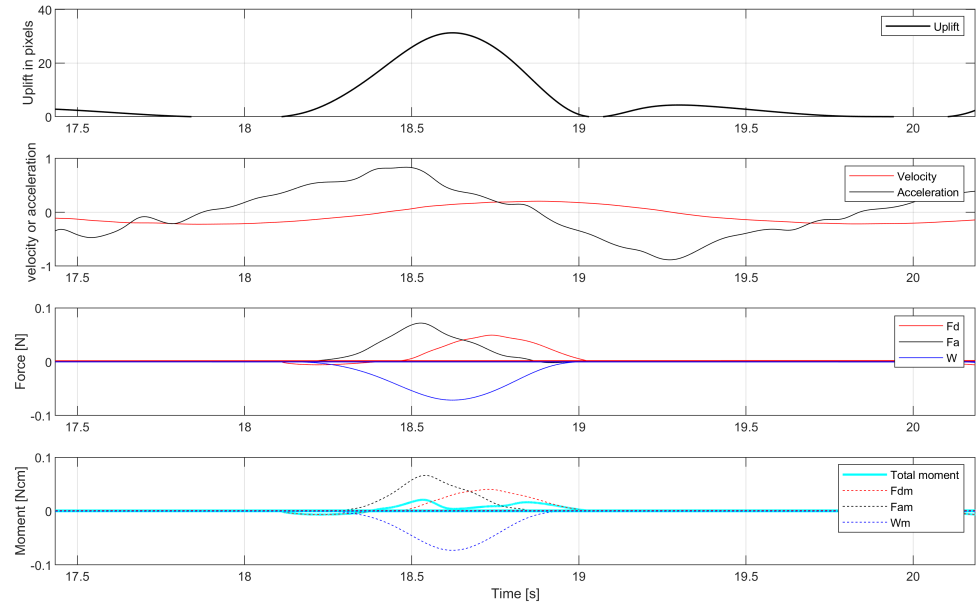

Figure 5.10: Time domain plot zoomed in on one uplift motion of test RWO_ 1bl_ 01

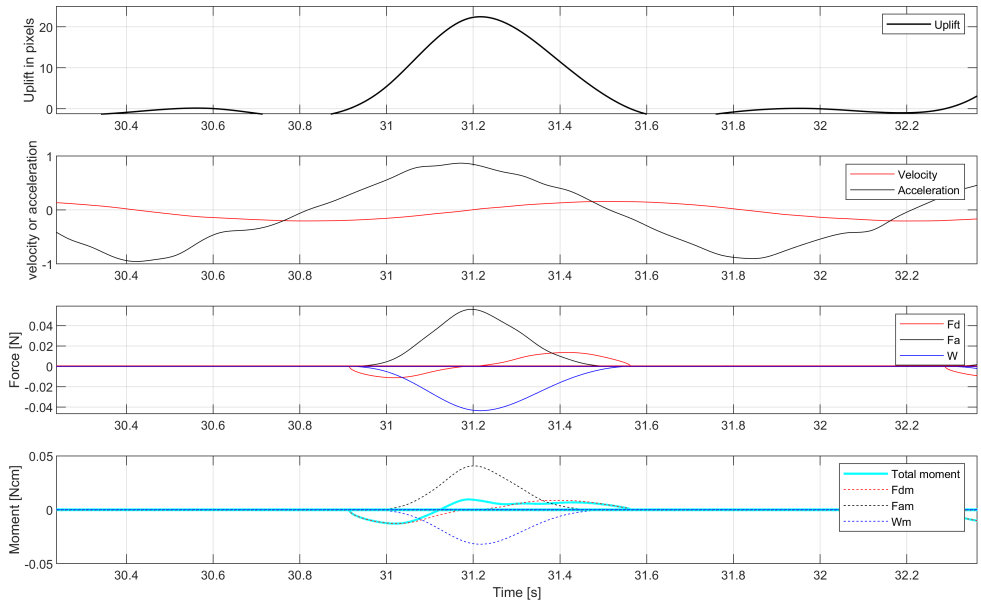

Figure 5.11: Time domain plot zoomed in on one uplift motion of test RWO_ 1bs_ 01

From this analysis it can be concluded that the fluctuating wave pressure cannot be neglected and initiates movement of the mattress. The uplift is inertia driven in all plots. This can be expressed by the inertia force with the horizontal acceleration. The plots show that the determination of F_i is not yet synchronized correctly. The length over which is lifted can be adjusted to provide a better fit. However, the current assumptions of three times the uplift already means the length over which is lifted is equal 14 cm, almost the total length of the mattress.

5.5 Evaluation

With the uplift recognition software, the mobility curve is determined for the BFM. This curve is determined by looking only at the movement of the BFM.

Using the instantaneous approach did not lead to the expected results. For the flat cable mattress there is no clear trend observed in the data and there is significant scatter, for the flexible and medium-flexible monopile mattresses the results are better.

For the flat cable mattress there is a lack of good data. There seem to be two directions of spreading of the data. One direction is expected; with an increase in force there is an increase in uplift. The second direction belongs to an increase in force but no increase in uplift. The latter direction is also seen at the upstream flexible monopile mattress and can not be explained. Also prior to different tests the cables seemed to have moved out of position from a previous test. Secondly, the mattresses, once uplifted, often slid out of position. Furthermore, some tests showed strange uplift behaviour that cannot be explained.

The flexible mattress did show behaviour as expected but showed different behaviour at the up- and downstream side of the pile. This has two reasons. One explanation is the KC-number, specific to the opposing

the wave motion, i.e. the trough of the wave creates a wake area at the upstream side of the pile and vice versa. The data shows that the KC number corresponding to the wave trough is bigger than the KC number of the wave crest. This was the results of the wave trough having, in most cases, a longer period and higher velocities compared to the wave crest. The wave trough creates a wake that is more developed than wake at the downstream side due to the wave crest. As found by Baykal et al. (2017) the wake area creates a low pressure zone. This more developed wake at the upstream side of the pile creates a lower pressure zone reducing the stability.
A second explanation can be the under pressure due to the wave trough, explained in section 5.4. For the downstream mattress, the inertia force starts prior to maximum under pressure due to the wave and the different processes do not succeed each other nicely as is the case at the upstream side. Where first the maximum under pressure occurs a followed by inertia and subsequently drag. This should however be further investigated by analysing the downstream mattress in time. Figure 5.12 show visually the different processes in time.

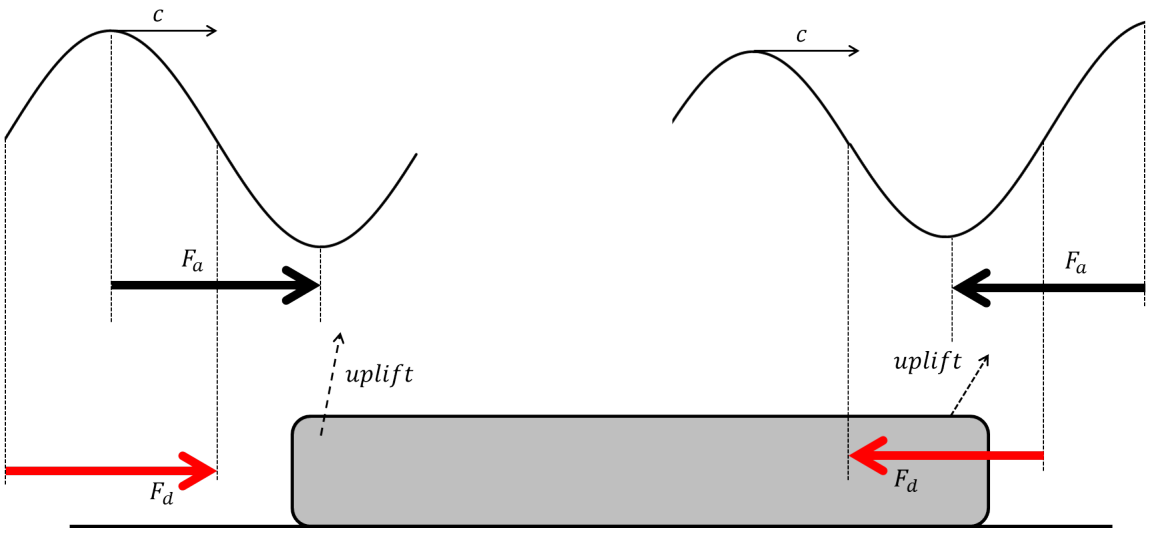

Figure 5.12: Visualisation of the forces and maximum uplift due to the fluctuating wave pressures. Wave travels from left to right.

This difference in up and downstream was not shown for the flat cable mattress and medium-flexible mattress.

The medium-flexible mattress plot should be interpreted with care. As explained in Chapter 3 and 4, the relative density for the two light mattresses differed significantly and while it was unknown which mattress was which, the lowest Δ was taken for the calculation of the mobility parameter. Also the medium-flexible monopile mattress does not lift as much as the flexible monopile mattress and is often followed by sliding. Both resulted in less data.
By comparing the plots the difference is clearly seen. The medium-flexible mattress does show a trend but is significantly different than the flexible mattress. This can be explained by the difference in uplift behaviour.

Comparing the flat cable mattress with the flexible monopile mattress, the point of initiation of motion does not differ much. The evolution of uplift seems to differ but no hard conclusion can be drawn with respect to this, the monopile mattress has significant more data. This difference was expected and due to the shape of the mattress. When looking at the full mobility parameter, a clear difference is observed for the flexible monopile mattress. The scatter decreased but the difference between the up- and downstream side remains and θ_{cr} shifts to the

right. When looking at the full mobility parameter for the flat cable and medium-flexible monopile mattress hardly any difference is seen expect a shift of the data points. For medium-flexible monopile mattress the points shift to the right, just like the flexible monopile mattress, but for the flat cable mattress the points shift to the left, reducing θ_{cr}.

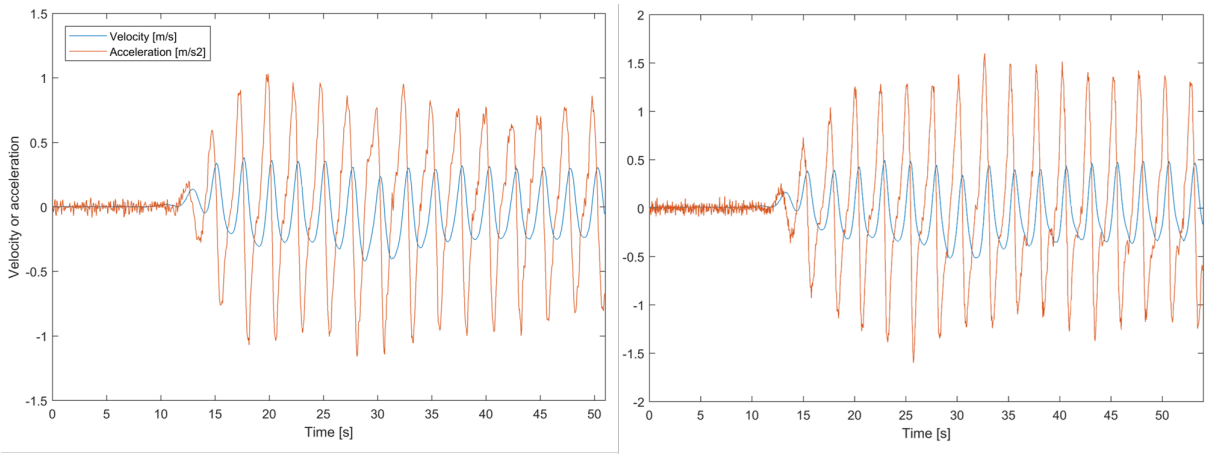

Figure 5.13: Two velocity and acceleration signals obtained from the EMS two different tests: RWO_ 1em_ 31 and RWO_ 1em_ 32

Concluding, the uplift recognition software provided us with more data to determine θ_{crit}. Secondly, it gives a promising result with respect to the mobility of the flexible mattress around a monopile and a possible explanation for the difference in the up- and downstream behaviour, but the latter must be investigated further. The time domain analysis did show that the uplift is primarily inertia driven. This however is not yet proven for the flat cable and medium flexible mattress.
The uplift recognition software was set on a limited pixel movement of 10 pixels. This could be decreased to generate more data, especially for the beginning of movement zone. However, the HSV-ranges are influenced by light. This already resulted in polygons not exactly drawn the same for two successive frames. When decreasing the limited pixel movement, more movements are found but more effort must be done to filter the correct movements from the changing light and moving of the rubber top layer.

From the uplift recognition analysis the following values are obtained.

	Flexible, monopile	Flexible, flat mattress cable	Medium-flexible, monopile	Method	Data
θ_{cr}	0.8	0.8	1.7	Uplift recognition	EMS
θ_{cr}	1.15	0.6	2.2	Uplift recognition	EMS/LWT

Table 5.3: Found θ_{cr} per , EMS = measured values and EMS/LWT = combined

6
DESIGN METHOD

6.1 INTRODUCTION

In this thesis the hydrodynamic stability of a ballast filled mattress under waves is being investigated. This is done with three different methods for regular waves. In this chapter the results are summarized and a design method is given to practically apply a ballast filled mattress for irregular waves.

To design a prototype ballast filled mattress it is necessary to define the important structural parameters. These are given in Chapter 4. Other aspects like mattress shape, installation and filling method have been left out of the scope of this research. The design method is based on the critical value of θ, obtained from the analyses done in this research. The flexibility of the ballast filled mattress is based on its ability to follow edge scour.

First the results from the different analysis are presented and a θ_{cr} is chosen that will be used for the design method. Then the design method is explained and followed by a case study.

6.2 DESIGN METHOD

6.2.1 DETERMINATION OF CRITICAL STABILITY NUMBER

A ballast filled mattress used as scour protection should not slide/flush away during a design storm but is allowed to lift to some extend. However, systematic uplifts and movement must be avoided but an occasional higher uplift is not assumed to be problematic. Furthermore, the mattress should be flexible enough to follow edge scour to mitigate undermining. For this reason the data of the flexible monopile mattress is used.

From the different analyses done in this research, multiple θ_{cr} are found, shown below in table 6.1. The θ_{cr} is either determined with linear wave theory, with the values obtained by the EMS or a combination of both, each with its own method. These methods are discussed in Chapters 4, 5 and Appendix D.

	Flexible, monopile	Flexible, flat cable mattress	Method	Data	Chapter
θ_{cr}	0.45	0.6	Stability	LWT	4
θ_{cr}	0.53	0.69	Mobility	LWT	Appendix D
θ_{cr}	0.8	0.48	Mobility	EMS	Appendix D
θ_{cr}	0.8	0.8	Uplift recognition	EMS	5
$\theta_{T,cr}$	1.15	0.6	Uplift recognition	EMS/LWT	5

Table 6.1: Found θ_{cr} for initial uplift per analysis for the Scheldt Flume tests. Method means which analysis method is used as described in this thesis. Data means if linear wave theory (LWT), the measured values (EMS) or a combination of both (EMS/LWT) is used for the determination of θ

The θ_{cr} differs significantly for the different methods. The difference is due to the different accuracies at which the analyses were performed. For the design method the value of $\theta_{cr} = 0.8$ obtained from the uplift recognition, using the maximum velocity is used. The uplift recognition provided enough data to give a safe first estimate for θ_{cr} and the development of uplift. Errors and uncertainties regarding this method have been explained in Chapter 5.

6.2.2 METHODOLOGY

θ_{cr} is found for regular waves and is applied in an irregular wave field. To translate this towards an irregular wave field a Rayleigh distribution, see eq. 6.1, is taken for the design storm.

$$P(\underline{H} > H) = \exp(-2(\frac{H}{H_{m0}})^2) \tag{6.1}$$

The design method requires the H_{m0}, T_{m02} and the water depth for the given location. With H_{m0} the probability of a certain wave height can be calculated which is subsequently used for the velocity determination according to linear wave theory given in eq. 6.2.

$$u_w = \frac{\omega H}{2sinh(kh)} \tag{6.2}$$

For the velocity determination T_{m02} should be used while Longuet-Higgins (1983) and Goda (2011) found that for the period of single waves for a narrow-banded spectrum higher waves tend to convert to T_{m02}.
With the known velocity, corresponding to a wave height and probability of occurrence, θ can be calculated according to eq. 6.3

$$\theta = \frac{u_w^2}{\Delta g d} \tag{6.3}$$

Due to the direct relation between the wave height and velocity, the resulting θ's can be assigned to the corresponding probability of occurrence. An estimate of the uplift height is given by eq. 6.4 per θ. The determination of this equation can be found in Appendix F.1.

$$Rul = \frac{uplift}{thickness} = 0.285\theta^2 + 1.679\theta - 1.57 \tag{6.4}$$

Finally, the Poisson distribution ,$P = (1 - (1 - P_{occurrence})^N$, is used to calculate the probability for exceedance

of a specific uplift obtained from eq. 6.4.

To conclude the hydrodynamics of the design method, it should be checked and designed for, such that

- for $H_{0.1\%}$, θ should equal to (or lower than) 1.2, this translate in a relative uplift of 1.
- A relative uplift of 3 (failure) should have a probability of exceedance smaller than 5%

This will give all information regarding the stability of the ballast filled mattress. The flexibility of the mattress should be such that the mattress is able to follow (edge) scour. No elastic modulus or effective bending stiffness is known and therefore the flexibility of the mattress is expressed in a practical design criteria. This criteria states that:

- if the uplift of the mattress is one time the thickness of the mattress, the uplift length, the length over which the mattress is lifted from the ground, should not exceed 2 times the thickness of the mattress.

This can be determined by applying the same procedure done in this research for the stiffness tests, and measuring the uplift length (the length over which the mattress is lifted). It is assumed that when this is the case, the mattress is flexible enough to follow (edge) scour. Resulting in a more streamlined and stable position according to Schiereck & Verhagen (2012). Furthermore it is less likely that failure due to sudden sliding of the mattress will not occur.

With the above mentioned steps and formulas a preliminary design can be made for the ballast filled mattress. A case study with the above given methodology is given below. The uncertainties with respect to this methodology can be found in section 7.4.2.

6.3 Case study: The German Bight

The ballast filled mattress and its installation system is a solution for the suction bucket jacket installed at a greater distances offshore and in deeper waters. For this reason, it is chosen take field data from the German Bight for an assessment of the stability of a prototype mattress.

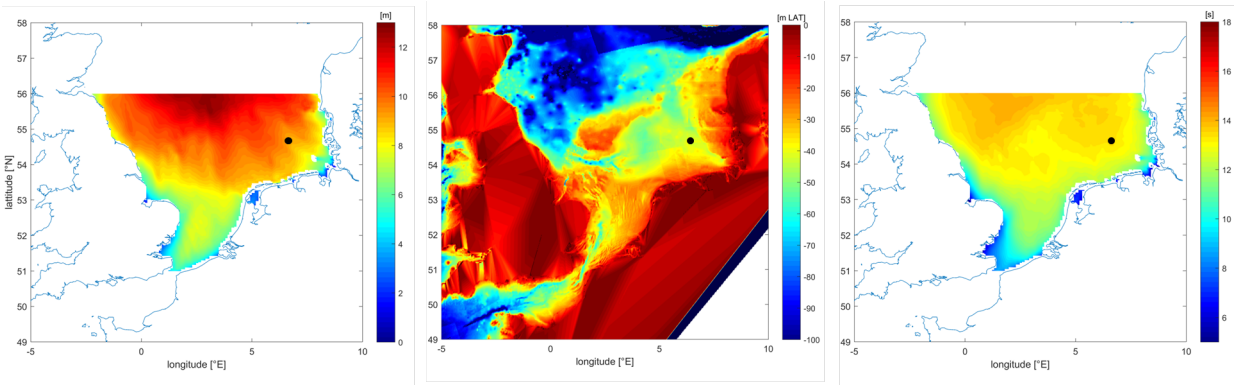

Figure 6.1: Left figure: North sea significant wave heights, middle figure: North sea water depth, right figure: North sea peak periods (Deltares, 2017). Black dot indicates the location

From Figure 6.1 the corresponding storm values are obtained, and together with the maximum ballast filled mattress characteristics presented in this research, are presented in Table 6.2.

		unit
H_s	11	m
T_p	14	m
T_{m02}	11.2	s
depth	41	m
Duration	1000	waves
Mattress thickness	0.6	m
Δ	1.1	-

Table 6.2: Typical 1/50 year storm characteristics for the German Bight

Assuming $H_s = H_{m0}$ and applying eq. 6.1, the corresponding θ's can be calculated according to linear wave theory given in eq. 6.2. This is shown in Figure 6.2.

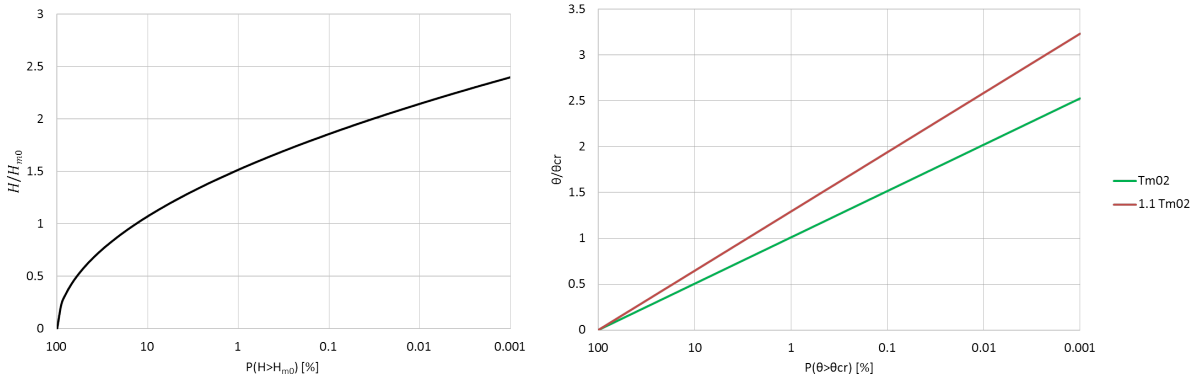

Figure 6.2: Left figure: probability of occurrence versus the normalised wave height, right figure: probability of occurrence versus a normalised θ

By applying eq. 6.4 together with the Poisson equation, the probability of exceedance of a certain uplift height is calculated.

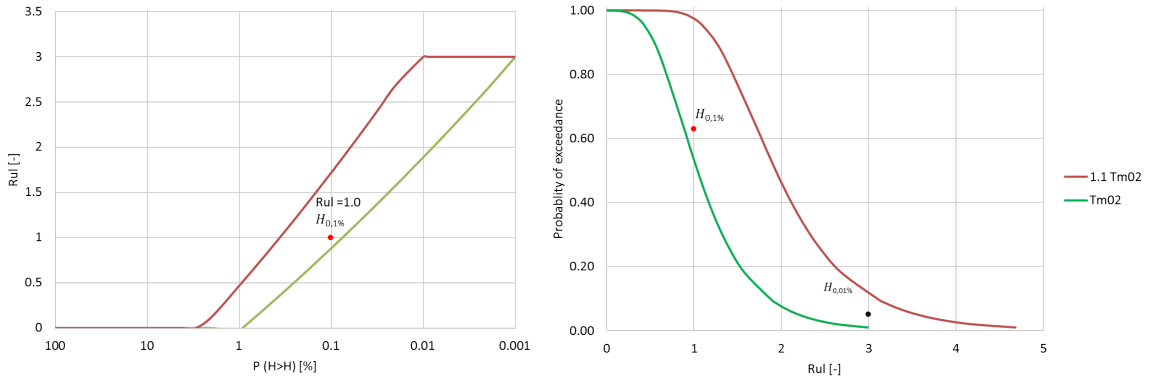

Figure 6.3: Probability of exceedance of a specific uplift height given for T_{m0} and 1.1 times T_{m02}. The red dot indicates $H_{0.1\%}$ for the first design criteria, the black dot indicates $H_{0.01\%}$ for the second design criteria

The design criteria are that for $H_{0.1\%}$, the relative uplift must be equal to or lower than 1. From the left graph of

Figure 6.3, the red dot indicated the first design criteria and it can be seen that this criteria is met for T_{m02}. The second criteria is obtained from the right graph of Figure 6.3 and it the probability of exceeding a relative uplift of 3 is below the black dot indicating 5%. Thus for this case, both conditions are satisfied and the ballast filled mattress can be applied for this location.

All figures presented in this case study showed two periods and the difference is clearly seen in the figures. If a higher period is used in the assessment of the ballast filled mattress for this case, it would not meet the design criteria. This is further discussed in section 7.4.2

7 DISCUSSION

7.1 INTRODUCTION

In the previous chapters, the different test set-ups have been explained, the scale models of the ballast filled mattress were introduced and the stability of the ballast filled mattress was studied with different methods resulting in a design method. In the following sections, topics that are relevant for the above mentioned categories are considered which can influence the validity and accuracy of the tests and results.

7.2 SMALL SCALE TESTS

In this section, aspects with respect to the small scale tests are discussed which could have had an influence on the behaviour and stability of the ballast filled mattress.

Reflected waves
The regular wave tests are performed within a wave flume and reflection of waves happen, even though a wave dissipation slope was placed at the end of the flume. The data has not been filtered with respect to reflected waves, as proposed by Mansard & Funke (1980). As this research mainly looked at regular waves, the reflection of waves is assumed to be small. As explained in Chapter 3, the wave dissipation slope could be adjusted per test for maximum wave damping but complete wave damping is not possible. As the interest was with the measured values by the WHM and EMS and there is no particular interest in the spectrum, the wave reflection is neglected. The WHM and EMS signal often showed the signal to change significantly after $\approx$ 40 seconds, the time a wave would approximately need to reflect and pass the EMS/WHM again.

The reflected waves could have an influence on the velocity at the location of the mattress. During the analysis it was unknown what the exact hydrodynamics were at the mattress and what possible effects the reflected waves had in this.

Gap-width
During the tests, multiple gaps occurred between the mattress and the flume bed. This gap width was not measured or taken in account when doing the scale tests, but it influences the stability of the ballast filled

mattress. The gap width allows a pressure to protrude below the mattress. The thickness of the gap together with the length, and evolution of the gap thickness over this length, determines the pressure distribution. During the tests there was no control of the variation of this gap thickness and the extent to which this pressure influenced the stability thus unknown.

Position of the flat cable mattress
From the photos and video recordings of the flat cable mattress it was not possible to determine if the mattress is still in correct position or was slightly moved out of position. The angle of the mattress with respect to the flow influences the stability.

7.3 Scale Models

The items treated in this section are about the scale models used in the different tests.

Degree of filling
The mattresses tested in the Scheldt Flume and Atlantic Basin were filled with a combination of loose rock in combination with another fill material or solely with loose rock. The degree of filling however was approximately only 50-60% for the Scheldt Flume cases, the filling of the Atlantic Basin mattresses were approximately 70-80%. The degree of filling greatly influences the flexibility of the mattresses. For the Scheldt Flume mattresses it was such that the rubber sheets, responsible for the stiffness off the mattress, had a significant slack. This will have influenced the stiffness, thus the stability of the ballast filled mattress.

Scale model
The scale model used for the Scheldt Flume tests consisted of two halves and the scale model used for Atlantic Basin test consisted of one mattress as a whole. A prototype mattress will consist of multiple mattresses connected to each other. The connection between the mattresses is most likely to be a stiff connection, changing the uplift behaviour of the mattress. The difference between the behaviour is shown in Figure 7.1 for the Delta Flume mattress.

Scaling of the mattress
The medium-flexible mattress is found to be too stiff to follow edge scour and therefore not included in the design method. The scaling of stiffness is complex and in general a flexible material on prototype scale will lead to a more stiff material once scaled down (Heller, 2011). The flexibility of the medium-flexible mattress could therefore on a prototype-scale be sufficiently flexible to follow (edge) scour.

Figure 7.1: Left photo showing loose ballast filled mattress components, right photo showing the ballast filled mattress connected to each other

Monopile tests only
Tests aimed at the stability of the mattress are only performed with a monopile. The most likely application of the ballast filled mattress is around the suction cans of a suction bucket jacket. If the stability of the mattress is influenced by the presence of a pile, this effect will be less for the suction bucket jacket due to the smaller dimensions with respect to a monopile.

7.4 Stability determination

The items treated in this section are about the accuracy of the different stability determinations.

7.4.1 Stability analysis

Movement determination
The determination of no movement and movement for the stability analysis in Chapter 4 is done by analysing the videos with respect to movement. It was hard to differentiate between very small uplifts or just movements of rubber. Especially at the far end of the mattress that was not visible on the camera. Tests corresponding to no movement can therefore have been assigned to movement due to uncertainty. Possible further research in the determination of movement and no movement will have this same problem with the available data.

The uplift recognition software was not calibrated for the purposed used in this research. The squares were not placed exactly in the middle at the most up- or downstream point of the mattress. Secondly, the mattresses were positioned slightly different throughout the tests, resulting in the squares being more towards or away from the most upstream point. The pixel to centimetre ratio has not been calibrated for each test and will in cases overestimate or underestimate the amount of uplift.
Also, the lack of calibration and the unknown angle of the video camera give errors in the conversion of the amount of uplift in pixels to centimetres.

Choice of θ
The stability parameter used in this research can give a good approximation for the initiation of motion for one specific mattress. But for describing and understanding the behaviour of the mattress, θ used in this research is not an universal parameter. For an universal expression that can be used for any mattress to asses the stability,

θ should be extended to the time domain as explained below.

Time domain analysis
The time domain analysis gave a more theoretical visualisation of the importance of the two parameters used in this research. This concluded that the upstream flexible mattress is inertia driven. The drag force due to the velocity seemed to have little effect on the evolution of uplift. It should be noted that the plots given in Chapter 5 are obtained with many assumptions. A better expression for the area of attack for drag and uplift length will provide an even better fit for the method applied in this research.

The timing of F_i was not synchronised yet with the start of uplift. This could be fitted by increasing the turning point, which will increase the inertia force due to the dependancy of the volume. This has limitations, the current turning point is estimated with three times the uplift height. The example given in Chapter 5 already showed that increasing the length, the length of the mattress is exceeded. This should be better determine by a new test series.

7.4.2 DESIGN METHOD

Determination of θ_{cr} and the evolution of uplift
θ_{cr} is taken from the uplift recognition analysis and obtained from looking at the lowest θ found. This θ represents a movement due to the fact that the uplift recognition script only detects movement of $\approx 0.2mm$ for the monopile mattresses and $\approx 0.15mm$ for the flat cable mattress. θ_{cr} is directly related to the limited pixel movement and the method to isolate the uplift height from the data. The detection of movement is sensitive to changes in light, location of the coloured square (with respect to the calibration image used for the pixel to centimetre determination in Chapter 5) and the moving of the rubber sheet. The determination of the uplift height with the uplift analysis script also includes small errors.
This means $\theta = 0.8$ is taken around the point where a significant noise is present and no further safety is given to this value and taken as start of movement.

The evolution of uplift, used in the design method is obtained by looking at the conservative side of all data and plotting the average. Due to the significant scatter in the data and the difference between the up- and downstream side of the monopile this again results in a conservative estimate for the uplift height, especially up to a relative uplift height of two.

Choice of linear wave theory
θ_{cr} from the design method given in Chapter 6 is obtained from velocities measured by the EMS. The proposed design method uses linear wave theory for practical reasons. Linear wave theory gives a good first prediction for the orbital velocities at the bottom. Comparing linear wave theory with the measures values from the EMS showed that for higher non-linear waves linear wave theory over predicts the velocity, see Figure D.2. For a better determination of the velocity for non-linear waves higher order stokes theory can be used, as shown in Figure D.5. For irregular waves, linear wave theory predicts the velocities at the bottom reasonably well and higher order stokes do not significantly increase the accuracy. For a better prediction of the velocity for irregular waves, numerical models can be used like the Boussinesq model or Swash.

Choice of velocity
The calculation of θ, assuming maximum velocity is responsible for the maximum uplift is found to be false. By including the inertia term the scatter was decreased and a better fit was obtained. However, using the full stability expression has a disadvantage. The hydrodynamics needed for this instantaneous approach can only be obtained by measuring equipment or by a complete CFD model, which both are not practical for a preliminary design.

Furthermore, the translation of the EMS signal towards the edge of the mattress by using linear wave theory, induces errors while linear wave theory is not valid. It does give an indication but should not be used determining the exact hydrodynamics at the time of uplift. The same accounts for assuming linear wave theory between crossing found from analysing the data, even though the signal showed high non-linearity. But by using these methods the importance of inertia becomes clear.

Regular wave vs irregular waves
θ_{cr} is based on regular waves but applied to irregular waves. For regular waves the hydrodynamics are more or less constant, which in most cases result in systematic uplifts. For irregular waves the hydrodynamics are constantly changing. This results in sudden uplifts. For this reason the design method, based on $theta_{cr} = 0.8$ is also performed on the irregular wave tests done in the Scheldt Flume. By calculating the corresponding H_{cr} that corresponds to $\theta_{cr} = 0.8$, an estimation can be given with the expected amount of movements. This is done by multiplying the probability obtained from H_{cr} with the total number of waves, which gives an average amount of waves that is higher. Table 7.1 gives the expected movements with respect to the observed movements.

IWO_1cm_01		unit			unit
H_{m0}	0.14	[m]	Δ	0.2669	[-]
movements	49	[-]	t	0.0106	[m]
waves	623	[-]	h	0.613	[m]
T_{m02}	1.37	[s]			
H_{cr}	16	%	$H_{\%}$	8	%
expected movements	100	[-]	θ_{cr}	1.19	[-]

IWO_1dm_31		unit			unit
H_{m0}	0.16	[m]	Δ	0.3705	[-]
movements	5	[-]	t	0.0126	[m]
waves	596	[-]	h	0.61	[m]
T_{m02}	1.54	[s]			
H_{cr}	18	%	$H_{\%}$	0.8	%
expected movements	108	[-]	θ_{cr}	2.32	[-]

IWO_1em_31		unit			unit
H_{m0}	0.18	[m]	Δ	0.3705	[-]
movements	20	[-]	t	0.0126	[m]
waves	594	[-]	h	0.613	[m]
T_{m02}	1.55	[s]			
H_{cr}	25	%	$H_{\%}$	3.3	%
expected movements	150	[-]	θ_{cr}	1.62	[-]

Table 7.1: Results of the irregular waves tests

A second check is to estimate the θ_{cr} based on the Rayleigh distribution. The observed amount of movements is divided by the total amount of waves. This gives an estimate for $P(\underline{H} > H)$ and the corresponding $H_{\%}$ is determined. Using linear wave theory, the corresponding θ_{cr} is calculated. This resulted in the following θ's: 1.19, 2.32 and 1.62.
Both checks showed that the design method based on $\theta_{cr} = 0.8$ with the design criteria of $H_{0.1\%}$ and linear wave

theory gives a conservative design for these specific cases. It is expected this is the case for most irregular wave cases but should be investigated further.

Choice of period

The design method presented in Chapter 6 showed the assessment of the ballast filled mattress for two different periods corresponding to a wave; T_{m02} and $1.1 \times T_{m02}$. The difference between the two periods is significant and whether the mattress satisfies the design criteria depends on which period is chosen. According to Longuet-Higgins (1983) and Goda (2011) using T_{m02} is a first good approximation. To get a better estimate on which period to use, a Monte Carlo simulation should be performed with the joint probability density function given by Longuet-Higgins (1983) and use this in the design method.

For safety reasons one could choose to use the higher period for the design of a ballast filled mattress. If this will not satisfy the design criteria,the structural parameters can be increased. This is explained below

Structural parameters

The velocity used θ is highly dependent on the period as shown in Chapter 6. A higher period will increase the velocity, thus θ. The assessment is based on the currently available thickness and Δ. But these can be further increased.

The thickness of the mattress is set at 0.6 m due to current constructional constraints. But can most likely be increased. The increase of thickness should not be more than 10-15% as the mattress will loose its thin layer advantage.

The maximum Δ can be increased with further research and testing. Compared with the thickness, Δ can be increased with more than 10-15%.

The difference of the increased structural parameters is applied to the case study of Chapter 6 and shown in Figure 7.2.

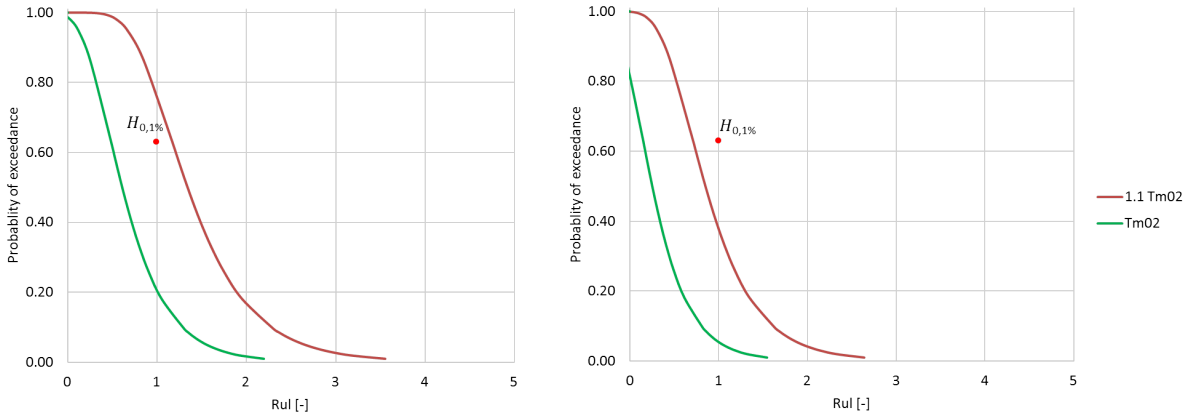

Figure 7.2: Probability of exceedance of a specific amount of uplift for three different wave periods. Left graph for $t = 0.7m$ and $\Delta = 0.6$, right graph for $t = 0.6$ and $\Delta = 1.5$

Choice of flexible mattress

The design method is based on the results from the flexible monopile mattress. However, as previously mentioned: a flexible prototype mattress will when scaled down behave more stiff. This is checked by a quick analysis of the Delta Flume mattress. The Delta Flume mattress is a scaled prototype mattress and will represent the flexibility better due to a smaller scale factor. From the left photo of Figure 7.1 the uplift behaviour is similar to that of the flexible monopile mattress from the Scheldt Flume as seen in Chapter 4. A

quick analysis performed on the stability of the Delta Flume mattress showed that minor uplifts happen for θ around 1.4. This would imply that the prototype mattress will behave similar as flexible mattress but has the stability of the medium-flexible monopile mattress.

Applying the design method explained in Chapter 6 and applying $\theta_{cr} = 1.4$ the result changes significantly. This is shown in Figure 7.3. The initiation of motion for the medium-flexible mattress (given by $\frac{\theta}{\theta_{cr}} = 1$) happens in the worst case for $H_{0.2\%}$ which is a significant improvement with respect to the flexible monopile mattress, for which occurs around $H_{3\%}$.

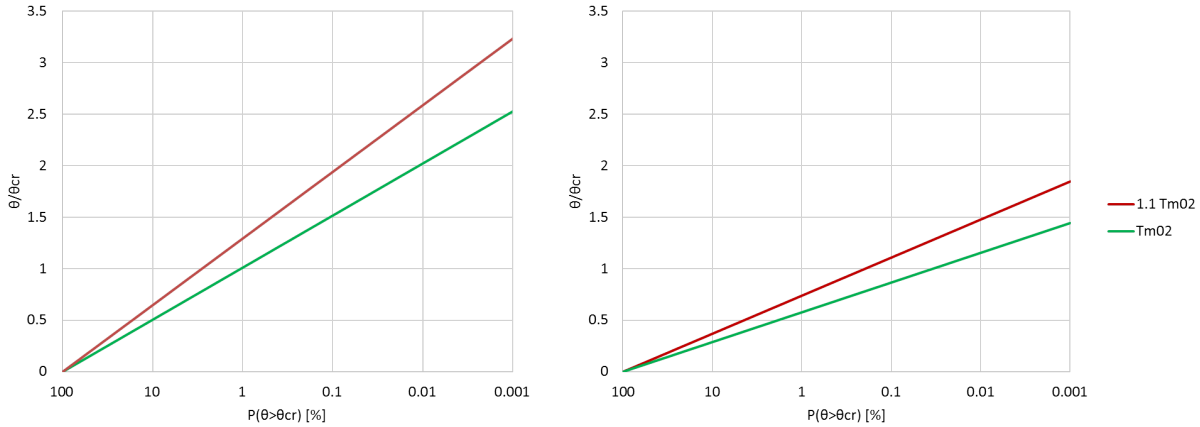

Figure 7.3: Left graph showing the flexible monopile mattress, right graph showing the medium-flexible monopile mattress

Flexibility criteria
The flexibility criteria is based on the stiffness tests of the flexible mattress performed in this research. The flexible mattress was able to follow the edge scour in comparison to the medium stiff mattress. During the stiffness tests the uplift length, the length over which the mattress is lifted, was not measured. But based on visual observations an estimate is given with respect to this uplift length, this estimate is the value given in the flexibility criteria. However it is unknown how this will translate to a prototype case and this criteria is based on a mattress which does not represent a prototype mattress well.

The idea behind the criteria is based on the turning point of the uplift. The closer the turning point is to the edge of the mattress, the easier the mattress can follow (edge) scour.

8 CONCLUSIONS

In this chapter the conclusions on the hydrodynamic stability of the ballast filled mattress are presented. This will be based on the research questions and sub-questions stated in Chapter 1 and ended with the design method.

8.1 CONCLUSIONS

The main goal is to investigate the hydraulic stability of a BFM under wave loads and to define a design criterion. In order to answer this question, the four sub-questions given in Chapter 1 must be answered. First, the failure mechanisms of the ballast filled mattress were identified. The failure mechanisms found in this research are uplift and undermining. Uplift is the lifting of the (edge) of the mattress. Once the mattress has lifted, the chance of sliding increases because the resisting friction force reduces with reducing contact area between the BFM and the seabed. Sliding always happens successively after an uplift event and happens fast. Therefore, both are categorized as uplift failure. Undermining is caused by scour of sediment from beneath the ballast filled mattress. These failure mechanisms are two-fold. Uplift is seen as the governing failure mechanism and when there are (hardly) no uplifts, undermining should be mitigated.

Secondly, the governing hydraulic parameters that can be used to asses the stability are found. The parameters found are the orbital velocity and the acceleration at the sea bed. The orbital velocity is responsible for a drag force on the mattress and the stagnation pressure, responsible for a lift force below the mattress once there is a small gap between the mattress and sea bed. From the uplift recognition analysis it was found that the acceleration of the orbital velocity is of importance to the forcing and significantly increased the fit for the flexible monopile mattress. With these two parameters the stability of the ballast filled mattress can be described reasonably well.
A time domain analysis showed that initiation of motion happens due the under pressure due to wave fluctuations. Furthermore, this showed that the uplift is actually inertia driven for the upstream flexible mattress, with little effect of the drag force. This also showed that for a correct stability formulation the time effect cannot be neglected. But these plots must be interpreted with care while they are obtained with many assumptions.

The governing structural parameters of the ballast filled mattress are the weight and bending stiffness. The analysis showed that the weight (Δd) of the mattress governs its stability. Secondly, the stability and mobility analysis showed that the stiffness influences the stability of the mattress. The more stiff a mattress is, the more resistant it is against uplifts. The bending stiffness determines the size of the lifted part. Thus the higher the bending stiffness, the more mass is mobilised and more mattress needs to be moved which increase the amount of added mass. Both are resisting against forces that oppose the uplift motion.
The stiffest mattress hardly shows any uplift, but the main mechanism is sliding. This can be seen as a stiff beam that need to be lifted as a whole. Once it is lifted it loses connection with the bed and the orbital motion of the wave will transport it in up- or downstream direction.
The bending stiffness of the ballast filled mattress is important for two reasons. First is increases the resistance against uplift thus benefiting the stability. Secondly, the bending stiffness is important for it ability to follow (edge) scour. Scour mitigation tests done in this research showed that only the flexible mattress was able to follow (edge) scour and stop undermining.

To finalize, it was tested with what mixture the mattress can be filled. One test regarding the filling of the mattress has been performed during this research. The mattress was filled with a mixture of water, bentonite clay and sand that is still pump-able. By adding the bentonite clay, the sand carrying capacity of the water increases. This assures the sand will stay in suspension and is equally distributed within the mixture. The mixture used in the tests had a density of approximately 1400 kg/m^2. When using the same materials and using barite as weighting agent, a mixture with a density up to 2100 kg/m^3 can be achieved. Literature showed even higher densities are possible.

How can the hydrodynamic stability of a ballast filled mattress under waves be described?

This research, done on the hydrodynamic stability of the ballast filled mattress under waves based on tests with regular waves, gives a first conservative estimation on the start of movement and the development of this movement for regular waves. The expression to describe a stable mattress, based on the flexible monopile mattress, is given below:

$$\Delta d = \frac{u^2}{0.8g} \tag{8.1}$$

in which: Δ = Relative density [-]
d = thickness of the mattress [-]
u = orbital velocity at the bed [m/s]
g = gravitational acceleration [$\frac{m}{s2}$]

Eq. 8.1 is obtained by using the expression $\theta = \frac{u^2}{\Delta g d}$ and using $\theta_{cr} = 0.8$. The hydrodynamic attack in this definition of θ is only based on the velocity and initial thickness of the mattress. The inertia term is not added for practical reasons. The velocity can be obtained by either linear wave theory, higher order stokes theories or numerical models like the Boussinesq model or Swash. Linear wave theory will over predict wave velocities and will provide a more conservative estimate of the velocity. Higher order stokes theories and numerical models will give a better prediction of the velocities at the sea bed. Eq. 8.1 gives a required Δd for the mattress to be stable. If one does not allow the mattress to move, this value should not be exceeded.

If some movement is allowed, the normal expression, given in eq. 8.2, can be used for an estimate of the amount

of uplift of the ballast filled mattress. This is further discussed in the section below.

$$\theta = \frac{u^2}{g\Delta d} \tag{8.2}$$

8.2 Design method

A design method for irregular waves is presented that can be used for a first assessment of the stability of the ballast filled mattress. When T_{m02}, H_{m0} and the water depth, h, are known for design storm, eq 8.3 can be used to predict the uplift height of the ballast filled mattress. Assuming a Rayleigh distribution for the wave heights and using linear wave theory to compute the orbital velocities, the corresponding values of θ can be calculated and subsequently the uplift height.

$$Rul = \frac{uplift}{thickness} = 0.285\theta^2 + 1.679\theta - 1.57 \tag{8.3}$$

The design criteria state that for

- $H_{0.1\%}$, θ should be equal to (or lower than) 1
- a relative uplift of 3 (failure) should have a probability of exceendance smaller than 5%

The velocity calculated according to linear wave theory will overestimate the velocity at the sea bed for irregular waves. A numerical model like Swash, that includes irregular waves, can be used to calculate the velocities more accurate. A quick analysis of the irregular wave test from the Scheldt Flume and Delta Flume showed that $\theta_{cr} = 0.8$ is conservative. The determination of the relative uplift is also taken conservatively, which conclude that using this design method gives a conservative preliminary design method.

The first criteria can be checked with eq. 8.3, the second criteria can be checked with the Poisson distribution for exceedance.

The flexibility of the mattress must be such that it is able to follow edge scour and for this a practical design guideline is given that

- if the uplift of the mattress is one time the thickness of the mattress, the uplift length, the length over which the mattress is lifted from the ground, should not exceed 2 times the thickness of the mattress.

This criteria will ensure the mattress is flexible enough to follow edge scour.

9 RECOMMENDATIONS

Based on the discussion and conclusions given in the presented in Chapters 7 and 8, recommendations are given with respect to further investigate the hydrodynamic stability of the ballast filled mattress.

1. No tests have been performed that include a dynamically stable mattress, thus occasional uplift but no failure, and a moveable bed. More tests should be performed to check the influence of a moving mattress on a moveable bed. This can check if the ability to follow (edge) scour is beneficial for the stability of the mattress and if a moving mattress has negative effects on the scour development.

    - The Scheldt Flume tests did not include a movable bed. During the Atlantic Basin test the mattress was stable and no uplifts were observed.

2. Instead of describing the behaviour of the ballast filled mattress, the initiation of motion should be further looked into for different hydraulic parameters. The critical value at which movement start is of more practical interest.

    - More movement categories should be applied to the stability analysis performed in this research. The categories should give more information about what kind of movement, how often the movement occurs and the magnitude of the movement. This should be done for irregular wave test. Because irregular waves are more realistic and such tests contain waves with many different wave heights, resulting in a wide range of uplift/no uplift events. This will make an accurate determination of the exact stability criterion easier.
    - A waveform approach could be applied in order to determine the effect of inertia on the initiation of motion. A parameter like H/L could be used or other acceleration parameters,like a_{spike} proposed by Drake & Calantoni (2001).

3. The Delta Flume tests should be analysed with respect to initiation of motion and the parameter used in this research.

    - The EMS in the Delta Flume is aligned with the upstream mattress and the time difference is zero. Resulting in the exact hydrodynamic conditions at the time of uplift. The velocity and acceleration can both be determined at the time of uplift.

4. The filling of the Delta Flume mattress represents a prototype filling better and should be checked on its ability to follow scour.
    - Furthermore, if the Delta Flume mattress is able to follow (edge) scour this will increase the stability criteria significantly from $\theta_{cr} = 0.8$ to around $\theta_{cr} \approx 1.4$.
5. The critical value and design method presented in this research must be applied to tests with irregular waves plus current.
    - No irregular wave plus current tests have been performed in the Scheldt Flume for the flexible mattress. New tests should be performed
    - The new tests should also include tests with waves in multiple direction with respect to the current.
    - Irregular waves plus current tests have been performed in the Atlantic Basin. But no movement was observed throughout these tests and the method can be applied to these tests to verify a stable mattress.
6. In general the stiffness of the Scheldt Flume mattresses should be tested (again) and the bending stiffness should be determined, with emphasis on the uplift length. The same accounts for the Delta Flume mattresses
    - The difference in bending stiffness above and below water should be checked to see what influence this has on the uplift length. The weight difference due to underwater tests could have an influence. This should be done to verify the validity of the in Chapter 6 mentioned design method for the bending stiffness.
7. During this thesis a start was made by looking at the force balance and determine the forces and moment step by step (time domain analysis). This would provide a better universal model that would describe the behaviour of a ballast filled mattress more accurate. If one is willing to continue on this and describe the behaviour of a ballast filled mattress in time, using an instantaneous approach with the Morison-type equations, a new set of test series should be performed aimed specifically at this purpose. Below a test set-up is described that should provide the data to describe the behaviour of a ballast filled mattress.
    - A more thorough test regarding the bending stiffness of the mattress should be done. In these tests, attention should be paid to the length over which the mattress is lifted, the uplift length. This length determines the amount of mobilised mass, responsible for the resistance against movement.
    - The hydrodynamic measurements must be taken closer to the edge of the mattress to translate the hydrodynamics to the forces. For this it is advices to either use laser doppler verlocity or PIV measurements. These allow for a better determination of the hydrodynamics around the edge of the mattress.
    - The recording frequency of the video camera should have the same frequency or a frequency close to that of the measuring devices. This will prevent the loss of information.
    - When testing the ballast filled mattress around a monopile, the effect of the pile should be investigated further. This can be done by placing pressure sensors on top of the mattress to check the influence of the wake. Due to the lack of time it was not possible to further investigate this in this research.
    - The amount of uplift and uplift length should be easily obtainable from the video recording made. Calibrating the video for this is essential to decrease errors.
    - During the tests there must be a better control of the (variations in) gap thickness between the mattress and bottom. As this greatly influences pressure below the mattress due to the stagnation pressure.

- These tests should again be performed with different mattresses with a different stiffness.
- With the known bending stiffness, exact hydrodynamics at location and a more detailed image of the hydrodynamics and uplift. The force balance can be applied and an universal formulation for any ballast filled mattress can be formulated and extended to the behaviour of the ballast filled mattress in time.
- The start made in this thesis can be continued knowing the errors made by translating the EMS signal to the edge of the mattress and uplift heights. For this it is necessary to determine the uplift length of the mattress to increase the accuracy of the mobilised weight and inertia force.

8. The ballast filled mattress should be tested on the effects of salt water and the attack of sediments on the coating and material on the long term.

REFERENCE

Adhiyasa, G. (2015). *Pipeline free span mitigation.* http://gadhiyasapipe.blogspot.nl/2015/01/pipeline-free-span-mitigation.html. (Accessed: 24-10-17)

AS, D. N. V. (2010). *On-bottom stability design of submarine pipelines* (Tech. Rep.). Author.

Baykal, C., Sumer, B., Fuhrman, D., Jacobsen, N., & Fredsøe, J. (2017). Numerical simulation of scour and backfilling processes around a circular pile in waves. *Coastal Engineering, 122*(Supplement C), 87 - 107.

Baykal, C., Sumer, B. M., Fuhrman, D. R., Jacobsen, N. G., & Fredsøe, J. (2014). Numerical investigation of flow and scour around a vertical circular cylinder. , *373*(2033).

Bolle, A., de Winter, J., Goossens, W., Haerens, P., & Dewaele, G. (2012). *Scour monitoring around offshore jackets and gravity based foundations.*

Bosboom, J., & Stive, M. (2011). *Coastal dynamics i.* VSSD.

Breusers, H. N. C., Nicollet, G., & Shen, H. (1977). Local scour around cylindrical piers. *Journal of Hydraulic Research, 15*(3), 211-252.

Chen, H., Yang, R., & Hwung, H. (2014). Study of hard and soft countermeasures for scour protection of the jacket-type offshore wind turbina foundation. , *2*, 551-567.

Dean, R., & Dalrymple, R. (1991). *Water wave mechanics for engineers and scientists.* World Scientific. Retrieved from https://books.google.nl/books?id=9-M4U_sfin8C

Deltares. (2017).

de Sonneville, B., Rudolph, D., & Raaijmakers, T. (2010). *Scour reduction by collars around offshore monopiles.*

Drake, T., & Calantoni, J. (2001). Discrete particle model for sheet flow sediment transport in the nearshore. *Journal of Geophysical Research: Oceans, 106*(C9), 19859-19868.

Escarameia, M. (1995). *Channel protection - gabion mattresses and concrete blocks* (Tech. Rep.). HR Wallingford.

EWEA. (2015). *Wind in power: 2014 european statistics.* https://windeurope.org/about-wind/statistics//european/. (Accessed: 19-09-17)

Garus, K. (2014). *First suction bucket jacket is complete.* http://www.offshorewindindustry.com/news/first-suction-bucket-jacket-complete. (Accessed: 16-10-17)

Glossary, O. (2017). *filter cake.* http://www.glossary.oilfield.slb.com/Terms/f/filter_cake.aspx. (Accessed: 07-09-2017)

Goda, Y. (2011). The observed joint distribution of periods and heights of sea waves. *Coastal Engineering Proceedings, 1*(16).

Godbold, J., Sackmann, N., & Cheng, L. (2014). *Stability design for concrete mattresses* (Vol. 1).

Guo, X., & Ma, H. (2009, 01). The study and application of high density drilling fluid technology. , *26*, 8-10.

Heller, V. (2011). Scale effects in physical hydraulic engineering models. *J of Hydraulic Research*, *49*(3), 293-306.

Ho, A., Mbistrova, A., Pineda, I., & Tardieu, P. (2017, January). *The european offshore wind industry. key trends and statistics 2016*.

Holthuijsen, L. (2010). *Waves in oceanic and coastal waters*. Cambridge University Press. Retrieved from https://books.google.nl/books?id=7tFUL2blHdoC

Hover, F., Miller, S., & Triantafyllou, M. (1997). Vortex-induced vibration of marine cables: Experiments using force feedback. *Journal of Fluids and Structures*, *11*, 307-326.

Hughes, S. (1993). *Physical models and laboratory techniques in coastal engineering*. World Scientific. Retrieved from https://books.google.nl/books?id=a5S5YR_TvTMC

Huisman, M. (1999). *Basiskennis boorvloeistoffen en foam* (Tech. Rep.). Delft Hydraulics.

Keulegan, G., & Carpenter, L. (1958). Forces on cylinders and plates in an oscillating fluid. *Journal of Research of the National Bureau of Standards*, *60*(5), 423-440.

Lamb, H. (1945). *Hydrodynamics*. Dover publications. Retrieved from https://books.google.nl/books?id=237xDg7T0RkC

Leeuwenstein, W., Bijker, E., Peerbolte, E., & Wind, H. (1985). *The natural self-burial of submarine pipelines*. Elsevier Science Publishers.

Longuet-Higgins, M. (1983). *On the joint distribution of wave periods and amplitudes in a random wave field* (Vol. 389).

Malarkey, J., & Davies, A. (2012). Free-stream velocity descriptions under waves with skewness and asymmetry. *Coastal Engineering*, *68*, 78 - 95. Retrieved from http://www.sciencedirect.com/science/article/pii/S0378383912000865 doi: https://doi.org/10.1016/j.coastaleng.2012.04.009

Mansard, E., & Funke, E. (1980). *The measurement of incident and reflected spectra using a least squares method* (Vol. 1).

Mastbergen, D. (2017). personal communication.

Melville, B., Ballegooy, R., & Ballegooy, S. (2006). Flow-induced failure of cable-tied blocks. *Journal of Hydraulic Engineering*, *3*(132), 324-327.

Morison, J., Johnson, J., & Schaaf, S. (1950). The force exerted by surface waves on piles. *Journal of Petroleum Technology*, *2*(5).

Mostafa, Y. E., & Agamy, A. F. (2011). Scour around single pile and pile groups subjected to waves and currents. *International Journal of Engineering Science and Technology, IJEST*, *3*(11), 8160-8178.

Nghiem, A., & Pineda, I. (2017, September). *Wind energy in europa: Scenarios for 2030*.

Peters, E. (2017). personal communication.

Petersen, T. U., Sumer, B. M., Bøgelund, J., Yazici, A., Fredsøe, J., & Meyer, K. E. (2015). Flow and edge scour in current adjacent to stone covers. *Journal of Waterway, Port, Coastal, and Ocean Engineering*, *141*(4), 0401-4044.

Petersen, T. U., Sumer, B. M., Raaijmakers, T. C., & Schouten, J. (2015). Edge scour at scour protections around piles in the marine environment - labaratory and field investigation. *Journal of Coastal Engineering*, *106*, 42-72.

Prasad, R., Vedula, S., & Indian Institute of Science, B. (2002). *Research perspectives in hydraulics and water resources engineering.* World Scientific. Retrieved from https://books.google.nl/books?id=n3ZqDQAAQBAJ

Raaijmakers, T. (2014, 12). *Scour & scour protection in the marine environment, lecture.*

Raaijmakers, T. (2017). personal communication.

Right, A. (2012). *Offshore wind turbines substructures.* http://www.renewablegreenenergypower.com/offshore-wind-turbines-substructures/. (Accessed: 24-10-17)

Sahin, B., Akilli, H., Karakus, C., Akar, M., & Ozkul, E. (2010). Qualitative and quantitative measurements of horseshoe vortex formation in the junction of horizontal and vertical plates. *Measurement*, *43*(2), 245 - 254. Retrieved from http://www.sciencedirect.com/science/article/pii/S0263224109002127 doi: https://doi.org/10.1016/j.measurement.2009.10.003

Sahroni, T. (2015). Modeling and simulation of offshore wind power platform for 5 mw nrel turbine. In *The scientific world journal.*

Schiereck, G., & Verhagen, H. (2012). *Introduction to bed, bank and shore protection.* VSSD.

Siam Gabions. (2011). http://www.siamgabions.com/Company.aspx. (Accessed: 21-11-2017)

Sonneville, B. (2015). *Review of scour protection below j-tubes at dolwin beta - results of desk study* (Tech. Rep.). Deltares.

Sumer, B., & Fredsøe, J. (2002). *The mechanics of scour in the marine environment.* World Scientific Publishing Co Pte Ltd.

Sumer, B. M., Christiansen, N., & Fredsøe, J. (1992). Scour around a vertical pile in waves. *J of Waterway, Port, Coastal, Ocean Engineering*, *118*(1), 15-31.

Sumer, B. M., & Fredsøe, J. (2001). Scour around pile in combined waves and current. *Journal of Hydraulic Engineering*, *127*(5), 403-411.

Trojanwoski, J. (2006, 12). *Water operation and maintenance bulletin* (Tech. Rep.). US Department of the Interior Bureau of Reclamation.

van Gent, M., & Wallast, I. (2001). *Stability of near-bed structures and bed protections - analysis of physical model tests with waves and currents* (Tech. Rep.). Delft Cluster.

Velzen, G. V., & de Jong, M. (2015). The stability of a block mattress under propeller induced loads. -.

WEU. (2013). *Weu offshore foundations report 2013 - report abstract* (Tech. Rep.). Wind Energy Update.

Whitehouse, R. (1998). *Scour at marine structures.* Thomas Telford Publishing.

Zaaijer, M. (2003). *Comparison of monopile, tripod, suction bucket and gravity base design for a 6mw turbine.*

Zaaijer, M., & Tempel, J. (2004). Scour protection: A necessity or a waste of money? In *Proceedings of the 43 iea topixal expert meeting.*

Zanganeh, M., Yeganeh-Bakhtiary, A., & Wahab, A. K. A. (2012). Lagrangian coupling two-phase flow model to simulate current-induced scour beneath marine pipelines. *Journal of Applied Ocean Research*, *38*, 64-73.

A

HYDRAULIC JACKING AND INERTIA

A.1 HYDRAULIC JACKING

Hydraulic jacking is due to a protruding object. The stagnation pressure at the base of this object builds up and is transferred below the object through a narrow gap. See Figure A.1.

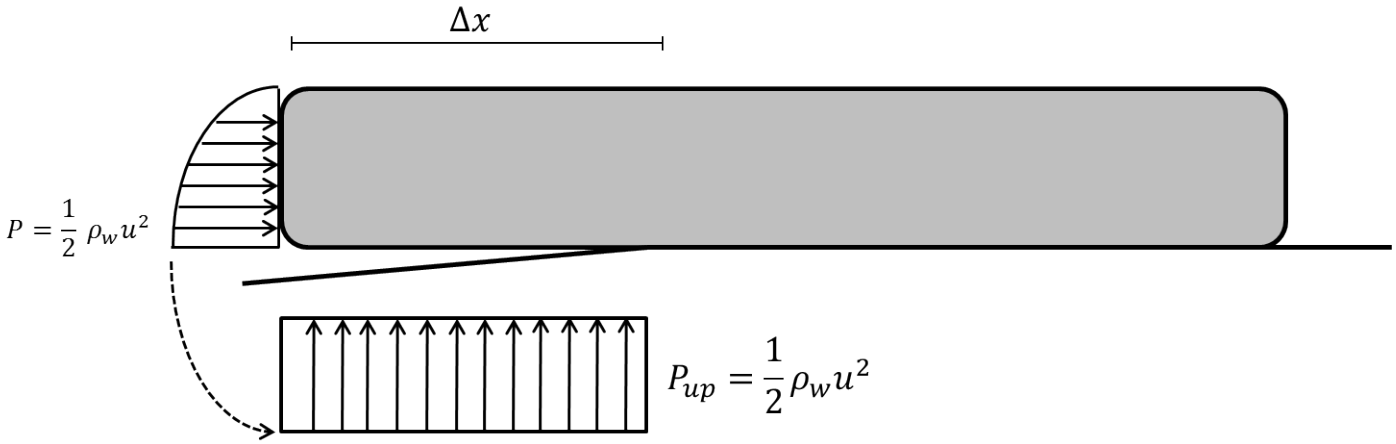

Figure A.1: Schematic representation of hydraulic jacking due to the stagnation pressure

The stagnation can be expressed as

$$P_{stagnation} = \frac{1}{2}\rho_w u^2 \tag{A.1}$$

This pressure is transferred below the mattress to the point of reattachment. This location of this reattachment point determines how far this pressure protrudes below the mattress and the decay of this pressure.

Multiplying the pressure with Δx will give the lift force due to this hydraulic jacking.

A.2 INERTIA

Acceleration around the mattress are caused by the pressure differences induced by the wave; the difference in wave phase induces a pressure difference over the length of the mattress. Since $L_{wave} >> L_{mattress}$ the pressure gradient over the length of the mattress is considered to be neglible. The pressure difference due to hydrostatic pressure and fluctuating wave pressures on top of the mattress are of more interest.

A wave passing over the mattress will induce a under pressure compared to the hydrostatic pressure at the bottom. If the mattress has a connection with the seabed this hydrostatic pressure cannot adjust and will create a pressure upward resulting in lift as shown in Figure A.2.

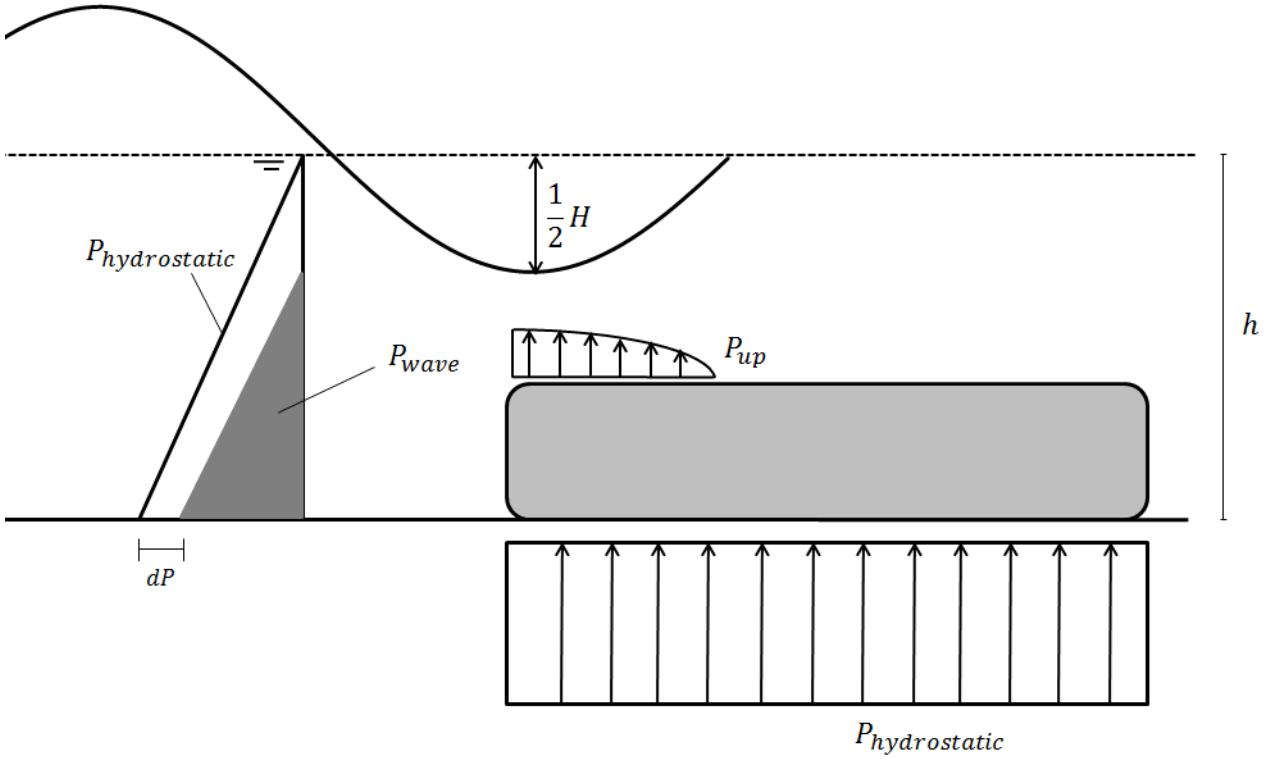

Figure A.2: Pressure difference over the mattress due to wave fluctuation on top of the mattress

Assuming a linear decay of the upward pressure, the pressure difference between the top and bottom becomes:

$$dp = \frac{dp}{dx}dx \tag{A.2}$$

Consequently, the force on the mattress will become:

$$F_p = \int\int\int dxdydz\frac{dp}{dx} = V\frac{dp}{dx} \tag{A.3}$$

From Euler is it known that

$$\nabla p = -\rho_w \frac{Du}{Dt} \tag{A.4}$$

Where

$$\frac{Du}{Dt} = \frac{\delta u}{\delta t} + u\frac{\delta u}{\delta x} \tag{A.5}$$

As there is no current imposed on top of the wave and the assumption of $L_{wave} >> L_{mat}$, so $u\frac{\delta u}{\delta x} \approx 0$. By combining eq. A.4 with A.5 will results in:

$$F_p = \rho_w a V \tag{A.6}$$

in which: F_p = pressure force
ρ_w = density of water
a = horizontal acceleration
V = volume

B

SCALE MODEL TESTS

B.1 SCHELDT FLUME

B.1.1 CABLE SECTION LAY-OUT

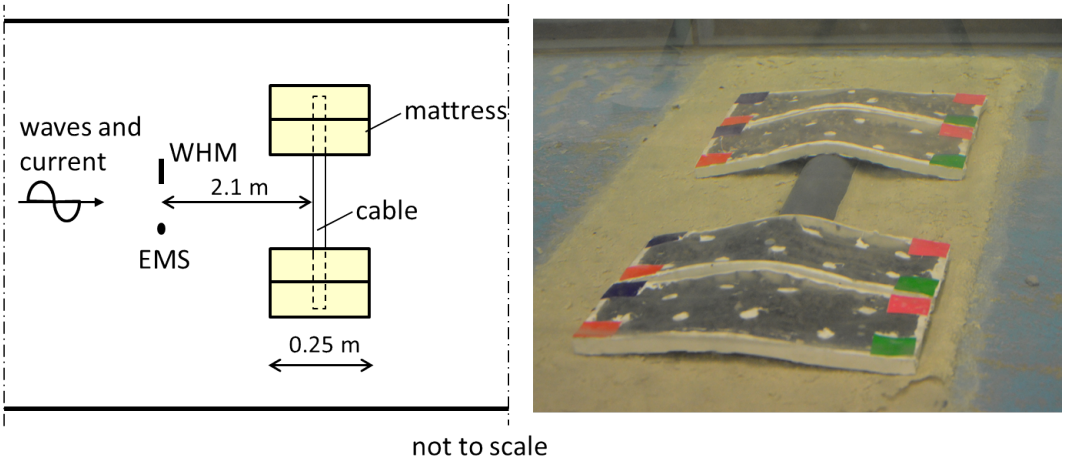

Figure B.1: Eastern Scheldt Flume cable test set-up (layout 2)

B.1.2 FULL TEST SERIES SCHELDT FLUME

Table B.1 and B.2 show the full test series for all wave/current conditions for the Scheldt Flume. The black line between tests indicates a sequence of tests.

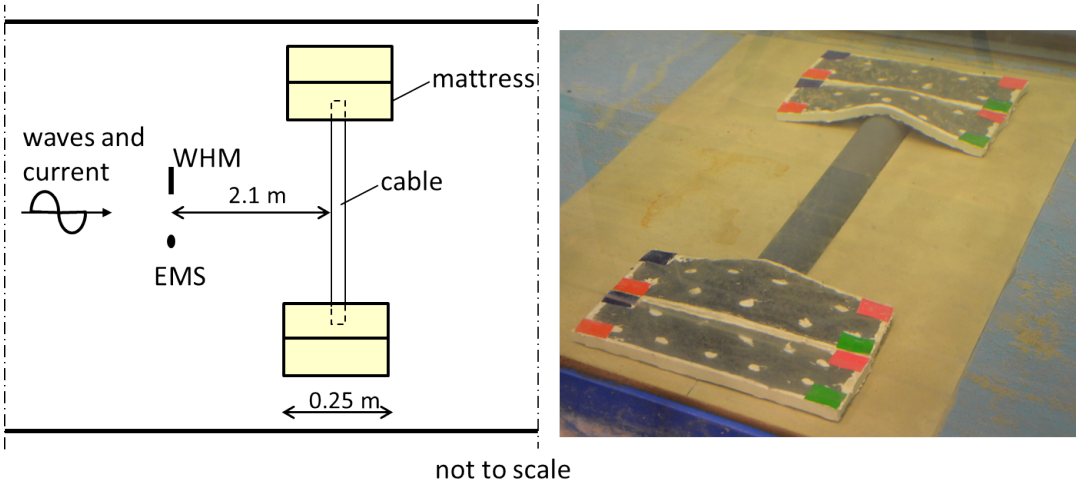

Figure B.2: Eastern Scheldt Flume cable test set-up (layout 3)

testID	hw [m]	Uc [m/s]	Hm0* [m]	Tp [s]	Duration [s]	Comments
CO-1b-01	0.600	0.145	-	-	900	Air pockets in mattress
CO-1c-01	0.609	0.206	-	-	720	Air pockets in mattress
CO-1d-01	0.611	0.255	-	-	720	Air pockets in mattress
CO-1e-01	0.614	0.289	-	-	900	Air pockets in mattress
CO-1e-02	0.611	0.298	-	-	900	Air pockets in mattress
CO-1f-01	0.611	0.339	-	-	720	Air pockets in mattress
CO-1g-01	0.614	0.400	-	-	720	Air pockets in mattress
CO-1b-11	0.612	0.146	-	-	720	
CO-1c-11	0.608	0.203	-	-	720	
CO-1d-11	0.610	0.254	-	-	720	
CO-1e-11	0.604	0.305	-	-	720	
CO-1f-11	0.609	0.352	-	-	720	
CO-1g-11	0.609	0.401	-	-	720	
RWO-1aM-01	0.596	-	0.097	1.386	61	Air pockets in mattress
RWO-1bM-01	0.597	-	0.156	1.811	67	
RWO-1cM-01	0.602	-	0.230	1.974	77	
RWO-1aS-01	0.604	-	0.107	1.109	61	Air pockets in mattress
RWO-1bS-01	0.604	-	0.150	1.385	54	Air pockets in mattress
RWO-1cS-01	0.604	-	0.207	1.622	60	Air pockets in mattress
RWO-1dS-01	0.602	-	0.240	1.821	51	Air pockets in mattress
RWO-1eS-01	0.601	-	0.349	1.885	49	Air pockets in mattress
RWO-1aL-01	0.603	-	0.101	1.576	52	Air pockets in mattress
RWO-1bL-01	0.603	-	0.165	2.000	48	Air pockets in mattress
IWO-1aM-01	0.605	-	0.099	1.429	700	
IWO-1cM-01	0.613	-	0.140	1.716	850	
IWO-1eM-01	0.609	-	0.176	1.939	950	
RWO-1bM-21	0.608	-	0.163	1.774	55	
RWO-1cM-21	0.607	-	0.217	2.000	56	

RWO-1dM-21	0.606	-	0.242	2.292	55	
RWO-1eM-21	0.602	-	0.312	2.476	52	
RWO-1cS-21	0.604	-	0.210	1.600	56	
RWO-1dS-21	0.601	-	0.247	1.833	55	
RWO-1eS-21	0.600	-	0.337	1.931	56	
RWO-1cL-21	0.604	-	0.255	2.320	58	
RWO-1dL-21	0.600	-	0.249	2.636	58	
RWO-1eL-21	0.598	-	0.304	2.905	61	
IWO-1dM-21	0.601	-	0.158	1.923	900	
IWO-1eM-21	0.603	-	0.176	1.939	950	
IWO-1fM-21	0.607	-	0.191	1.961	1000	
IWC-1eMc-21	0.623	0.202	0.161	1.939	950	
RWO-1bM-31	0.603	-	0.162	1.828	53	
RWO-1bM-31	0.603	-	0.181	1.828	53	
RWO-1cM-31	0.602	-	0.228	1.962	51	
RWO-1cM-31	0.602	-	0.246	2.040	51	
RWO-1dM-31	0.602	-	0.245	2.333	56	
RWO-1eM-31	0.599	-	0.330	2.571	54	
RWO-1cS-31	0.604	-	0.208	1.606	53	
RWO-1cS-31	0.604	-	0.223	1.606	53	
RWO-1dS-31	0.603	-	0.259	1.788	59	
RWO-1dS-31	0.603	-	0.272	1.788	59	
RWO-1eS-31	0.602	-	0.344	1.897	55	
RWO-1fS-31	0.600	-	0.264	2.120	53	Breaking waves
RWO-1bL-31	0.608	-	0.164	2.028	73	
RWO-1bL-31	0.608	-	0.183	2.028	73	
RWO-1cL-31	0.608	-	0.226	2.304	53	
RWO-1cL-31	0.608	-	0.252	2.304	53	
RWO-1dL-31	0.605	-	0.246	2.619	55	
RWO-1dL-31	0.605	-	0.245	2.619	55	
RWO-1eL-31	0.603	-	0.332	2.857	60	
IWO-1dM-31	0.610	-	0.159	1.923	900	
IWO-1dM-31	0.610	-	0.168	1.786	900	
IWO-1eM-31	0.609	-	0.177	1.939	950	
IWO-1eM-31	0.609	-	0.185	1.900	950	
IWO-1fM-31	0.606	-	0.201	2.000	1000	
IWO-1gM-31	0.605	-	0.217	2.120	1050	
IWO-1hL-31	0.606	-	0.230	2.529	1250	
RWO-1eM-32	0.600	-	0.261	2.550	51	
RWO-1eM-33	0.599	-	0.298	2.545	56	
RWO-1cM-41	0.603	-	0.213	2.000	54	
RWO-1cM-41	0.603	-	0.238	2.000	54	
RWO-1dM-41	0.602	-	0.242	2.333	56	
RWO-1dM-41	0.602	-	0.246	2.333	56	
RWO-1eM-41	0.600	-	0.255	2.522	58	
RWO-1eM-41	0.600	-	0.282	2.522	58	
RWO-1eM-42	0.599	-	0.329	2.478	57	
RWO-1eM-42	0.599	-	0.335	2.478	57	

RWO-1fM-41	0.595	-	0.210	2.643	37	Breaking waves
RWO-1fM-41	0.595	-	0.255	2.643	37	Breaking waves
RWO-1cL-41	0.604	-	0.240	2.292	55	
RWO-1cL-41	0.604	-	0.256	2.292	55	
RWO-1dL-41	0.601	-	0.240	2.591	57	
RWO-1dL-41	0.601	-	0.267	2.591	57	
RWO-1eL-41	0.598	-	0.299	2.900	58	
RWO-1eL-41	0.598	-	0.325	2.900	58	
RWO-1fL-41	0.596	-	0.244	3.154	41	Breaking waves
RWO-1fL-41	0.596	-	0.279	3.154	41	Breaking waves
IWO-1eM-41	0.606	-	0.177	1.939	950	
IWO-1fM-41	0.606	-	0.192	1.961	1000	
IWO-1fM-42	0.605	-	0.191	1.961	1000	
IWO-1gM-41	0.605	-	0.210	2.074	1050	
IWO-1hM-41	0.604	-	0.215	2.222	1100	
IWO-1hL-41	0.607	-	0.220	2.529	1250	
IWC-1eMc-41	0.621	0.206	0.161	1.939	950	
IWC-1fMc-41	0.621	0.207	0.176	1.961	1000	
IWC-1fMe-41	0.631	0.298	0.166	2.000	1000	
IWC-1hMe-41	0.616	0.303	0.190	2.222	1100	
IWC-1hLg-41	0.637	0.390	0.185	2.529	1250	
RWO-2bM-01	0.451	-	0.127	1.625	52	
RWO-2cM-01	0.449	-	0.170	1.806	56	
RWO-2dM-01	0.448	-	0.151	2.042	49	Breaking waves
RWO-2cL-01	0.450	-	0.192	2.077	54	
RWO-2dL-01	0.448	-	0.175	2.286	64	Breaking waves
RWO-2dL-02	0.450	-	0.170	2.346	61	Breaking waves
RWO-2dL-03	0.451	-	0.188	2.321	65	Breaking waves
RWO-2eL-01	0.447	-	0.221	2.423	63	Breaking waves
RWO-2fL-01	0.447	-	0.210	2.609	60	Breaking waves
RWO-2bM-11	0.451	-	0.136	1.586	46	
RWO-2bM-11	0.451	-	0.127	1.586	46	
RWO-2cM-11	0.448	-	0.169	2.000	50	
RWO-2cM-11	0.448	-	0.151	2.000	50	
RWO-2bL-11	0.450	-	0.164	1.885	49	
RWO-2bL-11	0.450	-	0.137	1.885	49	
RWO-2cL-11	0.451	-	0.239	2.069	60	
RWO-2cL-11	0.451	-	0.188	2.143	60	
RWO-2eL-11	0.448	-	0.183	2.375	57	
RWO-2eL-12	0.446	-	0.244	2.368	45	
RWO-3bM-01	0.753	-	0.183	1.800	63	
RWO-3bM-01	0.753	-	0.200	1.800	63	
RWO-3cM-01	0.751	-	0.225	2.000	52	
RWO-3cM-01	0.751	-	0.246	2.000	52	
RWO-3cM-02	0.751	-	0.224	2.000	56	
RWO-3cM-02	0.751	-	0.254	2.000	56	
RWO-3dM-01	0.750	-	0.307	2.320	58	
RWO-3dM-01	0.750	-	0.293	2.320	58	

RWO-3dM-02	0.751	-	0.297	2.259	61	
RWO-3dM-02	0.751	-	0.286	2.346	61	
RWO-3eM-01	0.749	-	0.318	2.500	60	
RWO-3eM-01	0.749	-	0.316	2.500	60	
RWO-3fM-01	0.747	-	0.334	2.700	54	
RWO-3fM-01	0.747	-	0.354	2.700	54	
RWO-3eM-02	0.750	-	0.328	2.500	55	
RWO-3dM-03	0.750	-	0.299	2.333	56	
RWO-3fL-01	0.746	-	0.357	3.000	21	Waves overtopping flume

Table B.1: Full test series monopile, Scheldt Flume

testID	hw [m]	Uc [m/s]	Hm0 [m]	Tp [s]	Duration [s]	Comments
CO-1b-01	0.600	0.145	-	-	900	Air pockets in mattress
CO-1c-01	0.609	0.206	-	-	720	Air pockets in mattress
CO-1d-01	0.611	0.255	-	-	720	Air pockets in mattress
CO-1e-01	0.614	0.289	-	-	900	Air pockets in mattress
CO-1e-02	0.611	0.298	-	-	900	Air pockets in mattress
CO-1f-01	0.611	0.339	-	-	720	Air pockets in mattress
CO-1g-01	0.614	0.400	-	-	720	Air pockets in mattress
CO-1b-11	0.612	0.146	-	-	720	Air pockets in mattress
CO-1c-11	0.608	0.203	-	-	720	Air pockets in mattress
CO-1d-11	0.610	0.254	-	-	720	Air pockets in mattress
CO-1e-11	0.604	0.305	-	-	720	Air pockets in mattress
CO-1f-11	0.609	0.352	-	-	720	Air pockets in mattress
CO-1g-11	0.609	0.401	-	-	720	Air pockets in mattress
RWO-1aM-01	0.596	-	0.099	1.386	61	Air pockets in mattress
RWO-1bM-01	0.597	-	0.171	1.811	67	Air pockets in mattress
RWO-1cM-01	0.602	-	0.208	2.026	77	Air pockets in mattress
RWO-1dM-01	0.602	-	0.266	2.250	45	Air pockets in mattress
RWO-1aS-01	0.604	-	0.108	1.109	61	Air pockets in mattress
RWO-1bS-01	0.604	-	0.154	1.385	54	Air pockets in mattress
RWO-1cS-01	0.604	-	0.201	1.622	60	Air pockets in mattress
RWO-1dS-01	0.602	-	0.254	1.821	51	Air pockets in mattress
RWO-1eS-01	0.601	-	0.282	1.960	49	Air pockets in mattress
RWO-1aL-01	0.603	-	0.099	1.625	52	Air pockets in mattress
RWO-1bL-01	0.603	-	0.148	2.000	48	Air pockets in mattress
RWO-1cL-01	0.603	-	0.245	2.286	48	Air pockets in mattress
RWO-1dL-01	0.601	-	0.222	2.600	52	Air pockets in mattress
RWO-1eL-01	0.599	-	0.367	3.000	51	Air pockets in mattress
IWO-1aM-01	0.605	-	0.100	1.471	700	
IWO-1cM-01	0.613	-	0.141	1.748	850	
IWO-1eM-01	0.609	-	0.174	1.863	950	
IWO-1fM-01	0.606	-	0.189	2.083	1000	
IWC-1fMc-01	0.621	0.202	0.174	2.041	1000	
IWC-1fMe-01	0.630	0.296	0.163	1.887	1000	
IWC-1fMg-01	0.646	0.383	0.149	1.961	1000	

IWC-1hMg-01	0.655	0.377	0.182	2.213	1096	
RWO-1bM-21	0.608	-	0.168	1.833	55	
RWO-1cM-21	0.607	-	0.225	2.000	56	
RWO-1dM-21	0.606	-	0.248	2.292	55	
RWO-1eM-21	0.602	-	0.319	2.476	52	
RWO-1cS-21	0.604	-	0.203	1.600	56	
RWO-1dS-21	0.601	-	0.251	1.833	55	
RWO-1eS-21	0.600	-	0.285	1.931	56	
RWO-1cL-21	0.604	-	0.252	2.320	58	
RWO-1dL-21	0.600	-	0.230	2.636	58	
RWO-1eL-21	0.598	-	0.376	2.905	61	
IWO-1dM-21	0.601	-	0.157	1.754	900	
IWO-1eM-21	0.603	-	0.175	1.863	950	
IWO-1fM-21	0.607	-	0.190	2.041	1000	
IWC-1eMc-21	0.623	0.202	0.160	1.863	950	
IWC-1fMc-21	0.622	0.204	0.166	2.041	1000	
IWC-1fMe-21	0.622	0.300	0.162	1.961	1000	
IWC-1fMg-21	0.634	0.390	0.146	1.961	1000	
RWO-1bM-31	0.603	-	0.171	1.828	53	
RWO-1cM-31	0.602	-	0.217	2.040	51	
RWO-1dM-31	0.602	-	0.257	2.333	56	
RWO-1eM-31	0.599	-	0.319	2.571	54	
RWO-1cS-31	0.604	-	0.200	1.606	53	
RWO-1dS-31	0.603	-	0.256	1.788	59	
RWO-1eS-31	0.602	-	0.286	1.897	55	
RWO-1fS-31	0.600	-	0.220	2.120	53	Layout restored before test; breaking waves
RWO-1bL-31	0.608	-	0.167	2.028	73	
RWO-1cL-31	0.608	-	0.225	2.304	53	
RWO-1dL-31	0.605	-	0.218	2.619	55	
RWO-1eL-31	0.603	-	0.390	2.857	60	
IWO-1dM-31	0.610	-	0.158	1.754	900	
IWO-1eM-31	0.609	-	0.176	1.863	950	
IWO-1fM-31	0.606	-	0.190	2.041	1000	
IWO-1gM-31	0.605	-	0.208	2.074	1050	
IWO-1hL-31	0.606	-	0.223	2.529	1250	
RWO-1eM-32	0.600	-	0.254	2.550	51	
RWO-1eM-33	0.599	-	0.296	2.545	56	

Table B.2: Full test series cable, Scheldt Flume

B.2 Atlantic Basin

B.2.1 Full test series

Monopile tests

The H_{m0} and T_p for the regular waves are the values imposed by the wave board.

Condition	h_w [m]	u_0 [m]	H_{m0} [m]	T_p [s]	Duration [s]
Regular waves	0.6	-	0.172 - 0.296	2.1 - 2.94	80
Tidal current	0.627	0.3-0.4	-	-	1800
Intermediate storm	0.6	0.075	0.183	1.92	2700
Intermediate storm	0.6	0.15	0.176	1.92	2700
Severe storm	0.6	0.1	0.224	2.17	2700
Severe Storm	0.6	0.2	0.219	2.17	2700

Table B.3: Test series monopile tests, Atlantic Basin

Suction bucket jacket tests

Test	Condition	h_w [m]	u_0 [m]	H_{m0} [m]	T_p [s]	Duration [s]
T01a	irregular waves	0.627	-	0.15	1.8	1800
T01b	mild storm	0.627	+ 0.3	0.15	1.8	1800
T01c	intermediate storm	0.7	+ 0.16	0.21	2.35	3838
T01d	severe storm	0.627	+ 0.16	0.233	2.173	3838
T02a	tidal current	0.627	+/- 0.2	0	0	1800
T02b	tidal current	0.627	+/- 0.3	0	0	1800
T02c	tidal current	0.627	+/- 0.4	0	0	1800
T02e	intermediate storm	0.7	+0.16	0.227	2.35	3838
T02f	severe storm	0.627	-0.16	0.25	2.17	1800

Table B.4: Test series SBJ tests, Atlantic Basin

B.3 Delta Flume

B.3.1 Full test series Delta Flume

Test set	Test ID	Condition	hw [m]	Uc [m/s]	Hm0 [m]	Tp [s]	Duration [s]
F02	F02-IW-1	Irregular waves	5.11	-	0.68	3.68	600
	F02-IW-2	Irregular waves	5.11	-	0.90	4.16	600
	F02-IW-3	Irregular waves	5.11	-	1.21	5.20	3600
	F02-IW-4	Irregular waves	5.11	-	1.18	5.26	410
	F02-IW-5	Irregular waves	5.11	-	1.26	5.60	360
	F02-IW-6	Irregular waves	5.11	-	1.57	6.21	652
F03	F03-IW-1	Irregular waves	5.11	-	1.01	4.55	3600
	F03-IW-2	Irregular waves	5.11	-	1.21	5.30	900
	F03-IW-3	Irregular waves	5.11	-	1.31	5.27	1800
	F03-IW-4	Irregular waves	5.11	-	1.38	5.73	900
	F03-IW-5	Irregular waves	5.11	-	1.63	6.08	803

Table B.5: Full test series Delta Flume

Test set	Test ID	Condition	hw [m]	Uc [m/s]	Hm0 [m]	Tp [s]	Duration [s]
F02	F02-IW-1	Irregular waves	5.11	-	0.68	3.58	600
	F02-IW-2	Irregular waves	5.11	-	0.88	4.16	600
	F02-IW-3	Irregular waves	5.11	-	1.18	5.27	3600
	F02-IW-4	Irregular waves	5.11	-	1.25	5.69	410
	F02-IW-5	Irregular waves	5.11	-	1.29	5.86	360
	F02-IW-6	Irregular waves	5.11	-	1.53	5.72	652
F03	F03-IW-1	Irregular waves	5.11	-	1.01	4.55	3600
	F03-IW-2	Irregular waves	5.11	-	1.22	5.30	900
	F03-IW-3	Irregular waves	5.11	-	1.29	5.27	1800
	F03-IW-4	Irregular waves	5.11	-	1.35	5.81	900
	F03-IW-5	Irregular waves	5.11	-	1.62	5.73	803

Table B.6: Full test series cable section Delta Flume

C

STABILITY AND VIDEO ANALYSIS

C.1 DATA ANALYSIS

A zero-down crossing analysis is performed for the data from the regular wave tests of the Scheldt Flume. The zero-down crossing analysis is performed after 22 seconds. This is not chosen arbitrarily; it is assumed that the waves are fully developed to the imposed wave height. From this section a mean wave height (H_{mean}) is computed with its standard deviation (σ). A zero-down-crossing is then performed on the total signal and if eq. C.1 is met, the corresponding wave is added to the waves that are analysed. Finally a mean wave height and mean wave period is computed from all waves that satisfy eq. C.1.

$$H_i > H_{mean} - \sigma \tag{C.1}$$

With the mean wave height known, the mean wave period is also computed from the data. The corresponding orbital velocity is calculated according to the full expression of linear wave theory. The acceleration is calculated by taking the derivative of the velocity. See eq. C.2 and C.3.

$$u_x = \omega a \frac{cosh(k(d+z))}{sinh(kd)} sin(\omega t) \tag{C.2}$$

and

$$a_x = \omega^2 a \frac{cosh(k(d+z))}{sinh(kd)} cos(\omega t) \tag{C.3}$$

With the velocity and acceleration the stability numbers are calculated and used for the first analysis.

C.2 FULL MONOPILE BOXPLOT

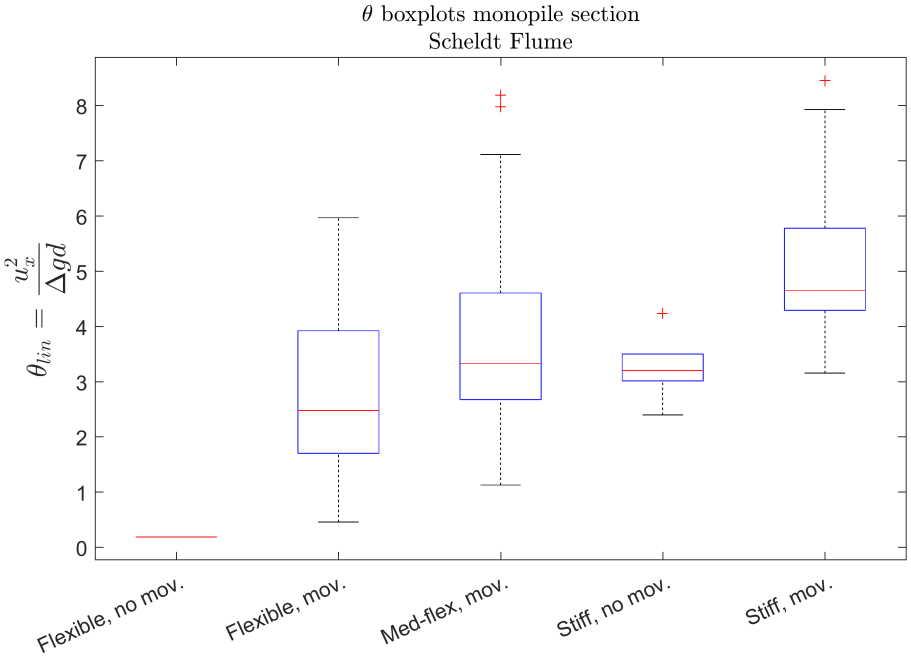

Figure C.1: θ_{lin} boxplots monopile section, Scheldt Flume

C.3 METHODOLOGY

Figure C.2 shows the flexible and medium-flexible mattress with gaps between the mattress and flume bed. The gaps are clearly visible and possibly decrease the stability of the mattress. Water pressure is transferred to the underside of the mattress and creates an upward force,due to the hydraulic jacking explained in Appandix A. The evolution of this gap thickness as well as the length to the reattachment point of the mattress is of importance. The evolution of the thickness determines the pressure dissipation, the length influences to where the pressure is transferred below the mattress. Both have not been taken in account during the test series. Figure C.2 show significant gaps, where even the smallest gap allows for water passing beneath the mattress, decreasing the overal stability of the mattress.

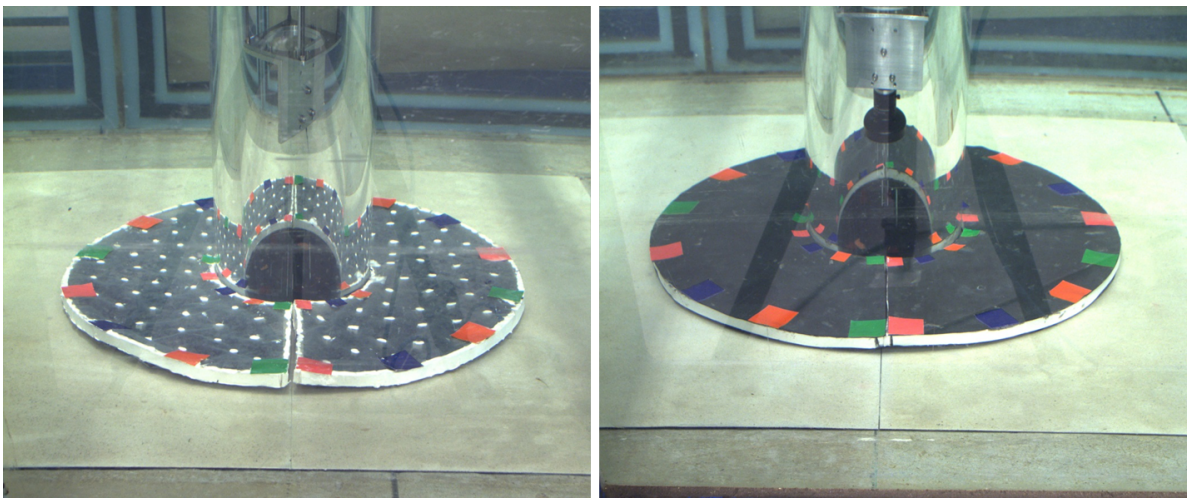

Figure C.2: Left: flexible mattress, right: medium-flexible mattress

C.4 Full Morison-equation

In order to understand the forcing due to drag and inertia the full Morison equation is plotted for different waves with an increasing wave height from the Scheldt Flume test obtained with linear wave theory. Figure C.3 shows that the inertial force is significant with respect to the force component due to drag. With increasing water level elevation, thus an increase in the orbital velocity the force due to drag increases but inertia is still dominant. When looking at the total force, it is possible to have a force in upstream direction when the orbital velocity is in downstream direction. With an increasing force due to drag, the time that opposing forces occur decreases. For the coefficients C_d and C_m unity has been used.

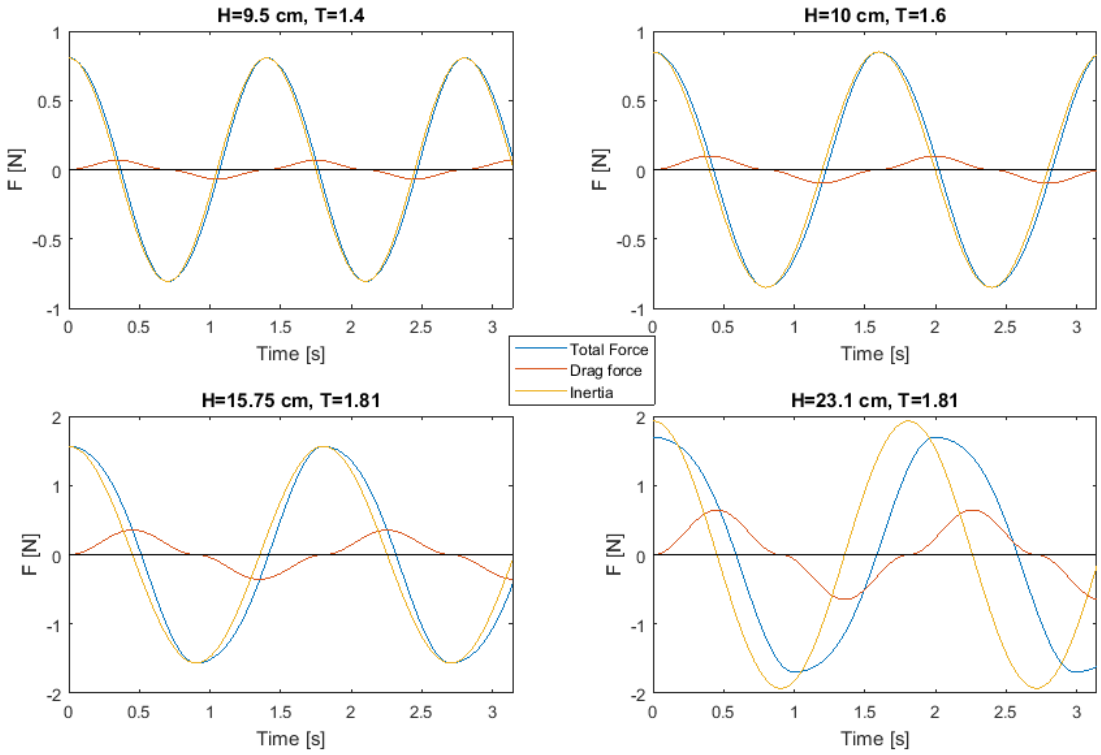

Figure C.3: Full force according to Morison for different wave heights

Figure C.4 show the same waves but instead of the Morison equation, the full mobility equation is used as given in eq. 4.8. The plot has changed significantly and the force due to velocity now dominates. For C_{all} unity is taken. The maximum mobility occurs just prior to the maximum velocity (which is the same as maximum mobility due to velocity). With an increasing contribution of acceleration this will shift more to the left and with an increasing velocity it will shift to the right as shown in the figure. The figure again shows the opposing forcing as explained above, the time again decreases with increasing orbital velocities. Any effect due to an uplift, thus an increase of drag force, has not been accounted for.

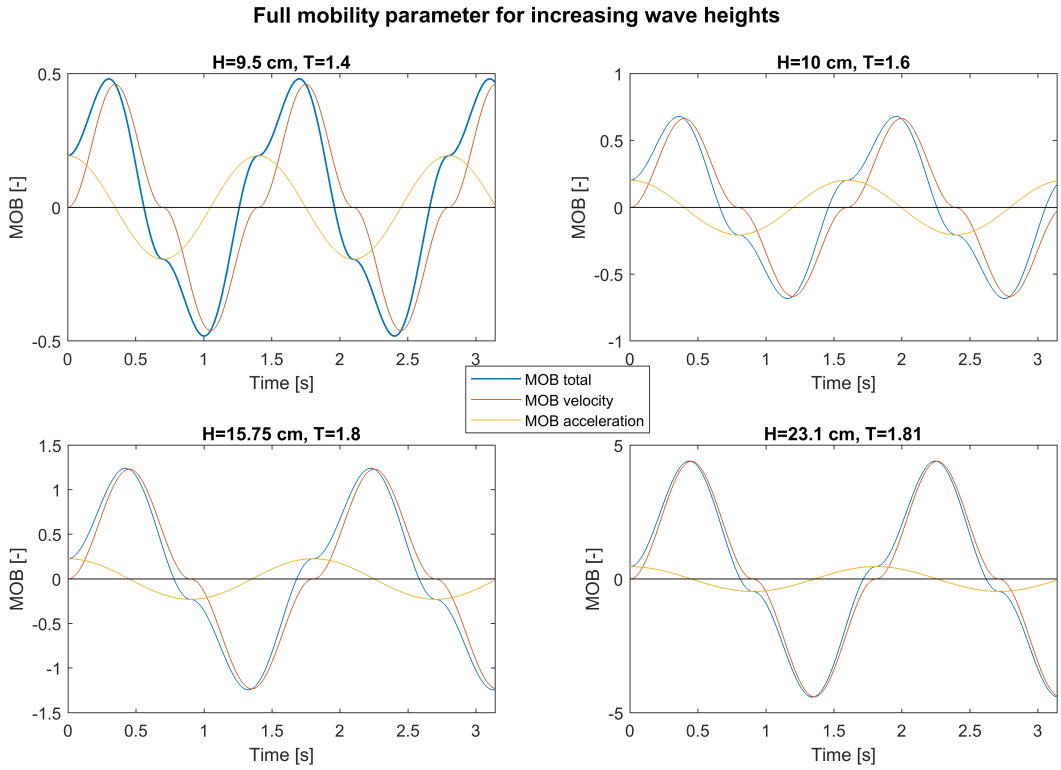

Figure C.4: Full mobility parameter for increasing wave height

Lastly, Figure C.5 shows the full mobility for different coefficients for one wave. The effect of the coefficient is clearly shown in the total mobility. The total mobility is shifted to the left and the maximum is increased. It does show that at the point of flow reversal inertia can be of importance with respect to the initiation of motion. The mobility around this point is already significant, solely due to the inertia component.

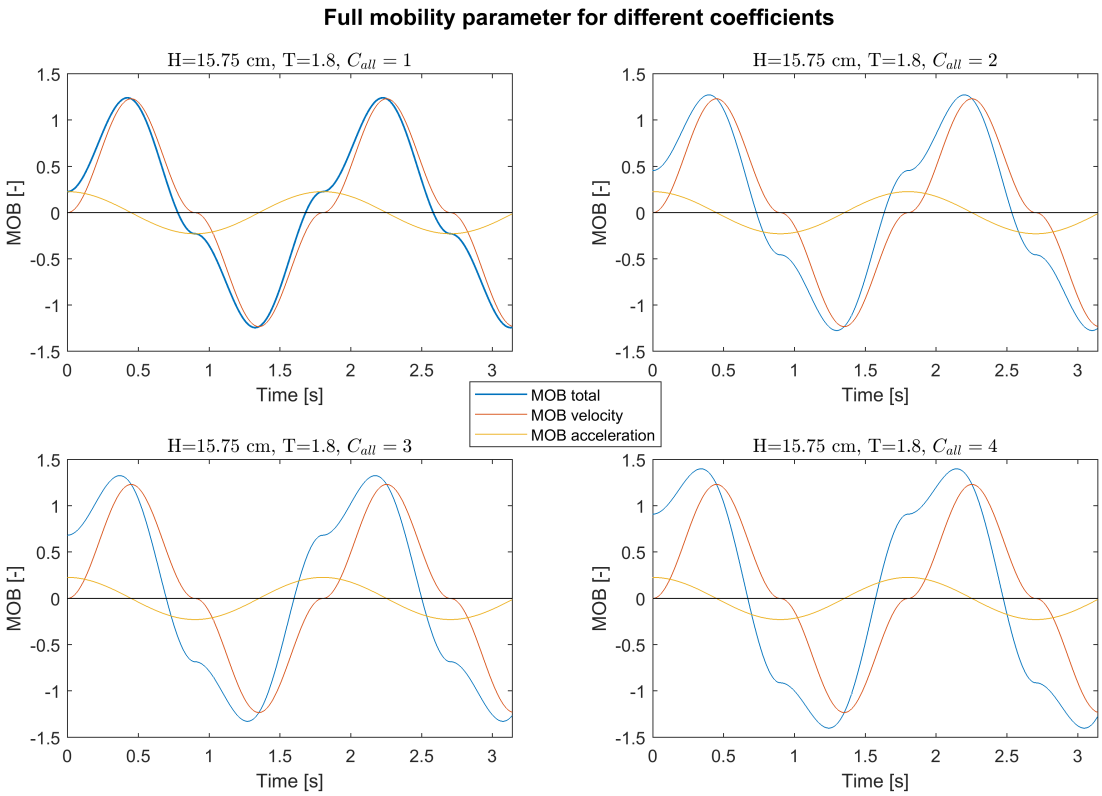

Figure C.5: Full mobility parameter for different coefficients

C.5 STIFFNESS MEASUREMENTS

The stiffness of the mattresses are tested with a simple set-up as shown in figure C.6. A force is applied on the most '*upstream*' side of the mattress close to the measuring rod. Different forces are applied (by means of a spring balance) and the uplift corresponding to the force is saved. Both dry and underwater tests have been performed to check the difference. For the dry tests, the mattress was fixed against sliding with a duct tape as seen in Figure C.6. For the underwater tests, the mattress was not fixed.

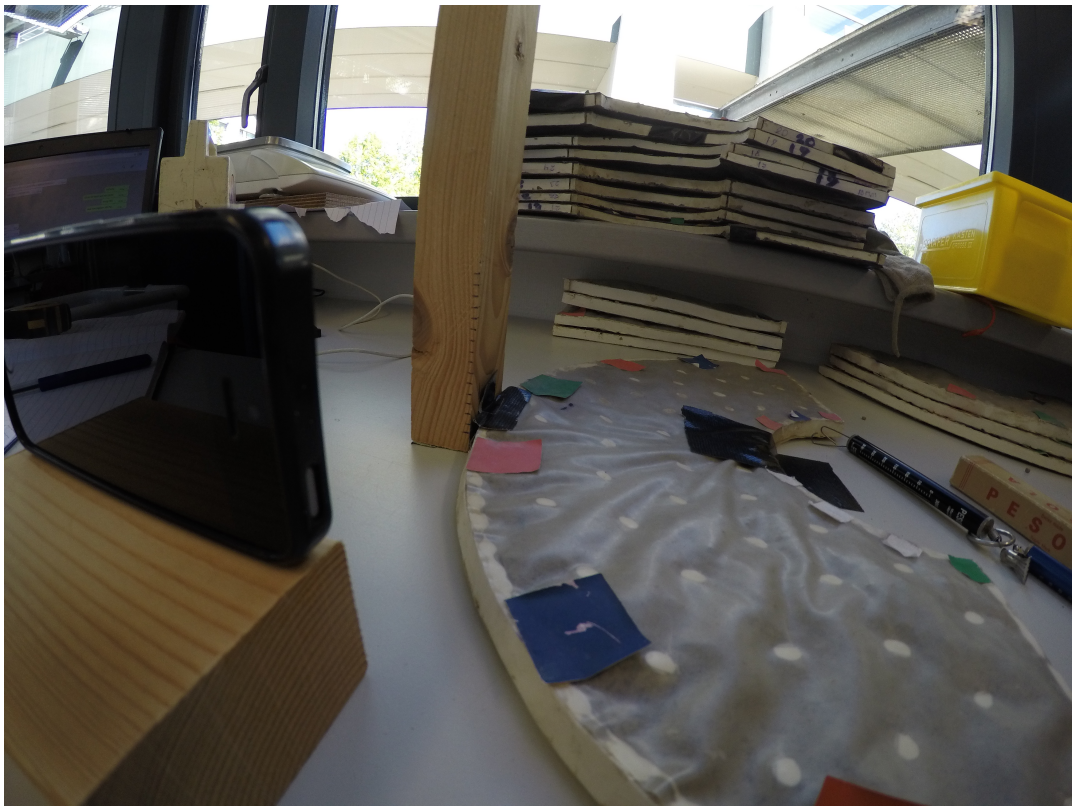

Figure C.6: Set-up of the stiffness measurements

The results as shown below show a trend that is expected, due to the shape of the mattress, the more a mattress is lifted the more mass is mobilised thus a higher force is needed to mobilize this mass. Where for the cable mattress a linear trend is expected due to the constant shape of the material. All mattresses tested were not completely filled up with material and had significant slack in the rubber sheets which determined the stiffness.

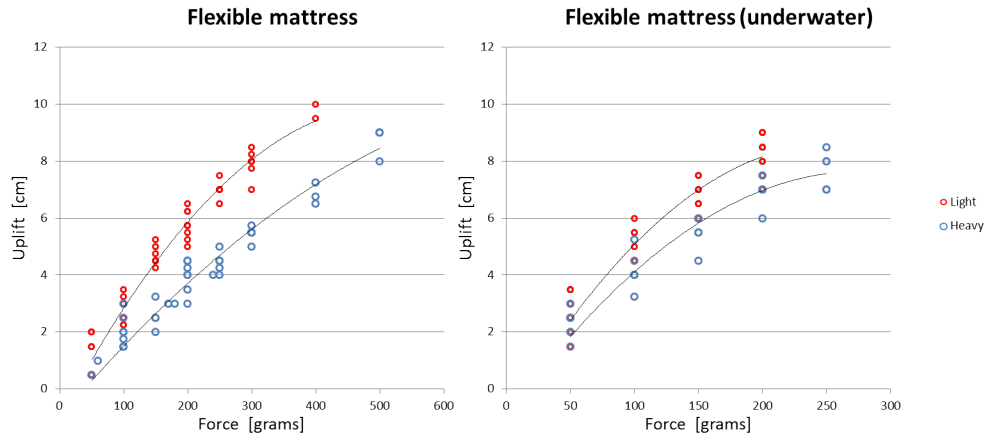

Figure C.7: Stiffness measurements flexible mattress, monopile

The flexible monopile mattress showed the non-linear behaviour as expected. The more the mattress is lifted, the more mass is being mobilised which in turn leads to a higher force needed to lift the mattress. Resulting in more force needed to lift the mattress higher. The behaviour of the above and underwater mattress is similar expect for the underwater tests the force needed to lift the mattress is significantly less. This is explained by the fact that underwater weight is less than the dry weight, thus less mass is mobilized.

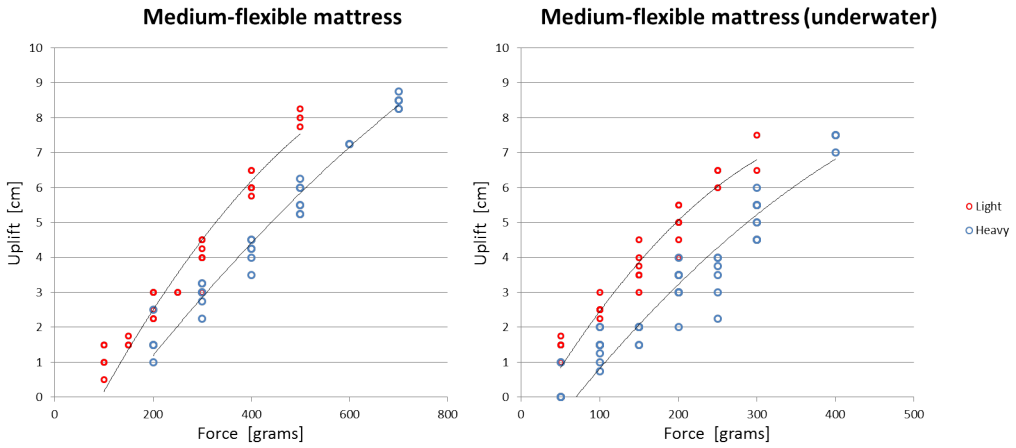

Figure C.8: Stiffness measurements medium-flexible mattress, monopile

The medium-flexible mattress showed similar uplift behaviour as the flexible monopile mattress, but as expected more force is needed to move the mattress. For the dry tests it can be concluded this is due to the bending stiffness of the mattress. As explained in Chapter 3 the light medium-flexible mattress has two halves with a different weight. The lightest mattress of the medium-flexible mattress weighted less than the light flexible mattress, see Table 3.2. But no difference is observed between the two light medium-flexible monopile mattresses, where it does show difference with the light flexible monopile mattress. The same is observed for the underwater tests.

Worth mentioning is that during the stability analysis in Chapter 4 the medium-flexible monopile mattress behaved more stiff and moved as a whole and had little uplift. No significant curvature was observed during

the stability tests as seen with the flexible monopile mattress shown in Figure 4.8. During the stiffness test a significant curvature is observed as shown in Figure C.9. Two possible explanations for this are formulated; during the stiffness tests multiple connections between the top and bottom sheet were broken. This could have influence on the behaviour of the mattress. Secondly the time scale of the force can be of importance. With the latter is meant that the wave exerted a force for no longer than 1.5 seconds, while for the stiffness tests the force is gradually applied. This hypothesis is not further tested.

Furthermore, Figure C.9 show that it looks like the whole mattress is being lifted when looking at the sides where it is not. This is due to the badly distributed ballast material within the mattress and the significant slack in the upper en lower sheet. This allows for the whole mattress to '*move*' while it still rests on the mattress below the uplift, which is not visible in the photos.

Figure C.9: Uplift behaviour of the medium-flexible mattress

For the stiff mattress it was expected to behave stiff and the maximum force would be half the weight. Instead it was still possible to apply smaller forces and get a small uplift. This can again be explained by the slack in the sheets and broken connection between the top and bottom sheet, as explained in the paragraph above. Once the mattress was lifted sufficiently, the force needed was half the weight of the mattress independent of the amount of uplift.
The same difference in force needed per uplift is observed for the dry and underwater tests.

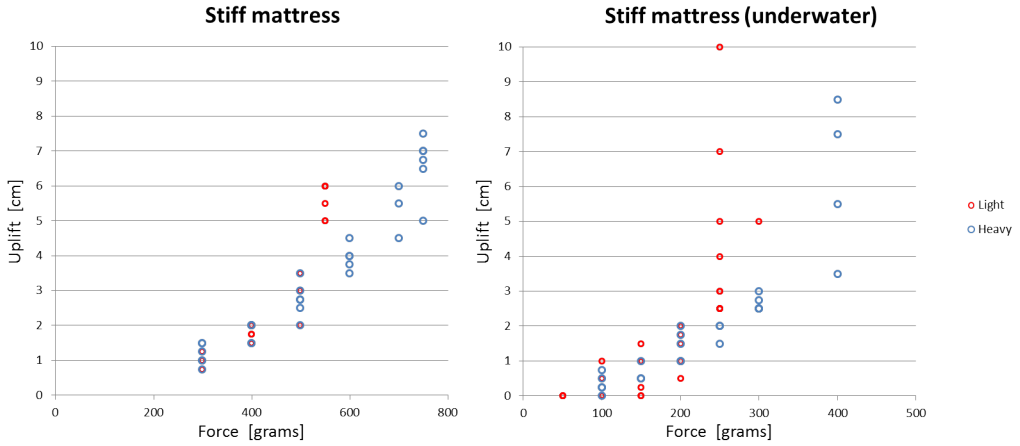

Figure C.10: Stiffness measurements stiff mattress, monopile

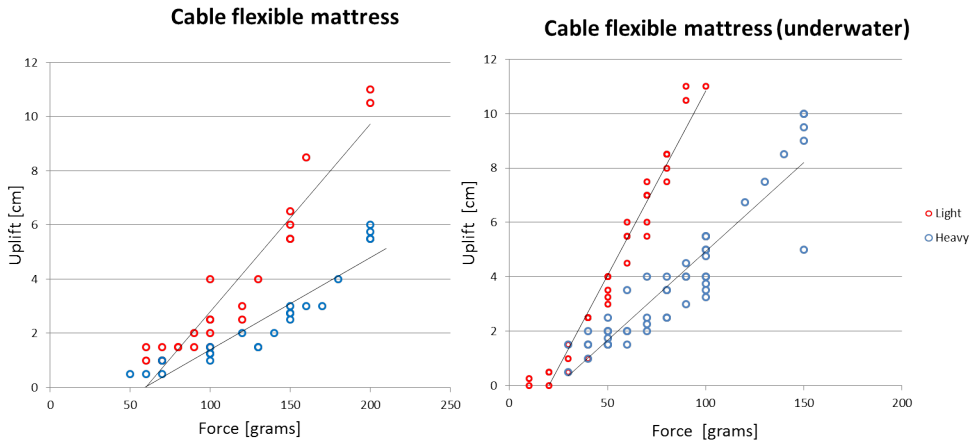

Figure C.11: Stiffness measurements flat mattress, cable

The flat mattress behaved differently than the other three mattresses which is due to its geometry. With respect to the monopile mattresses, the weight did not increase non-linear due to the shape and did behave linear. Furthermore the expected behaviour below water is observed.

During the stiffness tests the uplift length, the length over which the uplift took has not been measured.

D

MOBILITY ANALYSIS

Instead of looking at the initiation of motion, that is hard to define exactly, the Scheldt Flume tests are also analysed with respect an amount of uplift, thus the mobility. This is again done for θ and θ_i with linear wave theory and also the EMS data.

D.1 METHODOLOGY

The video recordings of the Scheldt Flume are analysed again but now quantitatively for the amount of uplift. Four or five stages are defined to categorize the uplifts and is explained below. First the whole video is analysed and checked whether multiple categories occurred during a test. If during a test only one category occurred, the maximum orbital velocity is taken. When multiple categories occurred, the lowest category is taken with its corresponding orbital velocities (from linear wave theory and the EMS).

When an uplift is observed, the corresponding wave and orbital velocity is used for the determination of θ_{lin} as given in eq. 4.7& 4.6. At the same time it is looked whether the uplift happens up- or downstream, with this also the corresponding EMS value is used in the following equation:

$$\theta_{ems} = \frac{u_{ems}^2}{\Delta g d} \tag{D.1}$$

The categories are defined as follows:

Category 0 No observable movement

Category 1 Movement of the edge of the mattress or constantly moving of the edge of the mattress

Category 2 Turning point up to ≈ three centimetres

Category 3 Turning point up to ≈ six centimetres

Category 4 Turning point up to ≈ nine centimetres

For the flat mattress at the cable section, the categorization only goes up to cat. 3. The distance of the turning point is defined while it is hard to estimate the amount of uplift. But it is assumed the higher the mattress is lifted, the further the turning point is on the mattress. Figure D.1.

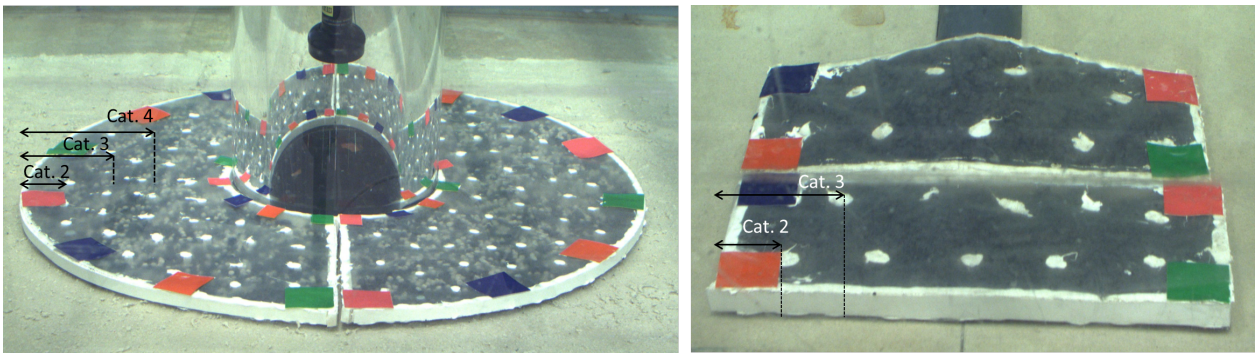

Figure D.1: Left: categories monopile mattress, right: categories cable mattresses

The medium-stiff and stiff mattress have not been analysed this way. The turning point is hard to define or do not have a turning point on the mattress at all. To quantify the amount of uplift with no reference point will results in big errors.

D.2 Visual Observations

Again, when analysing the video recording multiple things are observed that can have an influence on the stability of the mattress. Most of them have already been pointed out in section 4.3.2.

1. For the cable section the amount of uplift of the mattress at the far side from the camera is hard to determine exactly. The mattress at the end of the cable is in front of this mattress which makes it hard to define the turning point.
2. for the cable section, uplift of the flat mattress mostly starts at the same corner. This uplift is significantly higher than the uplift of the opposite corner on the same side.

D.3 Results

Figure D.2 and D.3 show the results with respect to the wave analysis. Both plots show the linear wave theory versus the measured values and it can be concluded that they agree reasonably well. For the monopile section the EMS data removes the biggest outliers. For the cable section the EMS data has a more significant influence, especially in the 3rd category. The difference between the linear wave theory and measure data is further explained in section D.4

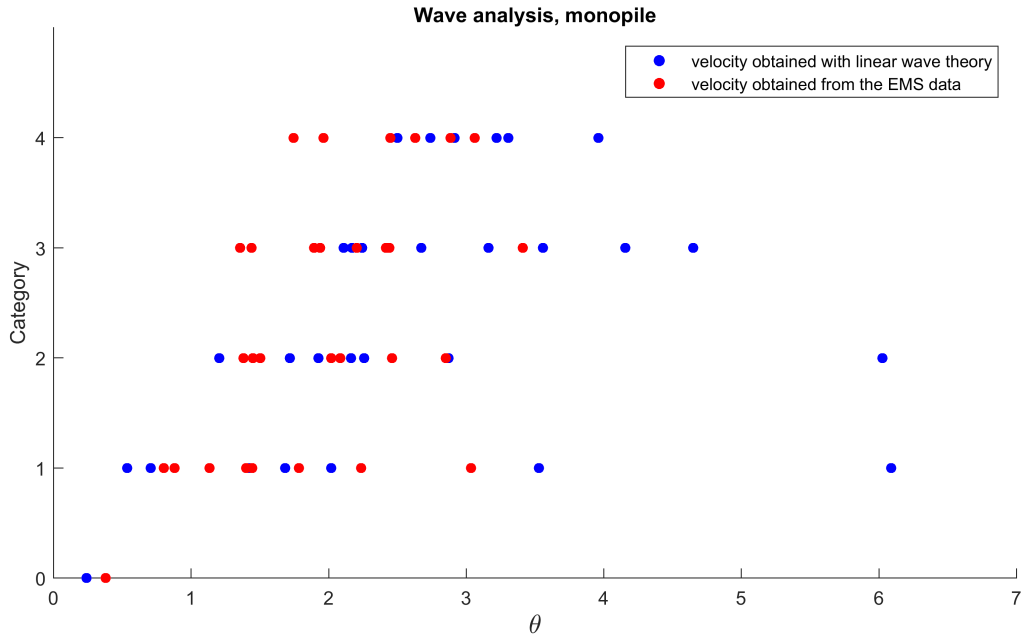

Figure D.2: Wave analysis, monopile

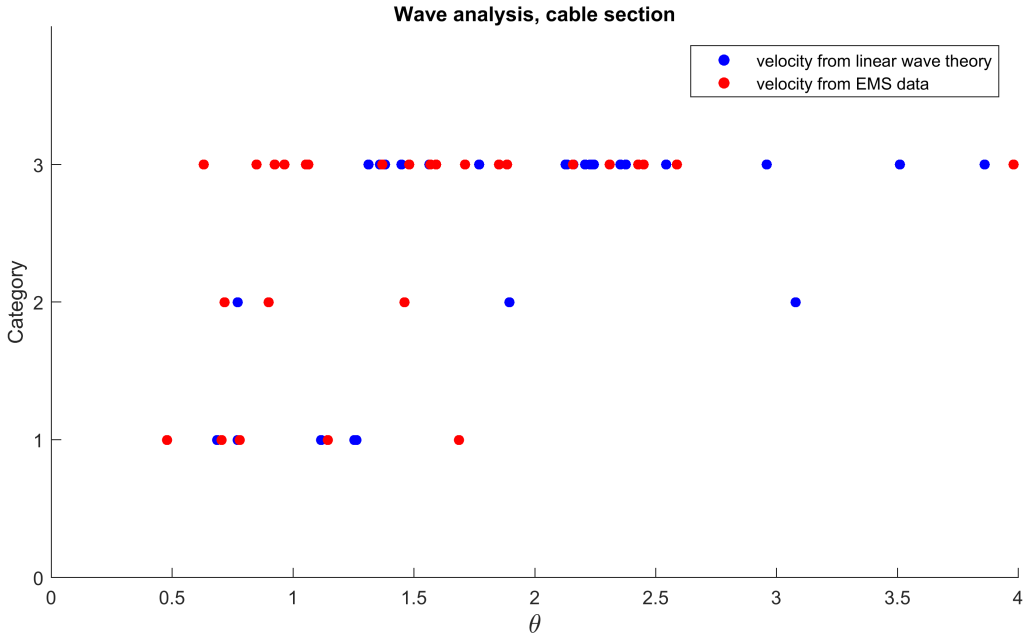

Figure D.3: Wave analysis, cable section

Lastly the full expression, shown in eq. D.2 is used. For a first analysis one coefficient is used for all test as before, where the coefficients between the forcing due to drag and inertia differ throughout a wave cycle and due to the geometry of the mattress, this has already been explained in Chapter 2. Eq. D.2 is only used for the linear wave theory and again it is assumed that the coefficient includes the difference in occurence of the forcing.

$$\theta_{T,lin} = \frac{u_x^2 + C_{all} a_x d}{\Delta g d} \tag{D.2}$$

Figure D.4 show four plots for different values for C_{all}. Only the data from the linear wave theory is used. In general all points shift to the right. Where per category the distance between the two most outer point does not differ much and the points in between seem to be moving randomly. The higher C_{all} the more pronounced the difference is between category 1 and 2. This can be explained by the fact that, in general, the hydrodynamics become larger. Leading to a higher acceleration. The inertia is assumed to be dominant in the early stages of movement, where for higher uplifts the area of attack increases, thus the drag.

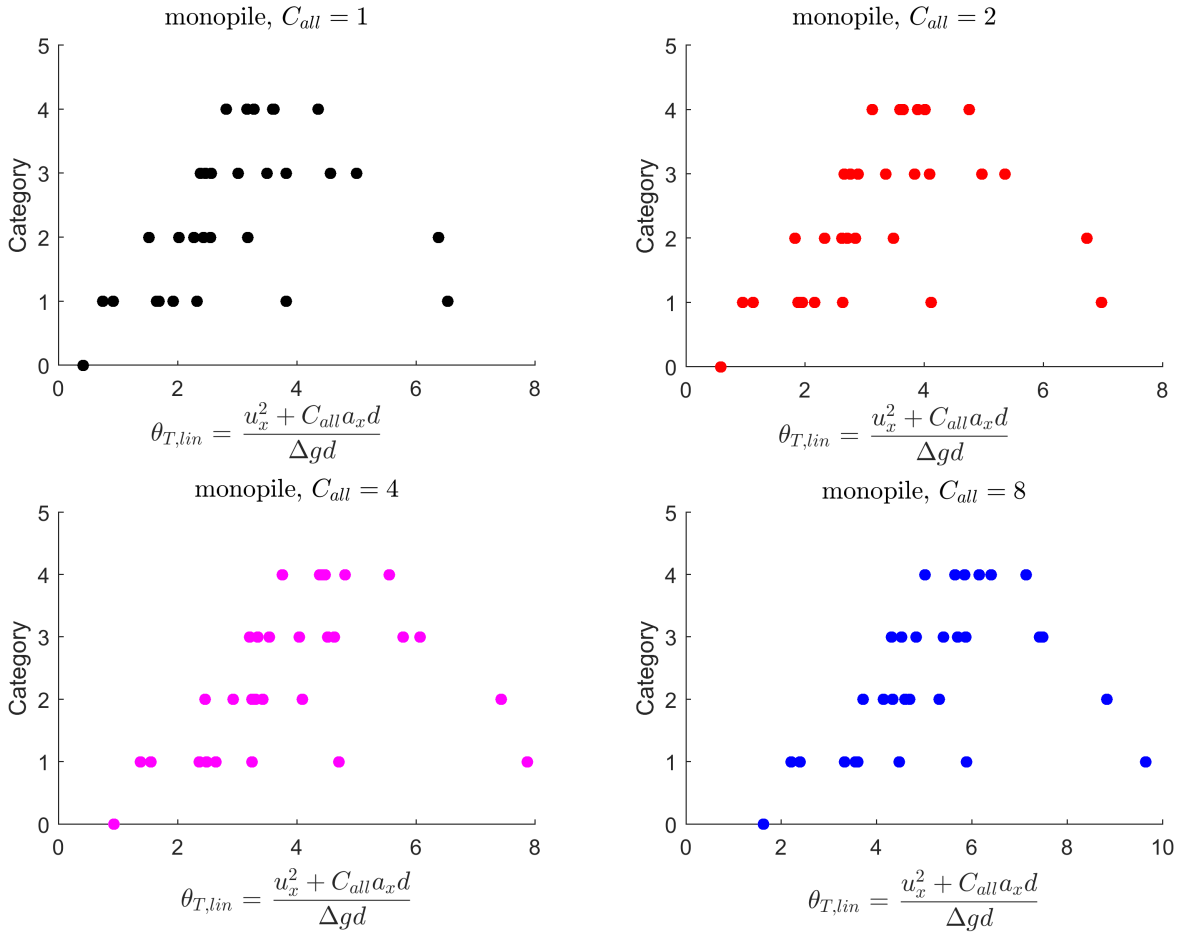

Figure D.4: Full mobility equation for different values of C

D.4 VALIDATION OF NEAR BED VELOCITIES

The velocity used in eq. D.1 is measured 5.0 cm from the flume bottom, where linear wave theory calculates the velocity at the bottom of the flume. This should introduce a first error, where the EMS should measure bigger velocities than calculated with linear wave theory due to the fact that the EMS is higher up the water column. Two other possible reasons for the difference in the velocity are:

1. Validity of linear wave theory
2. Wave boundary layer

The validity of linear wave theory is given in Figure D.5. This figure shows where the tests from the Scheldt Flume are within the validities of different wave theories. This shows that the range at which linear wave theory can be used is exceeded. However, linear wave theory still predicts velocities at the bottom reasonably well the less linear a wave will become.

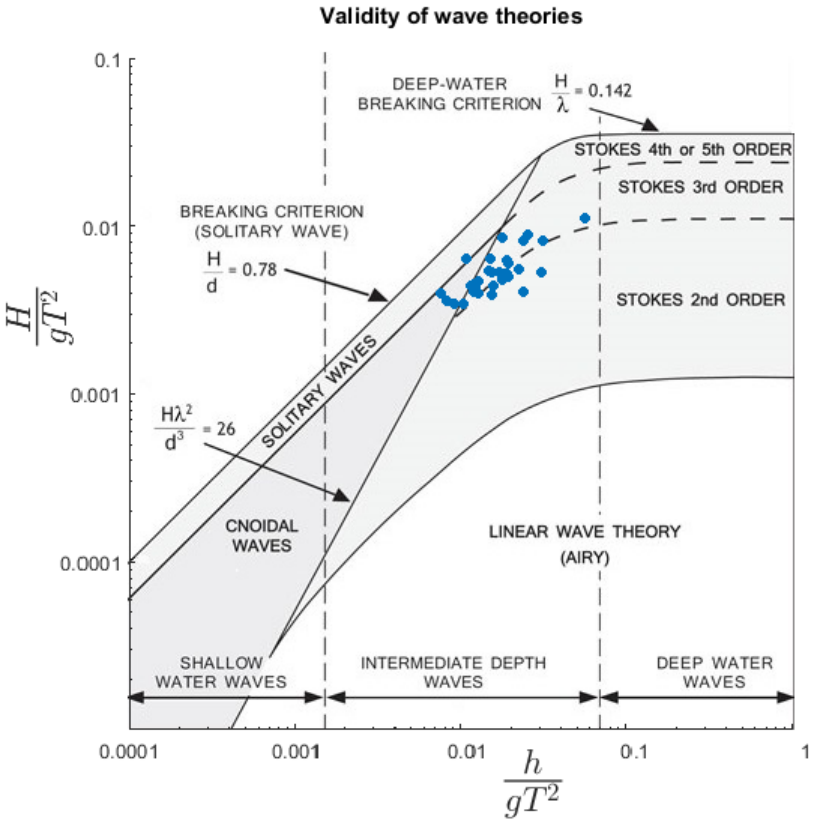

Figure D.5: Full mobility equation for different values of C

The disadvantage of the EMS is that it can not measure the velocities near the bed, for this reason it was placed 5 cm above the flume bed but this is not the height at which the velocity acts on the mattress. This velocity in turn would be lower due to the boundary layer. The height of this boundary layer can be approximated, according to Schiereck & Verhagen (2012), by:

$$\frac{d\delta}{dt} = ku_* \approx 0.4u_* \tag{D.3}$$

in which u_* is approximately $0.1 * u_{bed}$. When applying this to the lowest and highest value of the found velocities, it ranges between 1 mm to 3.5 cm. This concludes that the measured values from the EMS were taken well outside the wave boundary layer. But it does show that the mattress, for most waves (u_{ems} > 0.20 m/s and wave periode ≈2 seconds) is within the wave boundary layer.

The applicability of linear wave theory together with the height at which the EMS is measured can explain the small difference shown in Figure D.2 and D.3. The big two bigger outliers can be explained by looking at the Ursell number. The Ursell number indicates the non-linearity of waves (Holthuijsen, 2010). For the Ursell numbers > 26 the cnoidal theory is better. Figure D.6 shows the different Ursell numbers versus the wave steepness. From the three biggest values shown in Figure D.6 , two are the outliers. The rest of the data does not show a significant difference with respect to big Ursell numbers. The parameters in Figure D.6 are obtained with linear wave theory.

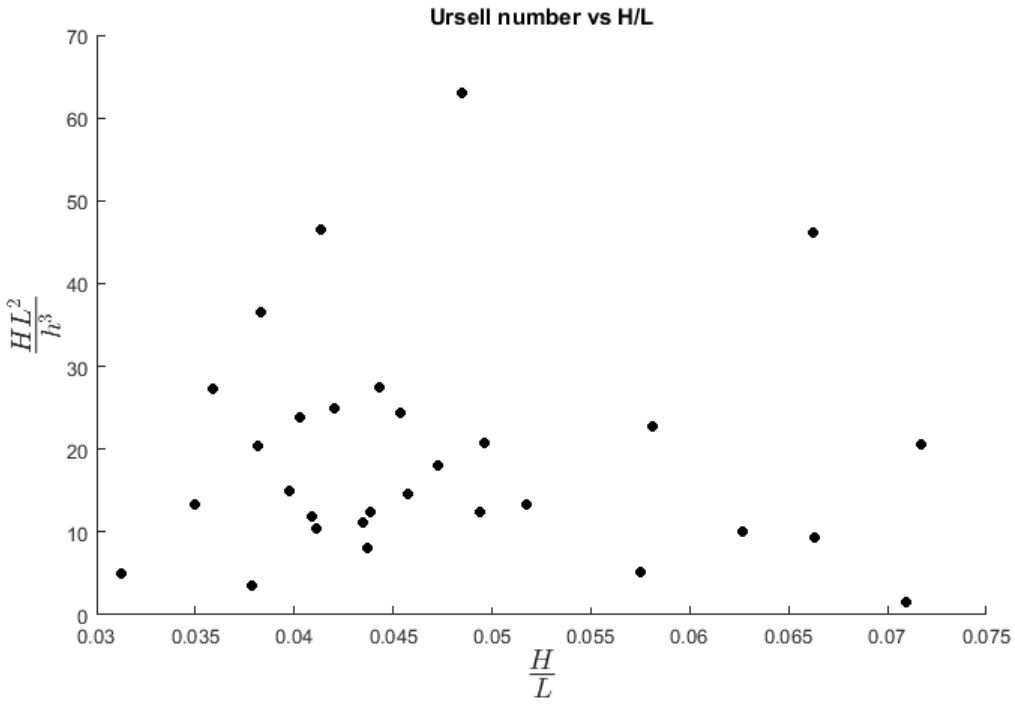

Figure D.6: Ursell number versus the wave steepness

E

UPLIFT RECOGNITION

E.1 EMS DATA AND LINEAR WAVE THEORY COMBINED

To apply the instantaneous approach, the exact velocity and acceleration must be known at the time of uplift. To do this, two methods are used to determine the exact hydrodynamics at the time of maximum uplift. The first method is already explained in chapter 5 and not repeated here. The second method uses the mean wave characteristics to calculate the wave celerity according to eq. E.1.

$$c = \frac{gT}{2\pi} tanh(kh) \tag{E.1}$$

in which: c = wave celerity [m/s]
T = mean wave period [s]
g = gravitational acceleration
k = wave number [-]
h = depth

With the wave celerity the time it takes for a wave to travel the distance between the EMS and the edge of the mattress is calculated. Subsequently, the whole EMS signal is translated according to this time shift and the exact hydrodynamics are obtained at the time of maximum uplift.
Figure E.1 shows the two methods for the cable and flexible monopile mattress. The methods agree well, which can be explained due to the fact that both methods assume the time shift according to linear wave theory. Where one assumed a sin-wave between the crossing, the other still keeps the original EMS signal.

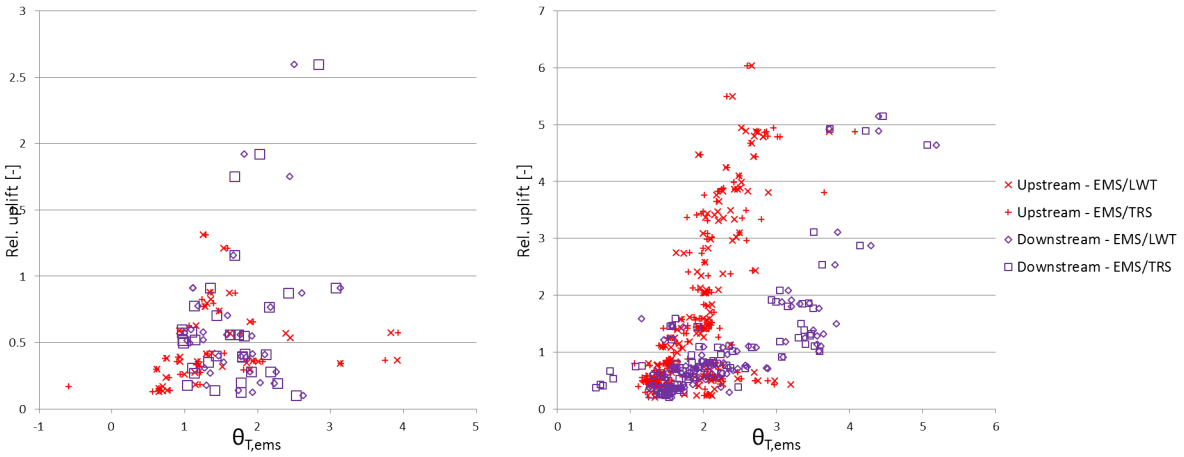

Figure E.1: Relative uplift against $\theta_{T,ems}$. Left graph shows the cable mattress, the right graph shows the flexible monopile mattress. Both plots us $C_{all} = 4$

Most of the tests for the medium-flexible monopile mattress are performed simultaneously with the cable mattress, assuming the same results. The negative results found for the flat cable mattress can be due to the assumptions of linear wave theory or a wrong detected movement by the software, as the relative uplift is small.

F

DESIGN METHOD

F.1 DETERMINATION OF RELATIVE UPLIFT

To determine the amount of uplift corresponding to a specific θ, the data from Chapter 5 is used and the lower bound is taken for safety. Figure F.1 shows the polynomial line taken from the data, this line with its equation is used to determine the uplift per given θ and gives a good agreement up to a relative uplift of two.

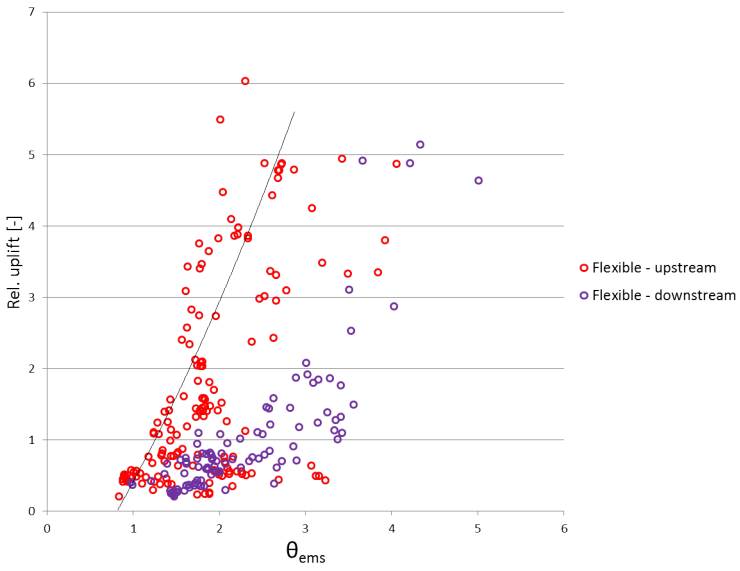

Figure F.1: Graph showing the polynomial function to calculate the uplift per given θ

The equation corresponding to this line is:

$$\frac{uplift}{thickness} = 0.285\theta^2 + 1.679\theta - 1.57 \tag{F.1}$$